72-17,167

SCHNEIDER, Bruce Stanley, 1946-
FLUORESCENCE OF MOLECULAR IONS; HBr^+, CS_2^+, AND N_2O^+.

Yale University, Ph.D., 1971
Physics, molecular spectroscopy

University Microfilms, A XEROX Company, Ann Arbor, Michigan

© 1972

Bruce Stanley Schneider

ALL RIGHTS RESERVED

Reproduced with permission of the copyright owner. Further reproduction prohibited without permission.

FLUORESCENCE OF MOLECULAR IONS; HBr^+, CS_2^+, AND N_2O^+

by

BRUCE STANLEY SCHNEIDER

B.S. TULANE UNIVERSITY OF LOUISIANA 1967

M. PHIL. YALE UNIVERSITY 1969

A Dissertation Presented to the Faculty of the

Graduate School of Yale University

in Candidacy for the Degree of

Doctor of Philosophy

1971

Reproduced with permission of the copyright owner. Further reproduction prohibited without permission.

PLEASE NOTE:

Some pages may have

indistinct print.

Filmed as received.

University Microfilms, A Xerox Education Company

Reproduced with permission of the copyright owner. Further reproduction prohibited without permission.

ABSTRACT

THESIS CHAIRMAN: Professor Allan Laslett Smith

The helium 584Å resonance line was used to photoionize a sample gas, and fluorescence was dispersed with a 0.25m monochromator and detected with a cooled photomultiplier tube coupled with photon counting equipment.

HBr^+ was the first molecule studied. Emission due to photoionization ($HBr\ (X^1\Sigma^+\ v'') + h\nu \rightarrow HBr^+\ (^2\Sigma^+,\ v') + e^-$) followed by fluorescence ($HBr\ (^2\Sigma^+,\ v') \rightarrow HBr^+\ (^2\Pi_i) + h\nu$ where i=1/2 or 3/2) was observed in the 3000-4000Å region. All bands with $v' \geq 2$ were missing from the spectrum. Franck - Condon calculations using Morse potentials combined with the photoelectron spectrum of HBr indicate equal intensities for the transitions $HBr^+\ (^2\Sigma,\ v'=1) \rightarrow HBr^+\ (^2\Pi_i, v''=0)$, and $HBr^+\ (^2\Sigma^+,\ v'=2) \rightarrow HBr^+\ (^2\Pi_i,\ v''=0)$. Therefore predissociation of the levels $v' \geq 2$ is strongly suggested. In addition, relative intensities for transitions from the v'=1 and 0 vibronic levels were measured. Theoretical Franck - Condon factors were computed under the assumption of a Morse potential. The ratio of the theoretical Franck - Condon factors for the 0-1 and 0-0 transitions differed significantly from the corresponding ratio obtained from the experimental relative intensities. Similar theoretical and experimental ratios for the 1-0 and 0-0 transitions barely agreed within experimental uncertainty. A further investigation was made by taking a photoelectron and ion emission spectrum, (photoionization was produced by microwave discharge). The ion emission results confirmed the accuracy of the F.C.F. ratios obtained from the fluorescent photoionization experiment. The photoelectron spectrum combined with information from previously published results indicates that the $^2\Sigma^+$ state is highly perturbed and has a potential maximum which facilitates predissociation by tunneling for v'=0 and 1 rovibronic levels. The incongruity between experimental and theoretical F.C.F.'s could not be fully explained but suggestions for further work were advanced.

Fluorescent photoionization spectra of CS_2^+ and N_2O^+ were also taken. The spectrum of N_2O^+ was not sufficiently resolved to yield any information about predissociation, but the CS_2^+ spectrum showed strong $CS(^1\Sigma-^1\Pi)$ transitions. The energetics of the CS_2^+ and CS_2 states suggest that the $CS(^1\Sigma-^1\Pi)$ fragment resulted from a Rydberg state of CS_2 not from a vibronic state of CS_2^+. Bonding characteristics for N_2O^+ and CS_2^+ electronic states were inferred from relative intensity measurements.

Reproduced with permission of the copyright owner. Further reproduction prohibited without permission.

TO MY PARENTS

AND

LYNETTE.

Reproduced with permission of the copyright owner. Further reproduction prohibited without permission.

ACKNOWLEDGEMENT

The author wishes to thank Dr. Allan Laslett Smith for his guidance and perseverance. The author would also like to express gratitude to Drs. Steven D. Colson and R. James Cross for their counseling.

The author is indebted to his many associates for their assistance and friendship and to the many skilled technicians who made construction of the equipment possible.

A special acknowledgement to the typist.

Reproduced with permission of the copyright owner. Further reproduction prohibited without permission.

TABLE OF CONTENTS

Page

I. INTRODUCTION.....1

II. EXPERIMENTAL.....13

Approaches to the Observation of Molecular Ions.....13

Experimental Details.....15
Fluorescence Chamber and He Purification System.....15
Vacuum System and Sample Gas Purification.....17
Optical System.....18
Detection System.....20

Conclusions.....22

III. THEORY.....23

IV. HBr^+.....34

Experimental Results.....35
Fluorescent Photoionization, N_2^+.....35
Fluorescent Photoionization, HBr^+.....36
Ion Emission, HBr^+.....38

Discussion.....40

Conclusions.....50

V. CS_2^+ AND N_2O^+.....52

Previous Work.....52

Experimental Results.....54
Observed Transitions.....54
Intensity Measurements.....55

Discussion.....57
Fragmentation Processes.....57
Electronic Structure and Bonding Characteristics.....59

Conclusion.....63

Reproduced with permission of the copyright owner. Further reproduction prohibited without permission.

TABLE OF CONTENTS

page

APPENDIX I : PROGRAM FOR COMPUTING ROTATIONAL SPECTRUM OF $^2\Sigma \rightarrow {}^2\Pi$ TRANSITIONS.....65

Reproduced with permission of the copyright owner. Further reproduction prohibited without permission.

INTRODUCTION

The interest in and study of molecular ions, which began in the early 1900's with spectroscopic investigations,[1,2] has expanded so rapidly that many experimental methods for determining properties of molecular ions now exist. If, however, attention is focused on vibronic properties of ions, five specific experimental techniques are most applicable. These are electron mass spectroscopy, observation of Rydberg series in V.U.V. absorption spectroscopy, photoionization mass spectrometry, photoelectron spectroscopy, and observation of emission from molecular ions produced by electron impact, microwave discharge, ion impact, or photoionization. Although the above methods are complimentary, all have their own strengths and limitations.

Electron impact[3] and photoionization mass spectroscopy[4,5] are experimentally similar techniques. In electron impact mass spectrometry a heated tungsten wire emits electrons which are given a pre-determined but adjustable velocity by voltage grids, and passed through a sample gas to produce ionization. The ions produced are then mass analyzed. Similarly in photoionization studies the Hopfield continuum produced by Helium discharges is used in combination with a V.U.V. monochromator as a source of monoenergetic high energy photons, whose absorption yields ions which are also mass analyzed. Data is taken by

Reproduced with permission of the copyright owner. Further reproduction prohibited without permission.

varying the energy of the ionizing source, (i.e. either kinetic energy of electrons or wavelength of photons), and graphing source energy versus number of ions of a particular charge to mass ratio detected. If the monitored ions are those obtained directly from ionization of the neutral, (i.e. parent ions are monitored), the data is called an ionization potential curve (I.P.). Similarly, if the monitored ions are those resulting from fragmentation of the parent ion the data is called an appearance potential (A.P.).

The interpretation of I.P. curves to give accurate energy separations of electronic states in the ion is only possible in a very limited number of cases. The analysis of any data depends on a sound theoretical framework. Because ionization by electron impact produces at least three particles, i.e. e^- (kinetic energy) + M (thermally excited) $\rightarrow$ e^- (scattered) + e^- (ionized) + M^+ (may fragment), a theoretical or experimental prediction of how the kinetic energy of the bombarding electron will be partitioned among the three products is presently infeasible. Even if both product electrons are assumed to have no kinetic energy, energies corresponding to breaks in I.P. or A.P. curves cannot be assigned to vibronic states of the ion. (This has been discussed at length by Chupka[6]).

Another limitation to electron mass spectrometry is the degredation of instrumental energy resolution, due to

Reproduced with permission of the copyright owner. Further reproduction prohibited without permission.

the Boltzman temperature distribution of source electrons and the inefficiencies in detecting ions. Often the exact onset of an I.P. curve is extremely hazy and can be determined to only ± .05ev. Mathematical devices have been used to correct for these difficulties. A Boltzman distribution corresponding to the temperature of the filament is convoluted with the spectrum as a correction.[6] Also first derivative curves of spectra are made to help determine onsets.

In contrast, photoionization mass spectroscopy does use a monoenergetic source. However, it does have many of the same problems as electron impact mass spectrometry. The two products resulting from the ionization process $h\nu + M(\text{thermal}) \rightarrow e^-(\text{ionized}) + M^+(\text{may fragment})$ still makes prediction of the energy partition impractical. Also the problems presented by the thermal energy of the neutral are still present. In addition, autoionization often obscures the added resolution a monoenergetic source provides.

A.P. curves can be used to obtain information on fragmentation processes. For example, if the appearance potential of NO^+ from N_2O is 16.57ev, and the closest I.P. is 15.5, then it takes 1.07ev of energy above the ground vibrational state of the 15.5 electronic state to cause fragmentation. Yet energy inaccuracies inherent in interpretation of I.P. curves only compound similar

Reproduced with permission of the copyright owner. Further reproduction prohibited without permission.

problems in A.P. curves. Thus energies of electronically excited ionic states and of fragmentation phenomena determined by mass spectrometric methods are at best approximate.

Use of both V.U.V. absorption spectroscopy[7] and of mass spectrometry began in the 1930's. However, the former grew much less rapidly than the latter. The source energy in V.U.V. absorption spectroscopy is an emission continuum, usually produced by a gas discharge, spanning the spectral region of interest. The continuum is passed through a sample gas and absorption is monitored on a spectrograph.[8]

I.P.'s are obtained from calculations determining the convergence limits of the observed Rydberg series.[9] If all the members of a series are correctly assigned, the I.P.'s can be quite accurate. If vibrational structure in the Rydberg series can be analyzed, then vibrational information is available assuming the vibrational structure in the ion is the same as in the Rydberg series.[10] This assumption has been shown to be true in a few instances. If the magnitude of a quantum defect is a good indication of the Rydberg electron's symmetry classification, an attempt to state the symmetries of ionic electronic state corresponding to the convergence of the Rydberg series is possible.[11] The usefulness of any spectrum, however, depends on the correct assignment of bands. Since Rydberg series often

Reproduced with permission of the copyright owner. Further reproduction prohibited without permission.

overlap and since bands are made diffuse by autoionization and predissociation, this is not always possible. Even if the spectrum can be interpreted, transition probabilities for neutral ion trnasitions depend on the unproven supposition that relative intensities in the vibronic components of the Rydberg series are the same as relative intensities in neutral-ion transitions. The amount of information obtainable from Rydberg series analysis depends strongly on the number of foregoing assumptions proved to be valid in the system under study.

Emission from electronically excited ionic states was first observed in the 1920's in electrical discharges.[12,13] In addition to hollow cathode and microwave discharges, electron or ion impact[14] on neutral molecules have augmented the means of producing emission from molecular ions. These methods produce relatively intense emission in which vibronic transitions with rotational structure can be completely resolved for many diatomic molecules. Although almost all of the original work in this field was done photographically, the intensity of the emission makes photoelectric detection also possible. The use of photographic methods allows typical energy resolution of $0.1cm^{-1}$. Therefore ion-ion vibronic transition energies can be determined quite precisely. Accurate vibrational frequencies of vibronic states can then be

Reproduced with permission of the copyright owner. Further reproduction prohibited without permission.

extracted from the transition energies. Photoelectric techniques make possible the measurement of emission intensity for each observed vibronic transition in the ion. Therefore information concerning ion-ion transition probabilities are obtainable. It is also possible to detect predissociation, if intensities of resolved rotational lines can be measured.[15]

The most recent technique developed for investigation of gas phase ions is photoelectron spectroscopy.[16,17,18] Briefly, a photoelectron spectrometer consists of a He resonance line light source (21.22ev) which is collimated by a capillary tube and passed through a sample gas to produce ions. The kinetic energy of the electrons which are ejected by the ionization process is then measured by an electrostatic or magnetic energy analyzer. A graph is then made of electron energy versus number of electrons detected at this energy. In the photoionization process, the 21.22ev of energy must be divided between kinetic energy of the ejected electron and the internal energy of the resulting ions and thus the internal energy states of the ion can be fully determined. Provided an ionic electronic state lies less than 21.22ev above the ground state of the neutral, the only limitation to observation in photoelectron spectroscopy is a small partial photoionization cross-section for production of that state. Generally this means that

Reproduced with permission of the copyright owner. Further reproduction prohibited without permission.

the ionization potentials and many of the vibrational frequencies of all electronic states of the ion lying less than 21.22ev above the neutral ground state can be obtained. Photoelectron spectroscopy also lends itself to qualitative predictions about ionic orbital bonding characteristics.[18] It is important to recognize the complimentary nature of photoelectron and molecular ion emission spectroscopy. P.E. spectroscopy determines the entire manifold of bound electronic states and emission spectroscopy studies the intensity and frequency of light emitted in transitions between these states.

Photoelectron spectroscopy is not a panacea. Thus far, the best resolution achieved has been 9mev ($72cm^{-1}$).[19] The symmetry of ionic electronic states can only be inferred indirectly, (i.e. the ionization potential determined from the photoelectron spectrum is the convergence limit for Rydberg series whose quantum defects may indicate the symmetry of the ionic state). Relative intensities of ion-ion transitions cannot be determined since little can be said concerning what happens to the ion once the ejected electron leaves the molecule. However, there is information available about ionic radiationless processes from line broadening. This can be demonstrated by a simple uncertainty argument. Average half lives of states which decay by radiative and by non-radiative

Reproduced with permission of the copyright owner. Further reproduction prohibited without permission.

processes are 10^{-7} and 10^{-13} sec. respectively. Using the uncertainty relations, $\Delta t \Delta E \simeq h/2\Pi$, ΔE's of 6×10^{-6} and 6 mev respectively are calculated. What this means physically is that the speed of non-radiative processes occuring from a discreet level determines the uncertainty of measuring transitions to this level. Thus line broadening in the photoelectron spectrum only indicates the presence of a non-radiative process with rates faster than about 10^{13} sec.$^{-1}$.

The last technique, (the one dearest to my heart), to be discussed is fluorescent photoionization.[20,21,22]

Ionization of the gas is achieved by irradiation with collimated 584Å light from a He discharge or by monochromatic light obtained from a continuum discharge coupled with a V.U.V. monochromator. The emission from the ions thus produced is dispersed by a grating spectrometer and monitored photoelectrically.

If the 584Å line is used as an ionizing source, relative populations of the ionic electronic states can be determined from the relative intensities of their corresponding peaks in the photoelectron spectrum.[23] The resulting excited ionic states can decay either radiatively or non-radiatively. For an allowed transition the relative rates of radiative and non-radiative decay from a vibronic level determine the intensity observed in fluorescent photoionization. By measuring

Reproduced with permission of the copyright owner. Further reproduction prohibited without permission.

what is essentially a fluorescence quantum yield, one may investigate the decay of vibronic states. If a quantum yield is lower than is expected a non-radiative process is probably occurring. If the quantum yield is unexpectedly zero there are two possibilities: (1) Symmetries of the relevant ionic states have been incorrectly assigned; (2) Non-radiative transitions completely dominate radiative ones. A thorough comparison of the results for all the vibronic states associated with one electronic state should eliminate one of the two preceding possibilities. Thus symmetry assignments can be checked concurrently with a search for non-radiative decay.

"Photoionization emission" techniques have certain limitations. The biggest restriction is very weak emission intensity. This causes a host of experimental problems which can only be solved by photon counting and low light level techniques. Even with sophisticated electronic counting equipment, rotational structure cannot at present be resolved. Thus nothing can be said about the rotational energy level, i.e. J dependence of predissociation.

It should now be apparent that no individual method is sufficient for a complete study of vibronic states of molecules. To study fragmentation products, especially of large molecules, photoionization mass spectrometry is particularly useful. However, the

Reproduced with permission of the copyright owner. Further reproduction prohibited without permission.

energetics of the fragmentation process is often inaccurate. Interpretation of electron impact data is difficult and of dubious use in augmenting fragmentation information.

Photoelectron spectroscopy is quite useful in determining the energies (to ± 14mev) of the complete manifold of ionic states attainable by photoionization. V.U.V. absorption spectroscopy is the most exact way of determining the I.P.'s to ionic states. However, often complete Rydberg series are unobtainable. Therefore, determining I.P.'s for all ionic states observed in P.E. spectra is usually impossible. Molecular ion emission is the best method to accurately (± 0.01cm^{-1}) determine energy separations of pairs of ioinc states involved in fluorescence. In addition, the vibrational and rotational structure of these pairs of states can be determined. Intensity measurements from both molecular ion emission and fluorescent photoionization can be useful to predict transition probabilities. Different ionization sources provide different populations of molecular ion vibronic states. Naturally the less populated a state the less intense fluorescence from this state will be. Therefore it is sometimes necessary to use a variety of emission techniques to optimize the amount of information obtainable.

Reproduced with permission of the copyright owner. Further reproduction prohibited without permission.

Combination of fluorescent photoionization and photoelectron spectroscopy is the best method of detecting non-radiative processes and assigning symmetry to electronic energy levels. Photoelectron spectroscopy gives possible energies of transitions, (i.e. where in the spectral range to look). Comparison of predictions from photoelectron spectroscopy with observed molecular ion emission spectra can confirm assignment of symmetries for all observed transitions. However, the forbidden nature of an ion-ion transition is not proven by its absence from the emission spectrum of the sources normally used in spectroscopy. It is quite possible that unfavorable population rates in these sources have precluded the appearance of a particular transition. This obstacle can be surmounted by using a technique in which ion population rates are known, namely fluorescent photoionization. Then a missing transition whose upper state is reasonably populated can be classified as either forbidden or predissociated and thus symmetry information is sometimes extractable.

In this thesis, the vibronic structure of three molecular ions, HBr^+, N_2O^+ and CS_2^+, will be investigated. Fluorescent photoionization and molecular ion emission experimental techniques are used in conjunction with published data from photoelectron spectroscopy and ion impact emission work. HBr^+ will be shown to exhibit

Reproduced with permission of the copyright owner. Further reproduction prohibited without permission.

a number of anomolies. Transition probabilities for N_2O^+ and CS_2^+ will be given. Also a new transition in CS_2^+ was discovered.

Reproduced with permission of the copyright owner. Further reproduction prohibited without permission.

EXPERIMENTAL SECTION

Approaches to the Observation of Molecular Ions

Before embarking on a rather detailed description of the equipment used to do the work for this thesis, a short discussion of previous work in fluorescent photoionization would help to explain our choice of experimental components. D.L. Judge in 1963[20] was the first investigator to observe emission from photo-ionized molecules. He used a line spectrum produced by a spark discharge in air combined with a Seya V.U.V. monochromator to obtain ionizing energies between 10 and 20ev. The wavelength band width was 5Å and the average intensity at the exit slit 10^{10} photons/sec. (No cross-sectional area for the photon flux was given). A fluorescence chamber was attached to the exit slit of the Seya, and a Czerny-Turner monochro-mator without entrance slits was mounted on the fluorescence chamber so that its optical axis was perpendicular to the axis of the vacuum U.V. photon beam. A cooled photomultiplier, gated on in synchro-nization with the pulsed discharge, was used to detect emission. The observed dark current was 1 count/min and detection efficiency 2% per photon emitted.

The B.S. Schneider - A.L. Smith apparatus, (see Figs. 1 and 2), uses a He microwave discharge

Reproduced with permission of the copyright owner. Further reproduction prohibited without permission.

collimated by a stainless steel capillary tube as an excitation source. The only radiation emitted by the source capable of photoionizing molecules was the helium resonance line $2^1P - 1^1S$ at 584Å (21.22ev), with a photon flux of 3×10^{10} photons/sec. mm^2. Emission from the sample gas is observed perpendicular to the photon beam through a Suprasil window and a quartz lens. The fluorescence is then dispersed by a 1/4 meter Jarrel-Ash spectrometer. The detection system consists of a cooled photomultiplier tube, photon counting electronics, and a Computer of Average Transients (C.A.T.) to store the data. Average dark counts of 2 counts/sec. (1.5 counts/channel) and typical fluorescence signals of 30 - 450 counts/sec. were observed. An N_2^+ spectrum with 18.0Å resolution was clearly defined from one wavelength scan.

The two afore-mentioned approaches differ mainly in the exciting source. A tunable source can be used to populate only a portion of the manifold of electronic states in the ion. The source can be set at an energy less than that needed for ionization to a particular ionic state. Since this state will not be populated, it will not fluoresce. Therefore the complication of energetically overlapping electronic transitions can be eliminated and the emission spectra can be more easily analyzed. (Judge has done this for CO_2^+).[21] Thus

Reproduced with permission of the copyright owner. Further reproduction prohibited without permission.

the use of a He discharge trades the flexibility and information obtainable from a variable energy exciting source for the convenience of high flux and the possibility of using population rates from photoelectron spectroscopy as a powerful tool in analysis. Since Judge's excitation source was not collimated, by the time the light passed through the exit slit of the Seya and into the fluorescence chamber it was a diverging beam. By collimating the 584Å source and observing emission produced close to the end of the capillary tube, we avoided this pitfall. We used a lens system to image the fluorescing volume on the entrance slit of the monochromator in order to optimize light gathering power. It is also noteworthy that if a discharge pulsed at 10^4 Hz could have been made monochromatic at 21.22ev without loss of intensity, our dark current would have been 1.2×10^{-2} counts/min.

EXPERIMENTAL DETAILS

Fluorescence Chamber and He Purification System

The He discharge source consisted of three components: (1) the helium purification system (see Fig. 3); (2) The discharge chamber; (3) a stainless steel capillary tube. Helium, 99.995% pure, bought from the Matheson Company was passed over two heated Cu-CuO columns to remove hydrogen and oxygen. The

Reproduced with permission of the copyright owner. Further reproduction prohibited without permission.

temperature of the columns was maintained at 200°F by nichrome heating wire and it was necessary to regenerate the Cu column every five to six runs.[25] (The Cu-CuO catalyst was bought from BASF).[26] The helium was then run through an activated charcoal trap cooled with liquid nitrogen to remove nitrogen and any organic impurity. This trap, which has a pathlength of about eight feet, consists of eight parallel one foot tubes arranged circularly and connected alternately on the top and the bottom. The helium then flowed through a 12mm quartz tube where a microwave discharge was produced with an air cooled Evenson microwave cavity run at 85 watts.[27] The intensity of the V.U.V. light after being collimated was about 3×10^{10} photons/sec. (The measurement was made at a tungsten plate about seven inches away from the discharge).[28] The He discharge contained a few strong visible He lines, (i.e. 3889Å, 5015Å).

A stainless steel capillary tube with a 0.020 inch bore connected the quartz discharge tube to a stainless steel ionizing chamber. A 1/8 inch hole was bored in the side of the capillary tube directly above the place where it entered the chamber and was connected to a Welsh pump. The size of this hole combined with the low conductance of the capillary tube made differential pumping of the helium quite

Reproduced with permission of the copyright owner. Further reproduction prohibited without permission.

easy. The stainless steel tube effectively collimated the He discharge while avoiding the hazards of light conduction through the tube walls and breakage inherent with glass capillaries.

The fluorescence chamber, (see Fig. 2), was made of type 316 stainless steel to facilitate the use of corrosive gases. A retractable mirror was installed at 45° to the capillary tube. Light from a He-Ne laser directed through a Pyrex window at the top of the quartz discharge tube can be used to align the entire optical system. A tungsten plate attached to a hermetically sealed BNC was placed at a 50° angle to the exciting source. The plate served the two-fold purpose of preventing most of the visible He radiation from reflecting back into the emission chamber and affording a means of measuring V.U.V. light intensities. The last addition to the chamber was a Wood's horn placed opposite the Suprasil window to prevent reflection of any scattered light into the optical axis.

Vacuum System and Sample Gas Purification

A fairly extensive vacuum system was necessary for the successful introduction of He and sample gases. Two Welsh forepumps and a C.V.C. 1 inch oil diffusion pump were used to maintain an optimum

Reproduced with permission of the copyright owner. Further reproduction prohibited without permission.

vacuum of 1 x 10^{-5} torr with a leak rate of 2 x 10^{-5} torr/sec. measured directly after the D.P. Under actual operating conditions 1 torr of He was maintained in the discharge tube while differential pumping kept the partial pressure of He in the fluorescence chamber less than 10^{-3} torr. Most experiments were run with a sample gas pressure of 100μ.

All gases were bulb-to-bulb distilled before use, and after use were condensed in a liquid nitrogen trap before they reached the diffusion pump. This made it unnecessary to turn off the diffusion pump during a run. To further minimize the inconvenience of using corrosive gases, only o-ring joints and stop-cocks were used in the sample pathway. The He pressure in the quartz discharge tube was maintained by filling the purification part of the system, which contained a two liter ballast bulb, and valving it off from everything except the differential pumping at the capillary tube. The sample gas pressure in the fluorescence chamber was maintained by similar means.

Optical System

The components of the optical system, including a 1 inch Suprasil window, 5cm. focal length quartz lens, and 1/4 meter Jarrel-Ash spectrometer were chosen to provide the greatest light gathering power

Reproduced with permission of the copyright owner. Further reproduction prohibited without permission.

possible. A 1/4 meter Jarrel-Ash spectrometer was used because of its very fast f number (f/3.6). Even so, the monochromator remained the limiting aperture in the system. (A Jarrel-Ash 1/2 meter spectrometer (f/8.6) was tried initially without success). Since only quartz was used in the optical system, wavelengths down to 2000Å could be observed. Resolution was limited; a reciprocal dispersion of 36Å/mm., coupled with 500μ or 100μ slits gave measured FWHM resolutions of 18Å and 3.6Å respectively.

Alignment of the optical system was a three part procedure. First, a laser beam was directed down the capillary tube and reflected into the emission optical axis by the retractable mirror. The spectrometer's entrance slit was positioned 20cm. from the optical axis of the discharge, quadruple the focal length of the lens and in the path of the laser beam. The lens was then put into the system and the tilt of the monochromator was adjusted so that the laser beam reflected back onto itself. Next, the light from the helium discharge was used instead of the laser and the signal obtained when scanning through a visible helium line was maximized. Finally, 50μ of air was introduced into the sample chamber, the retractable mirror was withdrawn from the optical axis, and the fluorescence signal from the 3914Å

Reproduced with permission of the copyright owner. Further reproduction prohibited without permission.

emission band of N_2^+ (B-X) was maximized. Without this procedure it was extremely difficult to obtain good signal to noise ratios.

Detection System

Once a reliable means of gathering and dispersing fluorescence was developed, an equally dependable method of detection was essential. At first, the signal from the photomultiplier tube was read directly on a Keithley picoammeter. However, only dark current was observed rather than signal. So the monochromator was removed and a bare photomultiplier tube was placed against the quartz window of the fluorescence chamber. A signal of 5×10^{-8} amp. due to scattered light was observed. I tried a prism photographic instrument but it proved ineffectual, (no emission, let alone scattered light was observed), probably because of its slow f number (ca. f/12). I then returned to the 1/4 meter instrument. This time a few additions were made. First, an EMI 6256S photomultiplier tube was cooled to -20°C in a PFR tube cooler, decreasing the dark current from 600 to 40 counts/sec. Then the photon counting circuitry described by Akins, Schwartz, and Moore was built.[29] The optimum discriminator voltage of 30mv.

Reproduced with permission of the copyright owner. Further reproduction prohibited without permission.

was determined by comparison of the differential change in counts for dark current versus signal current.[30] A 400 channel TMC Computer of Average Transients was used to store the information from the discriminator circuit and permitted repetitive scanning of a spectrum to maximize the signal to noise ratio. (The monochromator wavelength was scanned at 120Å/min. and the CAT channel address was advanced at 0.7sec./channel).

With all of the photon counting apparatus installed, dark current counts of seven per second were obtained. One final improvement, shutting off of the lab lights, reduced the count to 2/sec. After a few realignments of the optical system scattered light was easily detected, (Fig. 3A),(the atomic helium line at 3889Å was detected with a typical intensity of 2.8 counts/sec.). From a comparison of the efficiency of detecting weak emission by photographic, standard photoelectric, and photon counting methods, it is obvious that the latter has a definite advantage and should be used when intensities are a limiting factor.

The photon counting and optical systems described have a capability to detect signals as weak as 10 counts/sec. This limit is imposed not by the dark current but from the scattered light from the He discharge. Also the investigatable wavelength range was limited to the 2000-5000Å region by the spectral

Reproduced with permission of the copyright owner. Further reproduction prohibited without permission.

response of the 6256S photomultiplier. Wavelengths can be determined to within 3Å even when CAT and monochromator wavelength drives are started by hand. Emission in the 2000-4000Å region from most molecular ions can be detected, provided slit widths are not decreased below 500μ. Large molecules, however, usually have complex emission spectra, that is, too complex for the 18Å resolution obtainable with 500μ slits. Thus if vibronic or rotational analysis of polyatomics is desired, a photographic molecular ion emission technique should be employed. However, if identification of electronic transitions is the goal, fluorescent photoionization is quite useful.

Conclusion

The final problem is deciding which molecules are the most interesting and most practical to study. Three questions should be asked in making this decision. Does the gas have undetermined transition probabilities which cannot be determined from molecular ion emission experiments? Is predissociation suspected? Is a symmetry assignment in doubt? If the answer to any of the above questions is yes, a fluorescent photoionization study would probably be worthwhile.

Reproduced with permission of the copyright owner. Further reproduction prohibited without permission.

Figure 1

Overall View of the Fluorescent

Photoionization Apparatus.

And

Figure 3

The Helium Purification System

Including Charcoal Trap

and Cu-CuO Columns.

Reproduced with permission of the copyright owner. Further reproduction prohibited without permission.

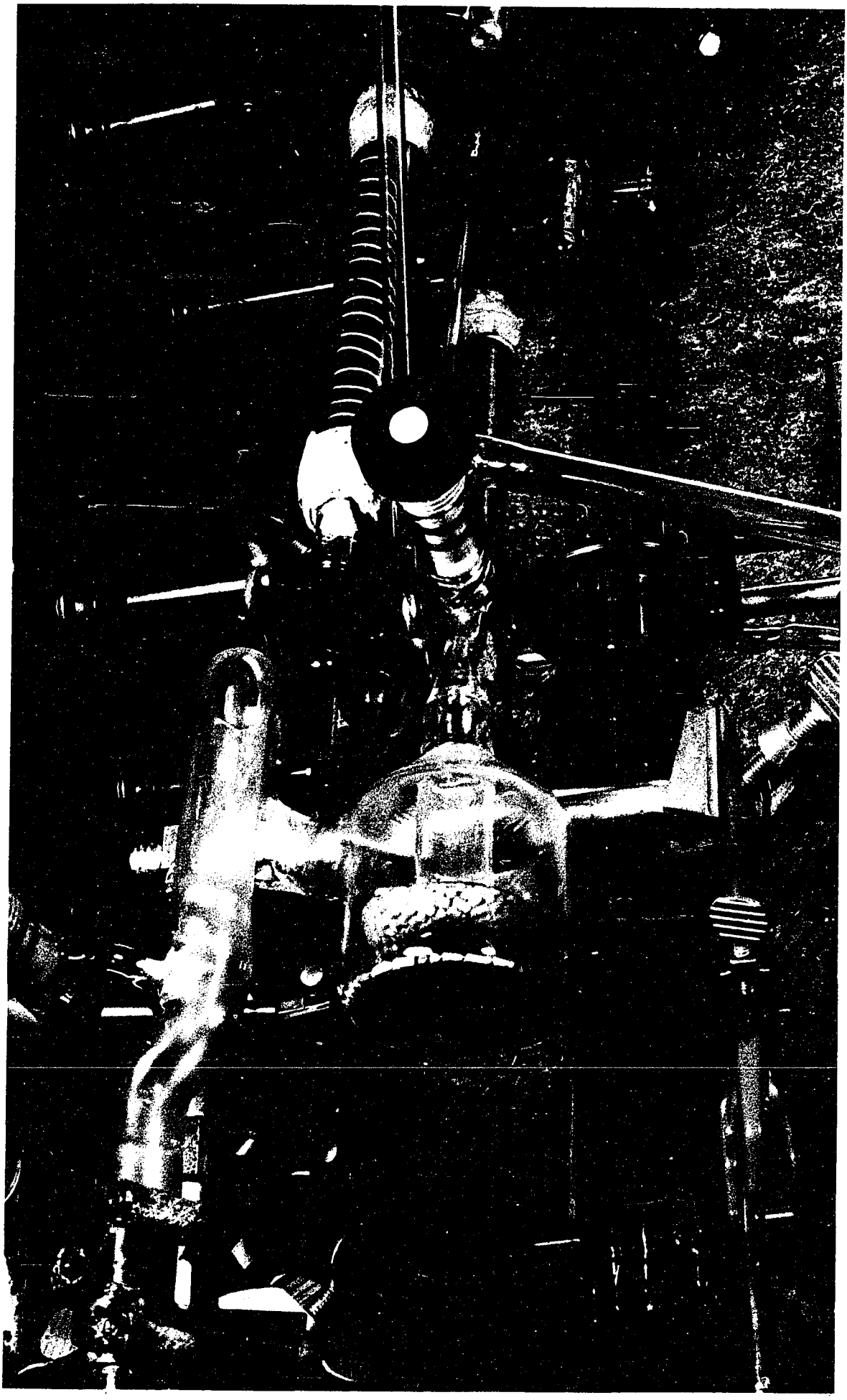

Reproduced with permission of the copyright owner. Further reproduction prohibited without permission.

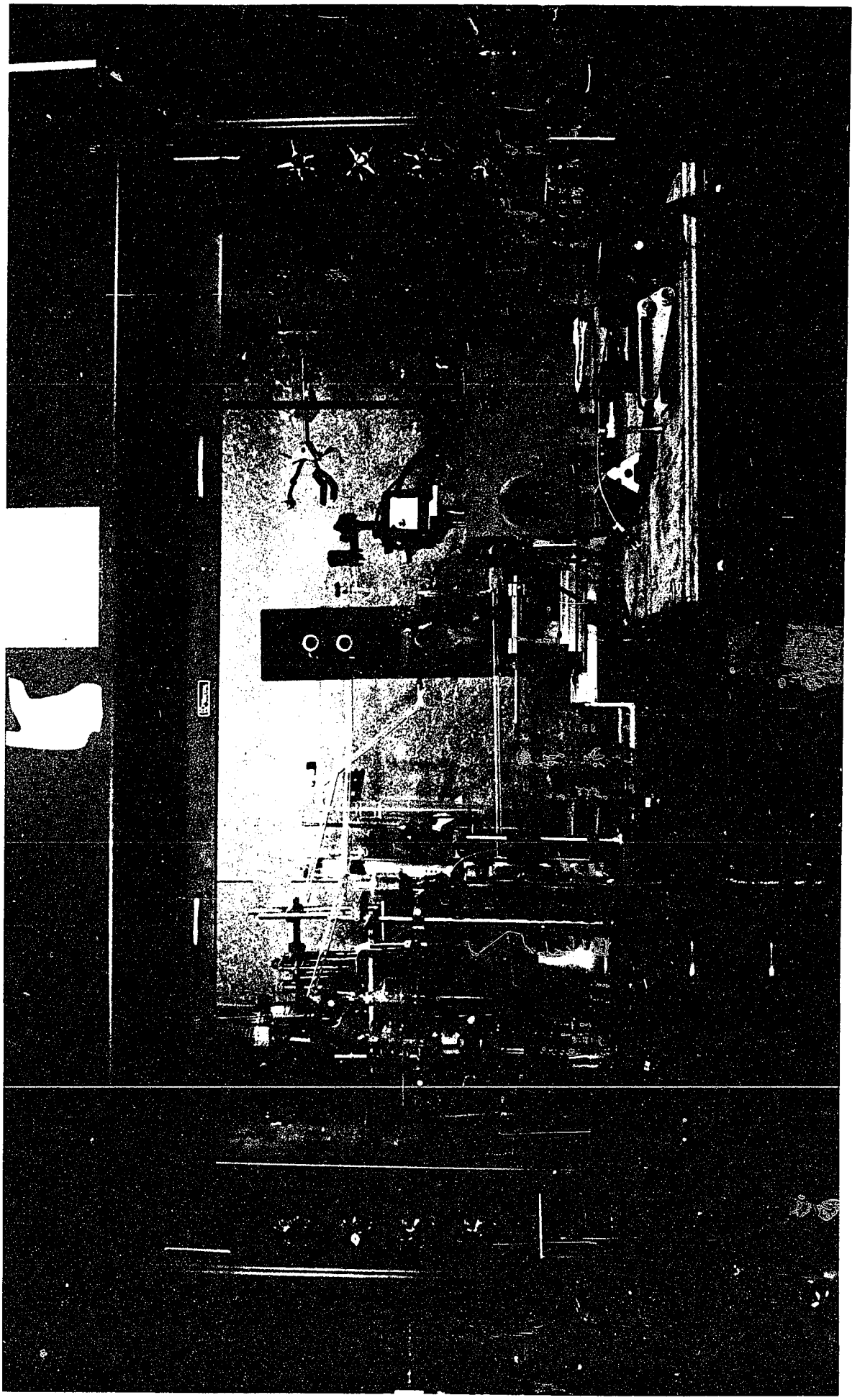

Reproduced with permission of the copyright owner. Further reproduction prohibited without permission.

Figure 2

Schematic Diagram of the Fluorescent Photoionization Apparatus.

Reproduced with permission of the copyright owner. Further reproduction prohibited without permission.

Reproduced with permission of the copyright owner. Further reproduction prohibited without permission.

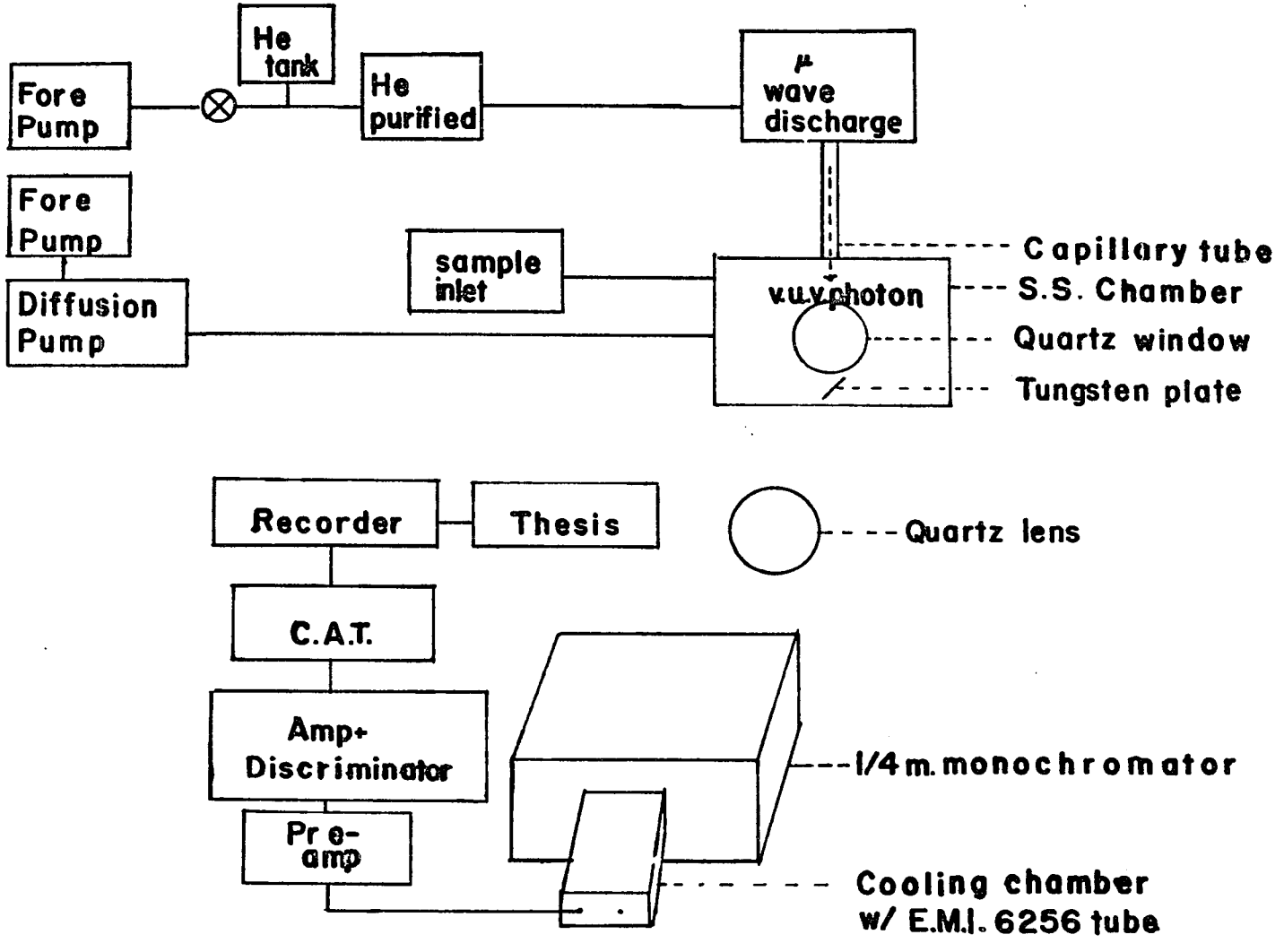

Figure 3A

Scattered Light Spectrum from the
Ionizing Source of the
Fluorescent Photoionization Apparatus
in the 2000-5000Å range.

Reproduced with permission of the copyright owner. Further reproduction prohibited without permission.

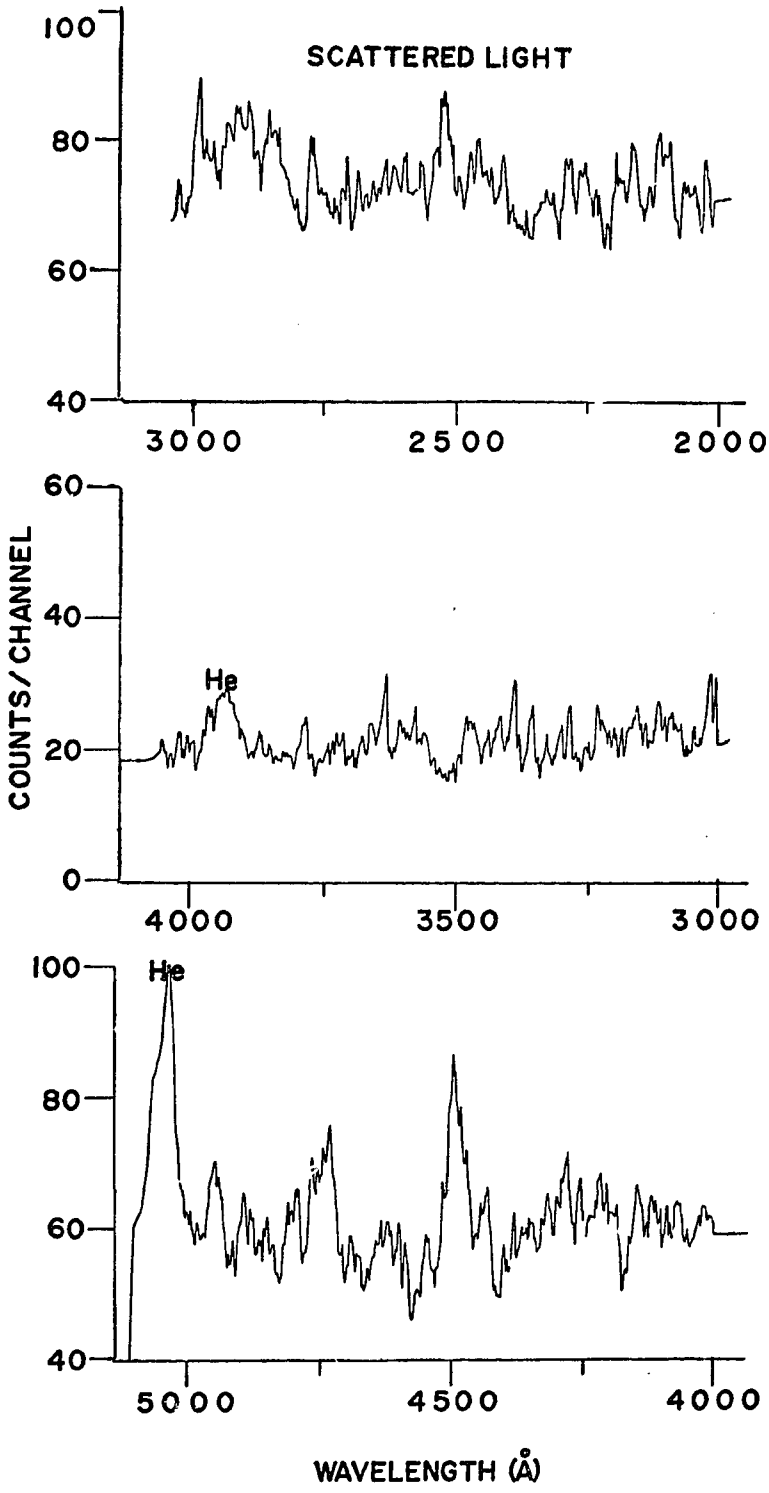

Reproduced with permission of the copyright owner. Further reproduction prohibited without permission.

THEORY

The relative intensities of molecular spectra have been discussed comprehensively by numerous authors.[31] Once a mathematical expression for the intensity of a transition has been derived, a method for relating this expression to experimental observations and a means for calculating Franck-Condon factors is necessary. If the electronic transition moment is assumed to be independent of internuclear distance, the relationship between emission intensity and F.C.F.'s for a diatomic molecule is:

$$I^{em}_{v',v''} = K\nu^3_{v',v''} N_{v'} \bar{R}_e q_{v',v''} \qquad (1)$$

where $I^{em}_{v',v''}$ = Intensity of emission in photons/sec. for the vibronic transition from vibrational state with quantum number(s) v' of the upper electronic state to vibrational state with quantum number(s) v" of the lower electronic state.

$K = (64/3)\Pi^4 h^{-1}$

$\nu_{v',v''}$ = frequency of the transition

$N_{v'}$ = steady state population of the vibrational level v', of the upper electronic state

$\bar{R}_e$ = the electronic transition moment

Reproduced with permission of the copyright owner. Further reproduction prohibited without permission.

$q_{v',v''}$ = F.C.F. for transition i.e. $|\int \psi_{v'}\, \psi_{v''}\, dr\,|^2$ where ψ_v's are vibrational wavefunctions

It can easily be proven that

$$\sum_{v'} q_{v',v''} = \sum_{v''} q_{v',v''} = 1 \qquad (2)$$

because of the complete orthogonality of vibrational states in a single electronic state. Therefore, substituting the second relationship of Eq. (2) into Eq. (1) and rearranging gives

$$N_{v'} = \left(\sum_{v''} I^{em}_{v',v''}/\nu^3_{v',v''}\right) / K\bar{R}_e \qquad (3)$$

Resubstituting in (1) gives

$$I^{em}_{v',v''} = \left(\sum_{v''} I^{em}_{v',v''}/\nu^3_{v',v''}\right)\nu^3_{v',v''} q_{v',v''} \qquad (4)$$

so

$$q_{v',v''} = \left(I^{em}_{v',v''}/\nu^3_{v',v''}\right)/\left(\sum_{v''} I^{em}_{v',v''}/\nu^3_{v',v''}\right) \qquad (5)$$

However, $I^{em}_{v',v''}$ is not the intensity of the signal observed experimentally. The experimentally observed signal can be related to $I^{em}_{v',v''}$ by

Reproduced with permission of the copyright owner. Further reproduction prohibited without permission.

$$I^{em}_{v',v''} \propto M^{em}_{v',v''}/\varepsilon_\nu \qquad (6)$$

where $M^{em}_{v',v''}$ = experimentally observed intensity (integrated area under a spectral peak)

ε_ν = efficiency of optical system at frequency ν

The quantity ε_ν can be determined by using a Black body light source (NBS standard lamp) to calibrate the intrument's efficiency. However, the results of this dissertation were derived by setting $\varepsilon_\nu = (\varepsilon_{p\nu}) \times (\varepsilon_{g\nu})$ where $\varepsilon_{p\nu}$ is the efficiency of the photomultiplier tube at frequency ν and $\varepsilon_{g\nu}$ the efficiency of the grating at frequency ν. Curves defining $\varepsilon_{p\nu}$ and $\varepsilon_{g\nu}$ were obtained from the manufacturers, E.M.I. and Jarrel-Ash respectively. Thus combining (6) and (5) gives

$$q_{v',v''} \propto (M^{em}_{v',v''}/\varepsilon_\nu \nu^3_{v',v''})/(\Sigma_{v''} M^{em}_{v',v''}/\varepsilon_\nu \nu^3_{v',v''}) \qquad (7)$$

This expression can be used to determine F.C.F.'s from the observed intensities of a progression in v". Ratios of F.C.F.'s can also be obtained from the relationship

$$q_{v',v_1''}/q_{v',v_2''} = (M^{em}_{v',v''}/M^{em}_{v',v_2''})(\varepsilon\nu^3_{v',v_2''})/\varepsilon\nu^3_{v',v''} \qquad (8)$$

Reproduced with permission of the copyright owner. Further reproduction prohibited without permission.

The situation is somewhat different for progressions in v'. Note that

$$\sum_{v'} I^{em}_{v',v''}/\nu^3_{v',v''} N_{v'} = K\bar{R}_e \qquad (9)$$

so that

$$q_{v',v''} = (I^{em}_{v',v''}/\nu^3_{v',v''} N_{v'})/(\sum_{v'} I^{em}_{v',v''}/\nu^3_{v',v''} N_{v'}) \qquad (10)$$

The usefulness of Eq. (9) in determining F.C.F.'s for v' progressions depends on whether the $N_{v'}$'s can be determined. If the electron detector of a photoelectron spectrometer was 100% efficient for electrons of any kinetic energy, then the area under a photoelectron spectral peak corresponding to vibronic state v' would be proportional to the rate molecular ions in vibronic state v' are produced. Therefore, ratios of $N_{v'}$'s can be obtained provided three assumptions hold: (1) The transmission of the spectrometer does not vary appreciably with electron kinetic energy, (spectrometers don't have the ideal energy variation calculated from their electron optics. Thus there is no easy way of calibrating spectrometer response); (2) The angular distribution of photoelectrons arising from photoionization to different molecular ion vibronic states

Reproduced with permission of the copyright owner. Further reproduction prohibited without permission.

is the same; (3) No nonradiative processes are occurring. Assumption (2) is necessary because an electron energy analyzer's aperture is much smaller than 4π radians. If a vibrational level, v', undergoes nonradiative as well as radiative decay then the steady state population $N_{v'}$ is not proportional to the population rate, (see discussion relating to Eq. (15)). Thus the necessity of assumption (3).

With the background of the preceding discussion a general procedure for determining F.C.F.'s can now be stated. Obtain F.C.F.'s for all observable progressions in v" using Eq. (7). If a v' progression is "complete," (i.e. none of its members predissociate), use Eq. (10) to calculate F.C.F.'s. If a v' progression is "incomplete," use Eq.(8) to determine relative F.C.F.'s for all the members which do not predissociate. Then if a member of a complete progression is also a member of an incomplete progression, all the relative F.C.F.'s can be normalized by comparison to the normalized F.C.F.'s common to the two progressions.

As can be seen in the foregoing paragraph, the occurrence of predissociation has an important bearing on the computation of F.C.F.'s. A means of detecting predissociation events from spectral data is necessary.

Reproduced with permission of the copyright owner. Further reproduction prohibited without permission.

Three general types of predissociation exist.[32] These are predissociation by rotation, radiationless transition from a rovibronic state into the dissociation continuum of another electronic state, and predissociation by vibration. The first two cases are discussed in great detail by Herzberg and many other authors. Therefore, no further attempt at explanation will be made. The third case occurs only in polyatomic molecules and could use a little illumination. The existence of more than one normal vibration in polyatomics necessitates the use of potential energy surfaces with the normal coordinates as the axes. A cross-section made by a plane cutting through the potential energy surface parallel to the x axis forms a potential energy curve for the x normal vibration with the other vibration coordinates fixed by the intercept of their axes with the plane. This curve's dissociation limit is reached for a finite value of v_x (the quantum number for the x vibration). Assume that a molecule is in a state with v_x vibrational energy which is below the amount needed for dissociation. Also assume that the vibrational energy in another normal mode, y, is also not enough to reach the dissociation limit on its cross-sectional curve. Until now, the validity of the normal mode analysis has been assumed. However, normal mode analysis

Reproduced with permission of the copyright owner. Further reproduction prohibited without permission.

depends on the assumption of a harmonic force field. However for a system to have a dissociation limit, the potential has to be anharmonic, and thus third order or even higher terms are important in the potential energy. The net effect is that some or all of the normal modes are no longer independent, but are weakly coupled to each other,(i.e. energy used to excite a normal mode, v', won't stay completely in that mode. Some energy will be transferred to the other normal modes coupled to v'). If sufficient vibrational energy is transferred from the y to the x mode, dissociation can occur,(i.e. there is enough energy in the system for dissociation). Similarly, if a pair of coupled normal modes have a dissociation limit but not enough energy to reach this limit, energy can also be transferred into the pair to cause predissociation. A quantitative description of this process can be found in many papers on unimolecular decay of polyatomics.[33,34]

Because all predissociation can be considered unimolecular decay, a steady state equation can be written for a vibronic excited state of an ion.

$$0 = dN_{v'}/dt = K_p^{v',\Lambda'}\{x\} - K_r^{v',\Lambda'}N_{v',\Lambda'} - K_n^{v',\Lambda'}N_{v',\Lambda'} \quad (10)$$

where {x} = concentration of the neutral species

Reproduced with permission of the copyright owner. Further reproduction prohibited without permission.

(concentration of gas before ionization)

$N_{v',\Lambda'}$ = steady state concentration of ion in vibrational state v' of electronic state Λ' ($cm.^{-3}$)

$K_p^{v',\Lambda'}$ = rate of production of ions in state Λ',v'. (These can be determined from photoelectron spectroscopy). (ions/sec.)

$K_r^{v',\Lambda'}$ = the radiative transition rate from state Λ',v' ($sec.^{-1}$)

$K_n^{v',\Lambda'}$ = the nonradiative predissociation rate from state Λ',v' ($sec.^{-1}$)

It is commonly known that[35]

$$I_\nu = I_\nu^0 \exp(-\sigma_{v',\Lambda'} N p/760\ 273/T\ \ell). \quad (11)$$

where I_ν = the intensity transmitted/sec. through unit area perpendicular to the photoionizing light at wave number ν

I_ν^0 = initial intensity of light

$\sigma_{v',\Lambda'}$ = partial photoionization cross-section for production of ions in state v',Λ' ($cm.^{-2}$)

ℓ = path length photoionizing light travels through (cm.)

N = Loschmidt's number (number of molecules/unit volume at S.T.P.)

P = pressure of gas (torr)

Reproduced with permission of the copyright owner. Further reproduction prohibited without permission.

T = temperature of gas (K°)

So the number of photons absorbed per second to produce ions in state v',Λ' is

$$K_p^{v',\Lambda'} = (I_\nu^0 - I_\nu) = I_\nu^0[1 - \exp(-\sigma_{v',\Lambda'} N \frac{p}{760} \frac{273}{T} \ell)]. \quad (12)$$

Expansion of the exponential in a Taylor series gives

$$K_p^{v',\Lambda'} = I_\nu^0[-\sigma_{v',\Lambda'} R + \frac{\sigma_{v',\Lambda'}^2 R^2}{2} + \ldots] \quad (13)$$

where $R = N\ p/760\ 273/T\ \ell$.

If the concentration of the neutral gas is small, then

$$K_p^{v',\Lambda'} = I_\nu^0\ \sigma_{v',\Lambda'}\ R. \quad (14)$$

Thus the area under a peak in a photoelectron spectrum is a measure of $\sigma_{v',\Lambda'}$ and therefore of the population rate. Rearranging (10) gives

$$N_{v'} = K_p^{v',\Lambda'}[x] \ / \ K_r^{v',\Lambda'} + K_n^{v',\Lambda'}. \quad (15)$$

(Note that to obtain $N_{v'}$ from partial ionization cross-sections determined from photoelectron spectra

Reproduced with permission of the copyright owner. Further reproduction prohibited without permission.

requires that $K_n = 0$ and either the v' dependence of the radiative decay rate can be determined experimentally or assumed constant), but remembering

$$N_{v'} = C \sum_{v''} M_{v',v''} / \nu^3_{v',v''} \varepsilon_\nu \qquad (16)$$

(C is a constant)

Substituting (16) into (15) gives

$$C \sum_{v''} M_{v',v''}/\nu^3_{v',v''}\varepsilon_\nu = K_p^{v',\Lambda'}[x]/[K_r^{v',\Lambda'} + K_n^{v',\Lambda'}] \; . \qquad (17)$$

The ratio N_1/N_2 is therefore

$$\frac{N_1}{N_2} = \frac{\sum_{v''} M_{1,v'}/\nu_1^3 \varepsilon_\nu}{\sum_{v''} M_{2,v''}/\nu_2^3 \varepsilon_\nu} = \frac{K_p^{(1)} [K_r^{(2)} + K_n^{(2)}]}{K_p^{(2)} [K_r^{(1)} + K_n^{(1)}]} \; . \qquad (18)$$

Assume that vibrational state 2 is predissociated but 1 is not. Then $K_n^{(1)} = 0$ and

$$\frac{N_1}{N_2} = \frac{K_p^{(1)}[K_r^{(2)} + K_n^{(2)}]}{K_p^{(2)}[K_r^{(1)}]} \; . \qquad (19)$$

Reproduced with permission of the copyright owner. Further reproduction prohibited without permission.

Since K_r usually varies only weakly with v', Eq.(19) simplifies to

$$\frac{N_1}{N_2} = \frac{K_p^1}{K_p^2}\left[1 + \frac{K_n^{(2)}}{K_r^{(1)}}\right] = \frac{\sum_{v''} M_{1,v''}/\nu_1^3\,\varepsilon_\nu}{\sum_{v''} M_{2,v''}/\nu_2^3\,\varepsilon_\nu} \qquad (20)$$

Since all the variables can be obtained from photoelectron or emission spectroscopy except $K_n^{(2)}$ and $K_r^{(1)}$, $K_n^{(2)}/K_r^{(1)}$ can be calculated. If this ratio is significant the existence of predissociation has been confirmed. Assuming there is no predissociation in the ground vibrational state of the upper electronic state of a transition, repetitive use of Eq. (20) can determine where and if predissociation occurs in the observed spectrum. Armed with this knowledge, (which might be a dangerous thing), we progress to the discussion of the experimental results.

Reproduced with permission of the copyright owner. Further reproduction prohibited without permission.

HBr^+

The study of HBr^+ began in 1935 when Norling took the first emission spectra of HCl^+ and HBr^+. Since then, a great deal of information has been compiled about HBr^+.[1] From the spectroscopic data, the symmetries for the ground and first excited electronic states, $^2\Pi_{3/2,1/2}$ and $^2\Sigma^+$ respectively have been determined. (Note: $^2\Pi_{3/2,1/2}$ is an inverted multiplet). Since Norling's experiments, many spectra from discharge sources have been taken photographically with high resolution.[2,3,4,5] From these measurements, rotational constants and other spectroscopic parameters, (i.e. γ, q, p, A, D_v), have been determined for the $^2\Pi_{1/2}$ and $_{3/2}$ (v = 0,1,2,3) and $^2\Sigma^+$ (v = 0,1) vibronic states.

Predissociation in the $^2\Sigma^+$ state of HBr^+ was first suspected when peak broadening appeared both in Turner's[6] and Price's[7] photoelectron spectra. This broadening started at v'=4, which suggested that predissociation took place above an energy corresponding to 4 vibrational quanta in the $^2\Sigma^+$ state. Recently Haugh and Bayes[8] have observed HBr^+ emission from an ion impact source; these spectra indicate that predissociation begins at rotational level N'=12 for v'=1 and N'=21 for v'=0. The onset of predissociation

Reproduced with permission of the copyright owner. Further reproduction prohibited without permission.

was discovered by making a plot of $\ell n\ I_{v',v''}^{em}/S_J$ versus E_{rot}. Haugh and Bayes also stated that the predissociating state was $^4\Pi$ and that this $^4\Pi$ state is bound. (A more detailed discussion of this will follow).

Since photoelectron spectra of HBr^+ have been reported in the literature, it is possible to obtain F.C.F.'s for the photoionization process to the $^2\Sigma^+$ state. However, F.C.F.'s for ion-ion transitions have not been tabulated. Although most spectra of HBr^+ have been recorded photographically, making good intensity measurements difficult, some emission has been detected photoelectrically,[8] but no analysis for F.C.F.'s was ever attempted. This lack of intensity information was the stimulus for this investigation.

EXPERIMENTAL RESULTS

Fluorescent Photoionization, N_2^+

Since the emission spectrum of the first negative bands of N_2^+ were taken in the process of aligning the optical system of the fluorescent photoionization apparatus, (see Fig. 4), it seemed expedient to use the v'=0 progression to indicate the accuracy of intensity measurements presented in this thesis. N_2^+ is a particularly convenient standard since F.C.F.'s

Reproduced with permission of the copyright owner. Further reproduction prohibited without permission.

have already been determined theoretically[9] and experimentally.[10] We have calculated both experimental F.C.F.'s from Eq. (7) and theoretical F.C.F.'s from wavefunctions obtained by using Zare's program[11] for numerical integration of the Schroedinger equation. (Morse potentials were assumed for initial and final states, with their parameters determined from the N_2^+ spectroscopic constants reported in Herzberg).[12]

A comparison of our F.C.F.'s with Judge's experimental and Nicholl's theoretical F.C.F.'s, (see Table 1), provides a number of important conclusions: (1) All four sets of F.C.F.'s compare favorably; (2) Theoretical and experimental values agree to ± 10%; (3) Since Nicholls has calculated F.C.F.'s for many molecules which are in good agreement with experimental results, our method of theoretical calculation is probably accurate if Morse potentials can be assumed. The discussion presented for HBr^+ and later for N_2O^+ and CS_2^+ will assume the validity of conclusions (2) and (3).

Fluorescent Photoionization, HBr^+

A fluorescent photoionization spectrum of HBr^+ was taken, (see Fig. 5), to provide F.C.F.'s and predissociation rates. Relative F.C.F.'s for the

Reproduced with permission of the copyright owner. Further reproduction prohibited without permission.

vibrational transitions observed were obtained using Eqs. (7) and (10) of the theory section and are presented in Table 2. In addition, theoretical F.C.F.'s were calculated with Zare's program, using the spectroscopic constants given in Table 3. The results appear in Table 4.

Since no fluorescence was observed from the v'=2 level of the $^2\Sigma^+$ state, the minimum detectable $M_{2,v''}$ for the strongest member of the v'=2 progression, (i.e. the member with the largest theoretical F.C.F.), is equal to the experimental error in determining $M_{1,v''}$. Eq. (10) of the theory section was used to estimate $M_{2,v''}$'s from $M_{2,0}$, (the limiting intensity for the strongest predicted v'=2 transition). Then a value of $K_n^{(2)}/K_r^{(1)} \geq 79$ was obtained from Eq. (20). The result confirms the conclusion of Haugh and Bayes that a radiationless process occurs at $v' \leq 2$.

Predissociation is not the only interesting problem associated with HBr^+. A quick comparison of theoretically and experimentally obtained values for $q_{1,0}/q_{0,0}$ and $q_{0,1}/q_{0,0}$, (see Table 2), reveals a striking incongruity for the latter and a barely satisfactory agreement for the former. Little more can be said about this anomaly from fluorescent photoionization data. Therefore a microwave discharge emission spectrum was taken to increase the accuracy

Reproduced with permission of the copyright owner. Further reproduction prohibited without permission.

of intensity measurements, and to extend the data presently available, and to help determine whether inaccurate rotational constants or perturbation effects are causing the trouble.

Ion Emission, HBr^+

The hardware needed to take a microwave spectrum was easily assembled. A charcoal trap identical to the one described in the experimental section was used to purify helium. A pressure of 0.10 torr of helium was maintained in a quartz 12mm. discharge tube by bleeding helium into a ballast tank while pumping on the entire system with a Welch pump. The HBr was introduced directly into the discharge tube through a needle valve. HBr pressure was maintained at 0.05 torr. Another ballast tank in combination with the needle valve was necessary to prevent fluctuations in HBr pressure. A discharge was struck in the He-HBr mixture with an Evenson microwave cavity. The entrance slit of a 1/2 meter Jarrel-Ash spectrometer was put directly against the slit in the microwave cavity. Dispersed radiation was detected with an EMI 6256S photomultiplier tube connected to a Keithley electrometer. There was sufficient intensity to permit using 0.070mm. slits and taking data in second order giving a resolution

Reproduced with permission of the copyright owner. Further reproduction prohibited without permission.

of 0.56Å which was sufficient to resolve much of the rotational structure. (The HBr spectra obtained are shown in Figs. 6 and 7).

A detailed discussion of the rotational branches which occur in $^2\Sigma$-$^2\Pi$ transitions, and the possible Hund's coupling cases which can occur, appear in Herzberg's Diatomics, pgs. 212-245, 257-264. To facilitate assignment of J values and branch types, a program was written to compute and display on a CRT screen the rotational fine structure of a $^2\Sigma^+$-$^2\Pi_1$ transition in emission, (see Appendix I). Energy expressions used in the program have been discussed by D.A. Ramsay.[13] Hill and Van Vleck[14] have formulated equations for intensities of transitions and Earls[15] has simplified them for the case of $^2\Sigma$-$^2\Pi$ emission and absorption transitions. The line spectrum obtained by combining intensity and energy expressions was convoluted with a triangular slit whose base is equal to the resolution used in the experimental work. This convoluted spectrum is displayed on a CRT and a 35mm. slide is taken. The slide is then put on an enlarger and compared with a graph of the line spectrum before convolution. Thus composite peaks on the slide can be indentified. By a similar process the slide can be compared to the experimental spectrum, and thus all peaks can be classified according to the fully

Reproduced with permission of the copyright owner. Further reproduction prohibited without permission.

resolved lines of which they are composed. The line, computed, and experimental spectra for the 0,0 and 0,1 transitions are compared in Figs. 6 and 7 respectively. A line graph of $\ln I^{em}_{v',v'',J',J''}$ versus E for all non-composite peaks was made, and a rotational temperature of 550°K was obtained, (see Fig. 8).

To obtain a more accurate rotational temperature and F.C.F.'s for the 0-0 and 0-1 transitions, a least squares fit of the computed spectral peak intensities to experimental ones was made by varying T_{rot} and $q_{0,1}/q_{0,0}$. The results obtained using a program written by Dr. Birss at the University of Alberta, Edmonton,[15a] were Temp = 519 ± 20°K and $q_{0,1}/q_{0,0}$ = 0.77_1 ± 0.03. Comparing 0.77_1 with a value of 0.85 ± 0.15 obtained from the photoionization emission experiment confirms the accuracy of the F.C.F. ratio determined from fluorescent photoionization. However, the discrepancy between computer calculated and experimentally obtained ratios for $q_{0,1}/q_{0,0}$ has not been changed at all.

Discussion

The first attempt to explain the discrepancy between the measured and calculated F.C.F. ratios consisted of adding a $K(K + 1)r^2$ potential energy term to the Morse potential used in Zare's program. This

Reproduced with permission of the copyright owner. Further reproduction prohibited without permission.

term corrects for the increasing centrifugal distortion the molecule undergoes as its rotational energy increases. As can be seen from Table 4, the theoretical F.C.F.'s even at K=8 do not vary significantly from the theoretical F.C.F.'s for K=0. Thus, the effect of centrifugal distortion on F.C.F.'s is too small to account for the discrepancy.

The next most obvious path is to check the accuracy of the rotational constants and thus the internuclear separations used in the computation of the Morse potential. A least squares fit was again used to check the values of the rotational constants $B_{v'}$, $B_{v''}$, γ, and $D_{v'}$. Rotational term values measured by Norling[1] and used in Barrow and Caunt's[2] analysis of the 0-0 band were compared to term values calculated using Barrow and Caunt's parameters and the program in Appendix I. Differentials were obtained by the analytical differentiation of the energy expressions. The fit produced the values listed in Table 5. The $B_{v'}$ and $B_{v''}$ lead to values of $r_{e''}$=1.4481 and $r_{e'}$= 1.6848, (these r_e's are obtained from the expressions $B_e=27.9830/I_e$; $I_e=\mu r_e^2$ where μ=reduced mass, and $B_e=B_v + \alpha(v + 1/2)$. Barrow's value of α was used). With these values of $r_{e'}$ and $r_{e''}$, F.C.F.'s were computed using Zare's program. The results of q_{0-0}= 0.192 and q_{0-1}= 0.343 makes the agreement with the

Reproduced with permission of the copyright owner. Further reproduction prohibited without permission.

experimental F.C.F.'s no better than before.

The only parameter which affects the transition energy but hasn't been considered yet, is the spin-coupling constant, A. A change in the coupling constant of only 0.1 from Barrow and Caunt's value produces changes in the transition energy of HBr^+ by 0.06cm.$^{-1}$ for the smallest K's. When transition energies derived with an A=-2651.65 or -2651.55 were used for the least square fit of $B_{v'}$, $B_{v''}$, $D_{v'}$, and γ, the constants in Table 5 were obtained. It is obvious that a small variation in A, 0.007%, causes large variation in spectroscopic constants and in F.C.F.'s. Since A is calculated by taking second differences between 0-0 and 0-1 rotational transitions, (0-1 transitions are accurate to 0.05cm.$^{-1}$), an uncertainty in A of $\pm$ 0.1cm.$^{-1}$ seems quite feasible; this uncertainty, however, is hardly sufficient to rectify the discrepancies in F.C.F.'s.

Morse potentials constructed from accurate spectroscopic constants can lead to theoretical F.C.F.'s which differ significantly from experimental ones for two possible reasons: (1) Morse potentials do not approximate the true potentials even at the bottom of the potential well; (2) An inaccuracy exists in the method used for determining F.C.F.'s from experimental relative intensities. To demonstrate the validity of

Reproduced with permission of the copyright owner. Further reproduction prohibited without permission.

explanation (1), F.C.F.'s were calculated by individually varying both the relative separations, (i.e. $r_{e'} - r_{e''}$), (see Fig. 9), and the shapes of the Morse potentials, (see Fig. 10). Fig 10 illustrates that large variations, (5%), in vibrational constants, and thus in the shape of the Morse potential, do not effect $q_{1,0}/q_{0,0}$ significantly or decrease $q_{0,1}/q_{0,0}$ below 1.00; and Fig. 9 indicates that the experimental values for $q_{0,1}/q_{0,0}$ and $q_{1,0}/q_{0,0}$ cannot be simultaneously duplicated for any value of $r_{e'} - r_{e''}$. Thus explanation (1) is quite plausible.

Implicit in all derivations of the theory section is the assumption that $\bar{R}_e$ is constant with v' or v". Often incongruities between experimentally and theoretically derived relative intensities are attributed to the variation of $\bar{R}_e$ with v' or v" and not to the inaccuracy of theoretically computed $q_{v',v''}$'s.[16] $\bar{R}_e$ is replaced by $R_e(\bar{r}_{v',v''})$ in the expression

$$I^{em}_{v',v''} = N_{v'}\nu^3_{v',v''} R_e(\bar{r}_{v',v''})q_{v',v''} \qquad (1)$$

where $R_e(\bar{r}_{v',v''})$ is the value of the electronic transition moment at $r_{v',v''} = \langle v'|r|v''\rangle$,(this is called the r-centroid approximation). The meaningful determination of $R_e(\bar{r}_{v',v''})$ from Eq. (1) depends strongly on the uncertainties in experimental $I^{em}_{v',v''}$'s

Reproduced with permission of the copyright owner. Further reproduction prohibited without permission.

and theoretical $q_{v',v''}$'s. Zare's[17] comparison of F.C.F.'s calculated from Morse and Rydberg-Klein-Rees potentials showed frequent deviations of 20% and 40%. However, in most cases, including the highly perturbed first positive bands of N_2, $R_e(\bar{r}_{v',v''})$ calculated from R.K.R. potentials showed no appreciable dependence on v' or v". (An exception was the Vegard-Kaplan N_2 bands which showed a variation in $R_e(\bar{r}_{v',v''})$ of over an order of magnitude). James[18] has added to the confusion by suggesting that the r-centroid approximation is invalid for a number of molecular systems and Smith[19] has questioned James' conclusions. Obviously there is considerable disagreement concerning the assumptions necessary for and means of calculating F.C.F.'s and relative intensities. However, a few conclusions can be drawn from the discussion of the preceding two paragraphs. It is almost certain that Morse potentials are not appropriate for HBr^+; the calculation of F.C.F.'s from R.K.R. potentials might rectify the difference in F.C.F.'s of Table 2; finally if use of R.K.R. potentials proves ineffective the r-centroid approximation could correct disagreements of the magnitude observed in HBr^+.

Until now, the discussion has barely touched on the predissociation of the $^2\Sigma^+$ state of HBr^+, because the data presented herein can only confirm the work

Reproduced with permission of the copyright owner. Further reproduction prohibited without permission.

of other investigators. However, a careful reading of the literature on HBr^+ has suggested important facts which have a direct bearing on the anomolous intensity ratios. The main experimental observations pertaining to predissociation which have already been mentioned in this chapter are: (1) Haugh and Bayes' experiments show a sudden break-off in rotational lines for the 1-0 transition at N=13 and a gradual break-off for the 0-0 transition starting at N=21 and ending at N=23; (2) Our experiments indicate no fluorescence from the v'=2 vibrational level of the $^2\Sigma^+$ state; (3) The dissociation energy for the $^2\Pi_{3/2}$ state, calculated from the limiting curve of predissociation, closely corresponds to results obtained thermochemically.[8]

Turner's work has added an additional two observations: (4) Vibrational levels up to v'=4 of the $^2\Sigma^+$ state are observed in the photoelectron spectra, (level v'=4 and possibly v'=3 are broadened);[6] (5) The Birge-Sponer plot made from photoelectron data shows an unusual behavior.[20] To characterize this unusual behavior a photoelectron spectrum of HBr was taken, (see Fig. 11), on a Perkin-Elmer PS 16 photoelectron spectrometer. HBr obtained from Matheson was used without further purification. Calibration of the energy scale was done by taking the O_2 spectrum as a standard. Then a Birge-Sponer plot was made for the

Reproduced with permission of the copyright owner. Further reproduction prohibited without permission.

first six vibrational peaks of the $^2\Sigma^+$ state of HBr^+, (see Fig. 12). Although many Birge-Sponer plots deviate from linearity, few exhibit such a radical shape. As discussed in the introduction, observation (4) suggests that predissociation rates are approaching 10^{+14} sec.$^{-1}$ at v'=4. Observation (5) indicates the predissociating state, (i.e. the state causing the predissociation of the $^2\Sigma^+$ v'=4 level), produces a strong perturbation which disturbs the usually weak departures from harmonic vibration embodied in a linear Birge-Sponer plot.

Since band broadening in the photoelectron spectrum does not start until v'=4, observations (1) and (2) are necessary for an understanding of the predissociating state's effect on less energetic vibronic levels. The gradual disappearance of spectral lines for the 0-0 transition indicates that predissociation rates are increasing only gradually with increasing K. The sudden break in the 1-0 transition at K=21 suggests that the predissociation rate has increased to approximately 10^{+7} sec.$^{-1}$, (since the radiative lifetime of the $^2\Sigma^+$ state has not been measured yet, the preceding value is just an estimate), and observation (2) fixes the predissociation rate at $> 8 \times 10^{+9}$ sec.$^{-1}$ for the v'=2 level.

A full consideration of the potential energy curves and energetics involved would help to elucidate and

Reproduced with permission of the copyright owner. Further reproduction prohibited without permission.

to expand on the preceding claims. The six lowest lying states of the separated atoms are: $H(^2S_{3/2}) + Br^+(^3P_2)$, $H(^2S_{1/2}) + Br^+(^3P_1)$, $H(^2S_{1/2}) + Br^+(^3P_0)$, $H(^2S_{1/2}) + Br^+(^1D_2)$, $H^+(^1S_0) + Br(^2P_{3/2})$, and $H^+(^1S_0) + Br(^2P_{1/2})$. Their correlation to molecular state symmetry and their energy relative to these molecular states have been discussed by Haugh.[21] In Fig. 13 the $^2\Sigma^+$ and $^2\Pi$ potential energy curves have added to Haugh's correlation diagram. The v'=4 level of the $^2\Sigma^+$ state is obviously much less energetic than the $H(^2S_{1/2}) + Br^+(^1D_2)$ dissociation continuum. Thus the significant broadening in the v'=4 level of the photoelectron spectrum can only be explained by predissociation. The sudden increase of the predissociation rate from 10^{+9} sec.$^{-1}$ in the v'=2 level to 10^{+14} sec.$^{-1}$ in the v'=4 level and the large perturbation inferred from observation (5) indicates that a curve crossing occurs around the v'=4 level and that this curve crossing produces a potential maximum. (Haugh has shown with symmetry arguments that the $^4\Pi$ state is the predissociating one).[21] Paradoxically, the predissociation rate is appreciable at v'=0, K=23 and does increase gradually with K. However, if the potential barrier formed by the curve crossing is narrow, tunneling processes could account for both the significant size and gradual increase of predissociation at low v'. Fig. 14 illustrates the relative positions

Reproduced with permission of the copyright owner. Further reproduction prohibited without permission.

of the potential curves with no interaction and Fig. 15 shows the resultant perturbed potential curves.

There is a possibility of another perturbation to the $A^2\Sigma^+$ state. The energy separation of the $H^+(^1S_0)$ + $Br(^3P)$ and $H(^2S_{1/2})$ + $Br^+(^1D_2)$ dissociation products is much less than lev. It is quite possible that the $A^2\Sigma^+$ state wants to dissociate into $H^+(^1S_0)$ + $Br(^2P)$ and the $B^2\Sigma^+$ state into $H(^2S_{1/2})$ + $Br^+(^1D_2)$. Thus there would be an avoided crossing which would perturb the $A^2\Sigma^+$ state within lev. of the dissociation limit. Although this perturbation certainly couldn't effect the v'=0, 1 or 2 vibronic levels it could contribute to the eccentricities of the Birge-Sponer plot around v'=5.

Haugh's conclusion that the $^4\Pi$ state is bound and his calculation of a dissociation energy for the $^2\Pi_1$ state relies on the assumption that predissociation at or above a curve crossing is the only radiationless process occurring and that a limiting curve of dissociation can be drawn, (i.e. that dissociation does not start until the energy of the curve crossing is reached and that once it starts it is complete). If predissociation by tunneling is indeed the dominating process neither assumption is valid. The agreement of Haugh's calculated dissociation energy with the thermochemical value is probably due to tunneling fortuitously dominating fluorescence at a rovibronic

Reproduced with permission of the copyright owner. Further reproduction prohibited without permission.

energy correpsonding to the dissociation energy of the $^2\Pi$ state.

It would seem that the tunneling model explains the experimental observations better than straight predissociation. However, so far no quantitative evidence has been presented to confirm the existence of tunneling. Since tunneling depends totally on perturbations of potential energy curves to produce potential barriers, it is necessary to prove the presence of these perturbations. Hopefully, any demonstration of perturbations will also help to explain the anomolies in the F.C.F.'s.

The rotational energy of a state can be represented by $F_i(J) = B_vJ(J+1) + D_v(J+1)^2+...+\Phi_i(J)$. The term $\Phi_i(J)$ is caused by perturbation of a rovibronic level by another electronic state or states. When rotational constants are calculated the coefficient of the J(J+1) term in the rotational energy expression is taken as B_v. Yet the calculated $B_v^{eff} = \delta_i + B_v^{true}$ where B_v^{true} is the rotational constant needed for determining equilibrium internuclear distances. Since B_v^{eff}'s are used to calculate r_e's, a relatively large value of δ_i can strongly affect the accuracy of r_e which in turn affects the calculated F.C.F.'s irrespective of the assumed potential. As demonstrated by the dependence of Morse F.C.F.'s on $r_{e'} - r_{e''}$, a shift in $r_{e'}$ probably

Reproduced with permission of the copyright owner. Further reproduction prohibited without permission.

will not entirely correct the intensity anomoly, but the use of inaccurate r_e's in constructing any potential will almost certainly prevent solution of the relative intensity problem.

The detection of perturbations and their effect on B_v is quite important. However, implicit in any method of detection is a good theoretical framework to which experiments can be fitted. Presently construction of an expression for the energy of a rovibronic level which is highly perturbed involves many approximations. Therefore, the uncertainty in energy measurements or intensity measurements, (which are usually more sensitive to perturbations), combined with the uncertainty of the theoretical model makes it extremely difficult to obtain B_v^{true}, thus r_e^{true}, instead of B_v^{eff} or r_e^{eff}.

The conclusions of this chapter can now be summarized as follows. There are probably strong perturbations which produce a potential maximum in the $A^2\Sigma^+$ state. Tunneling is probably the nonradiative process which is dominant below the $v'=4$ or 3 level. There is an anomoly between experimental and theoretical relative intensities which is much greater than experimental error. These conclusions indicate that the investigation of HBr^+ has just started. A possible battle order of research on HBr^+ could be: (1) Molecular ion emission spectra should be taken to obtain relative

Reproduced with permission of the copyright owner. Further reproduction prohibited without permission.

intensities for as many bands as possible. The more complete the set of relative intensities, the easier it will be to define and study the nature of the problem; (2) F.C.F.'s should be calculated from R.K.R. potentials for all observed vibronic bands; (3) If R.K.R. F.C.F.'s do not agree with experimental F.C.F.'s r-centroid electronic transition moments should be obtained either by computer calculation or by the graphical method. Then experimental relative intensities should be compared to theoretical ones calculated from R.K.R. F.C.F.'s and r-centroid transition moments. If there is still no agreement, the presence of perturbations in HBr^+ probably makes the R.K.R. potential model inapplicable and/or produces an r_e^{eff} significantly different from r_e^{true} ; (4) In any case, a fluorescent photoionization spectrum of DBr^+ should be taken. Isotopic substitution does not affect the potential but does decrease any tunneling rate and the vibrational energy spacing. If $K_n^{v'}/K_r^{v'-1}$ shows a smaller dependence on v' than in HBr the presence of tunneling and of strong perturbations is proven; (5) Once proof of a perturbation is established and if theoretical and experimental intensities still do not coincide, a method of discovering r_e^{true} must be developed or an a priori SCF calculation attempted.

Reproduced with permission of the copyright owner. Further reproduction prohibited without permission.

TABLE 1

N_2^+ F.C.F.'s: Theoretical and Experimental

Transition $N_2^+ \ ^2\Sigma_u^+ \rightarrow \ ^2\Sigma_g^+$	Judge Experimental	Nicholls Theoretical	Schneider Experimental	Schneider Theoretical
0-0	.57 ± .04	.66	.62 ± .03	.68
0-1	.30 ± .04	.25	.24 ± .03	.25
0-2	.10 ± .06	.06	.08 ± .03	.06

Reproduced with permission of the copyright owner. Further reproduction prohibited without permission.

Reproduced with permission of the copyright owner. Further reproduction prohibited without permission.

TABLE 2

HBr^+ F.C.F.'s: Experimental and Theoretical

$HBr^+ {}^2\Sigma^+ \rightarrow {}^2\Pi_{3/2}$ v'	v"	F.C.F.'s Experimental $q_{v',v"}$ (arb. units)	Ratios of F.C.F.'s Experimental $q_{v',v"}/q_{0,0}$	Theoretical $q_{v',v"}/q_{0,0}$
0	0	2.1 ± .2	1.0	1.0
1	0	2.4 ± .3*	1.14 ± .24*	1.33
0	1	1.8 ± .2	0.86 ± .15	1.79
$HBr^+ {}^2\Sigma^+ \rightarrow {}^2\Pi_{3/2}$				
0	0	2.6 ± .2	1.0	1.0
1	0	3.0 ± .4*	1.15 ± .25*	1.33
0	1	——****	——**	——**

* The value of $N_1/N_0 = 2.3$ obtained from P.E. spectrum was used to obtain this value

** The 0-1 transition for the $^2\Sigma^+ \rightarrow {}^2\Pi_{1/2}$ system was covered by the 3889Å He line.

TABLE 3

Spectroscopic Constants for HBr^+*

	Upper State $^2\Sigma^+$	Lower State $^2\Pi_i$
B_0	5.8464	7.9538
B_e	5.9702	8.0720
D_0	4.293×10^{-4}	3.477×10^{-4}
r_e	1.684Å	1.448Å
α	0.2476	0.2363
γ_0	2.105	———
p_0	———	2.070
q	———	-0.01
A	———	-2651.65
ω_e	1407	2445.6
$\omega_e x_e$	48 ± 6	48.6

*unless noted units are in $cm.^{-1}$

Reproduced with permission of the copyright owner. Further reproduction prohibited without permission.

TABLE 4

Theoretically Computed F.C.F.'s

Transitions v' v"	F.C.F.'s K=0 (Schneider)	F.C.F.'s K=0 (Haugh)	F.C.F.'s K=8 (Schneider)
0-0	.204	.207	.187
0-1	.349	.351	.341
0-2	.276	.274	.282
1-0	.273	.277	.251
2-0	.220	.220	—
2-1	.005	.004	—
2-2	.150	.152	—

Reproduced with permission of the copyright owner. Further reproduction prohibited without permission.

TABLE 5

Rotational Constants and Equilibrium Internuclear Distances Obtained from Least Square Fit of Ion Emission Spectra

	$^2\Pi_{3/2}$ A=-2651.65	$^2\Pi_{3/2}$ A=-2651.55	$^2\Pi_{1/2}$ A=-2651.65
B_0'	5.8398	5.8462	5.8479
B_0''	7.9444	7.9457	7.9641
B_e'	5.9636	5.9700	5.9717
B_e''	8.06255	8.06385	8.08225
B_{etrue}''	8.07147	8.0728	8.09211
r_e'	1.6848	1.6838	1.6836
r_e''	1.4481	1.4480	1.4463
Std. Dev. of line fit	.106	0.092	0.113
F.C.F.'s computed for rotational level K=5 with above r_e' and r_e''			
0-0	.19151	.19403	.19025
0-1	.34351	.34472	.34289
0-2	.28036	.27910	.28099
1-0	.25416	.25592	.25327
1-1	.08339	.08139	.08493
1-2	.02346	.02499	.02271

Reproduced with permission of the copyright owner. Further reproduction prohibited without permission.

Figure 4

Fluorescent Photoionization Spectrum of N_2^+ First Negative Bands; 500μ Slits, 18Å FWHM, 2 Runs, 150μ N_2 Pressure.

Reproduced with permission of the copyright owner. Further reproduction prohibited without permission.

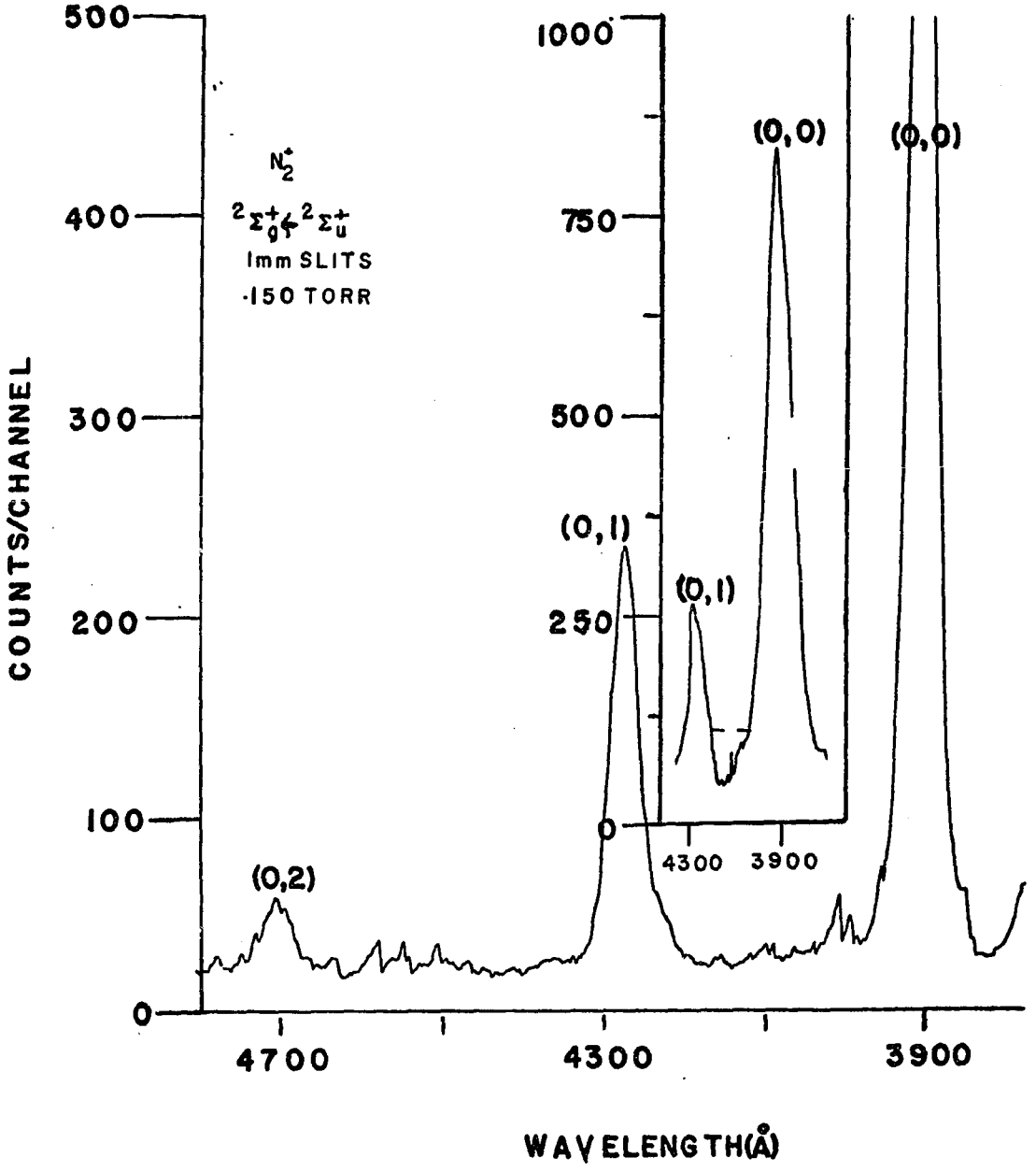

Reproduced with permission of the copyright owner. Further reproduction prohibited without permission.

Figure 5

Fluorescent Photoionization Spectrum of the $HBr^+ \ ^2\Sigma^+ \rightarrow \ ^2\Pi_{1/2,3/2}$ Transition in the 3000Å - 4000Å Region; 500μ Slits, 18Å FWHM, 2 Runs, 100μ HBr Pressure.

Reproduced with permission of the copyright owner. Further reproduction prohibited without permission.

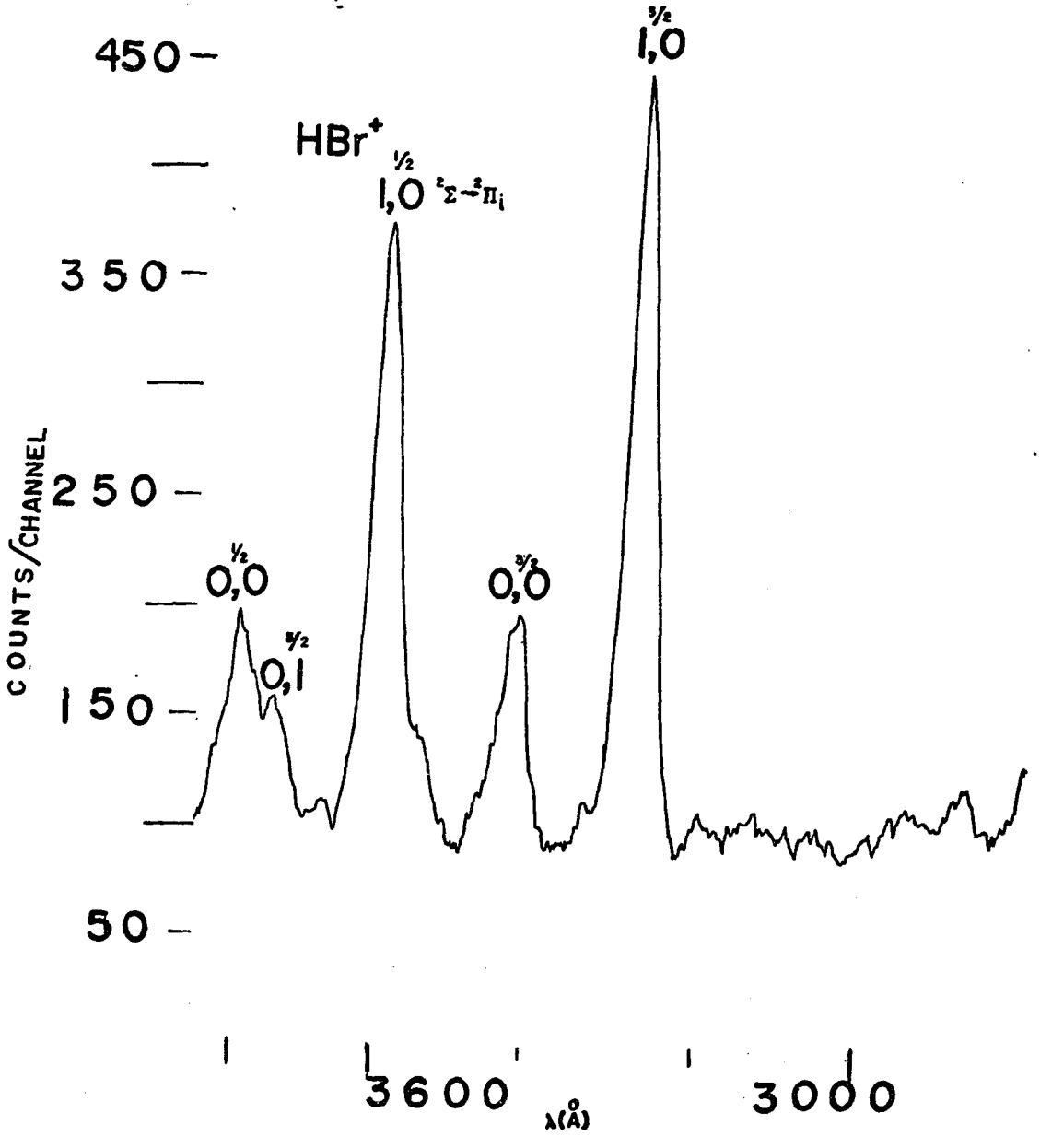

Reproduced with permission of the copyright owner. Further reproduction prohibited without permission.

Figure 6

Ion Emission Computed Line and Convoluted Line Spectra of the $HBr^+ \ ^2\Sigma^+_{v'=0} \rightarrow \ ^2\Pi_{3/2 \ v''=0}$ Rovibronic Transitions. Experimental Conditions for the Ion Emission Spectra were: 50μ HBr Pressure, 40 Watt Microwave Power, 900v on Photomultiplier Tube, 1000μ He Pressure.

Reproduced with permission of the copyright owner. Further reproduction prohibited without permission.

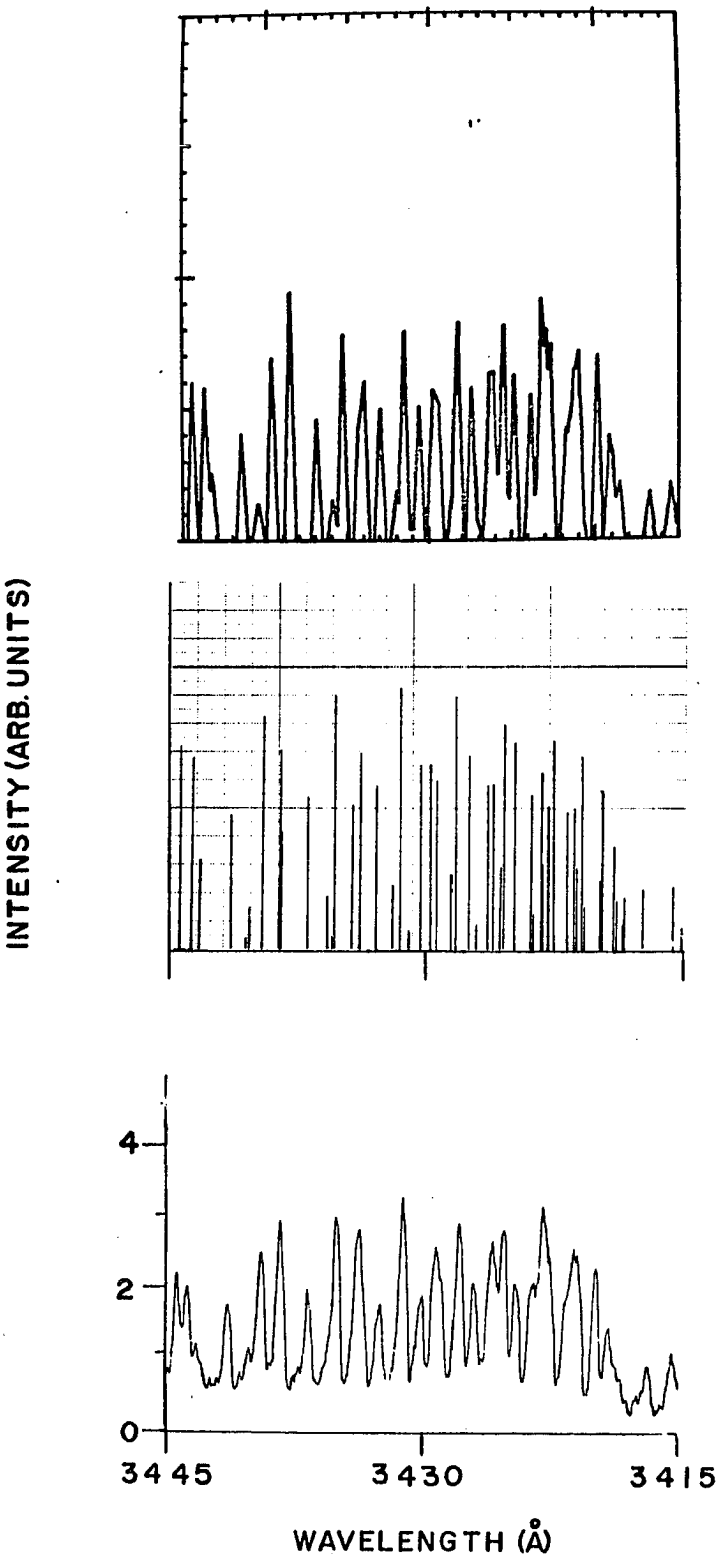

Reproduced with permission of the copyright owner. Further reproduction prohibited without permission.

Figure 7

Ion Emission Computed Line and Convoluted Line Spectra of the $HBr^+ \ ^2\Sigma^+_{v'=0} \rightarrow \ ^2\Pi_{3/2} \ v''=1$ Rovibronic Transitions. Experimental Conditions For the Ion Emission Spectra were: 50μ HBr Pressure, 40 Watt Microwave Power, 900v on Photomultiplier Tube, 1000μ He Pressure.

Reproduced with permission of the copyright owner. Further reproduction prohibited without permission.

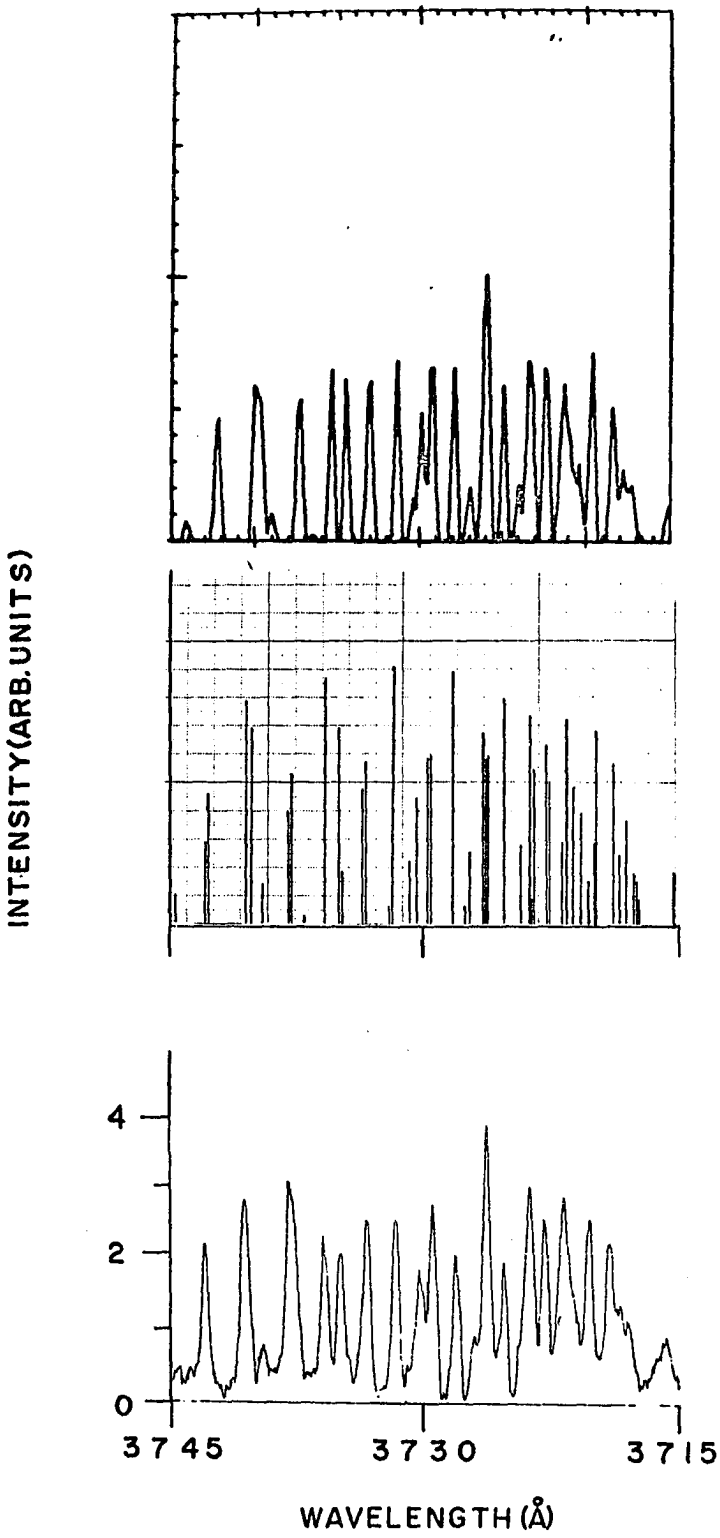

Reproduced with permission of the copyright owner. Further reproduction prohibited without permission.

Figure 8

Plot of Rotatioanl Energy versus I/S_j. Plot of all Non-Composite Rotational Lines of the HBr^+ $^2\Sigma^+_{v'=0} \rightarrow {}^2\Pi_{3/2v''=0}$ Band.

Reproduced with permission of the copyright owner. Further reproduction prohibited without permission.

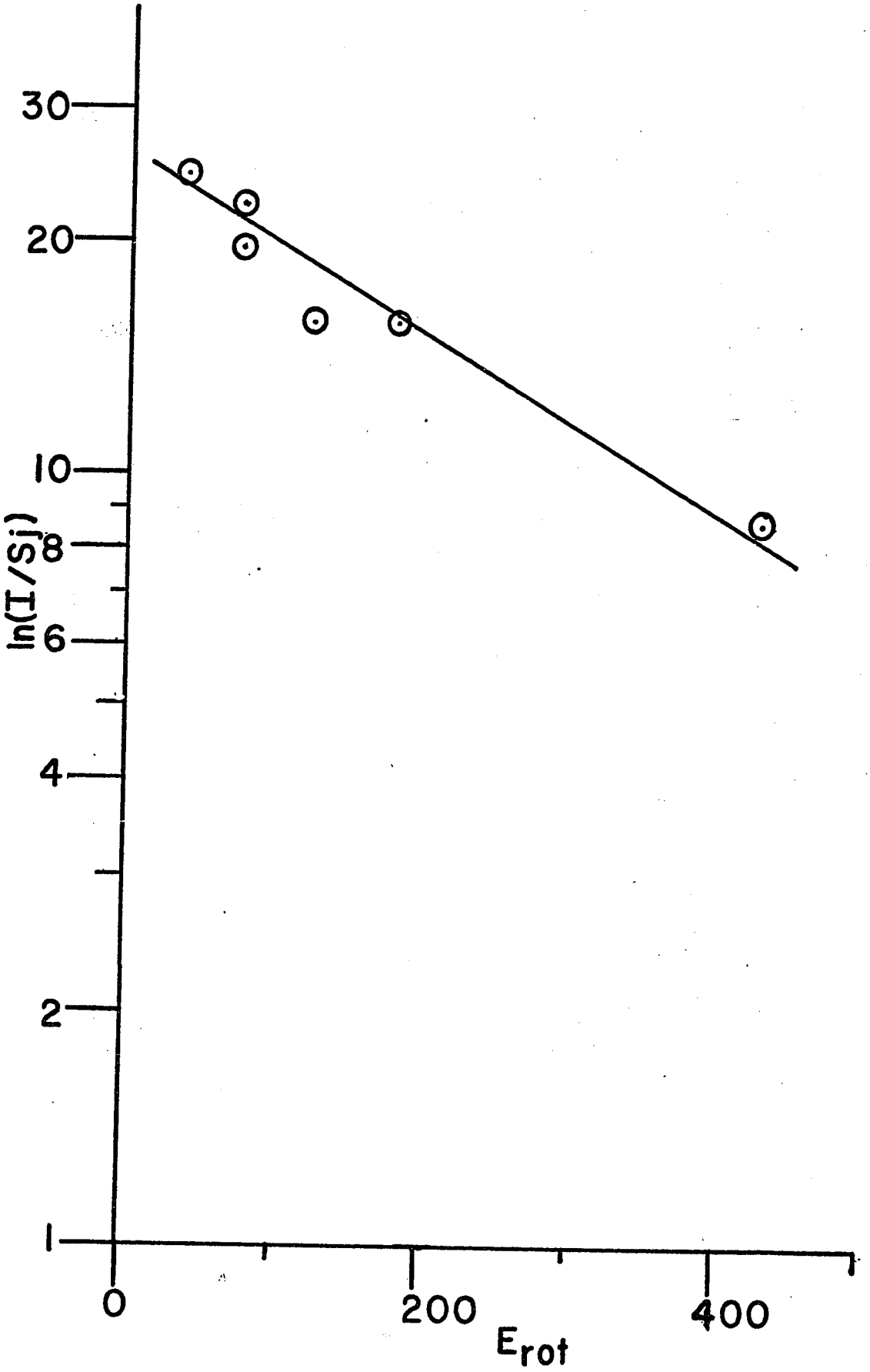

Reproduced with permission of the copyright owner. Further reproduction prohibited without permission.

Figure 9

Plot of $r_e'-r_e''$ versus $q_{0,1}/q_{0,0}$ (X) and $q_{1,0}/q_{0,0}$ (•). The Vertically Shaded Region Indicates the Value of $q_{1,0}/q_{0,0}$ Obtained from Fluorescent Photoionization Data and the Inherent Experimental Uncertainty. Similarly the Diagonal Shaded Region Indicates the Experimental $q_{1,0}/q_{0,0}$ Value.

Reproduced with permission of the copyright owner. Further reproduction prohibited without permission.

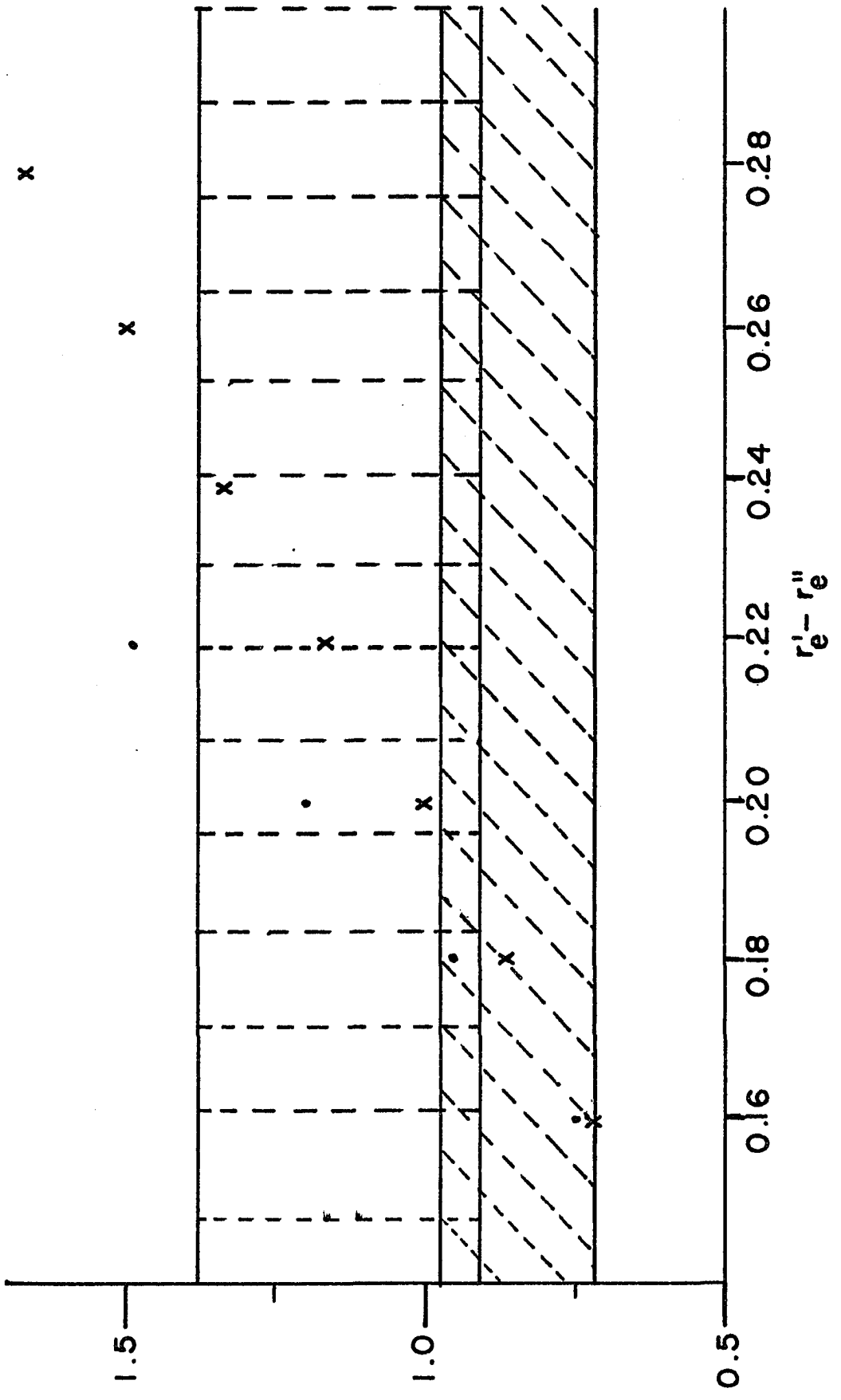

Reproduced with permission of the copyright owner. Further reproduction prohibited without permission.

Figure 10

Plot of Theoretically Calculated Values of $q_{0,1}/q_{0,0}$ (⊡) and $q_{1,0}/q_{0,0}$ (⊙) Versus Vibrational Constants used in the Computation. The Upper Row of Numbers Along the x Axis Indicates the Percentage Difference from Accepted Spectroscopic Vibrational Constants of both ω_e' and ω_e'' used in the Calculation. The Lower Row Indicates the Percentage Change in both $\omega_e x_e'$ and $\omega_e x_e''$.

(i.e. since $\omega_e'=1407$, $\omega_e''=2445$, $\omega_e x_e'=48.6$, $\omega_e x_e''=48$ are the accepted spectroscopic constants an entry along the x axis of $\overset{+10}{+50}$ would indicate the values $\omega_e'=1547$, $\omega_e''=2689$, $\omega_e x_e'=72$, $\omega_e x_e''=72$ were used in the calculation of $q_{0,1}/q_{0,0}$ and $q_{1,0}/q_{0,0}$). Note the experimentally obtained value for $q_{0,1}/q_{0,0}=.86 \pm .15$, and that no reasonable combination of vibrational spectroscopic constants yields this value.

Reproduced with permission of the copyright owner. Further reproduction prohibited without permission.

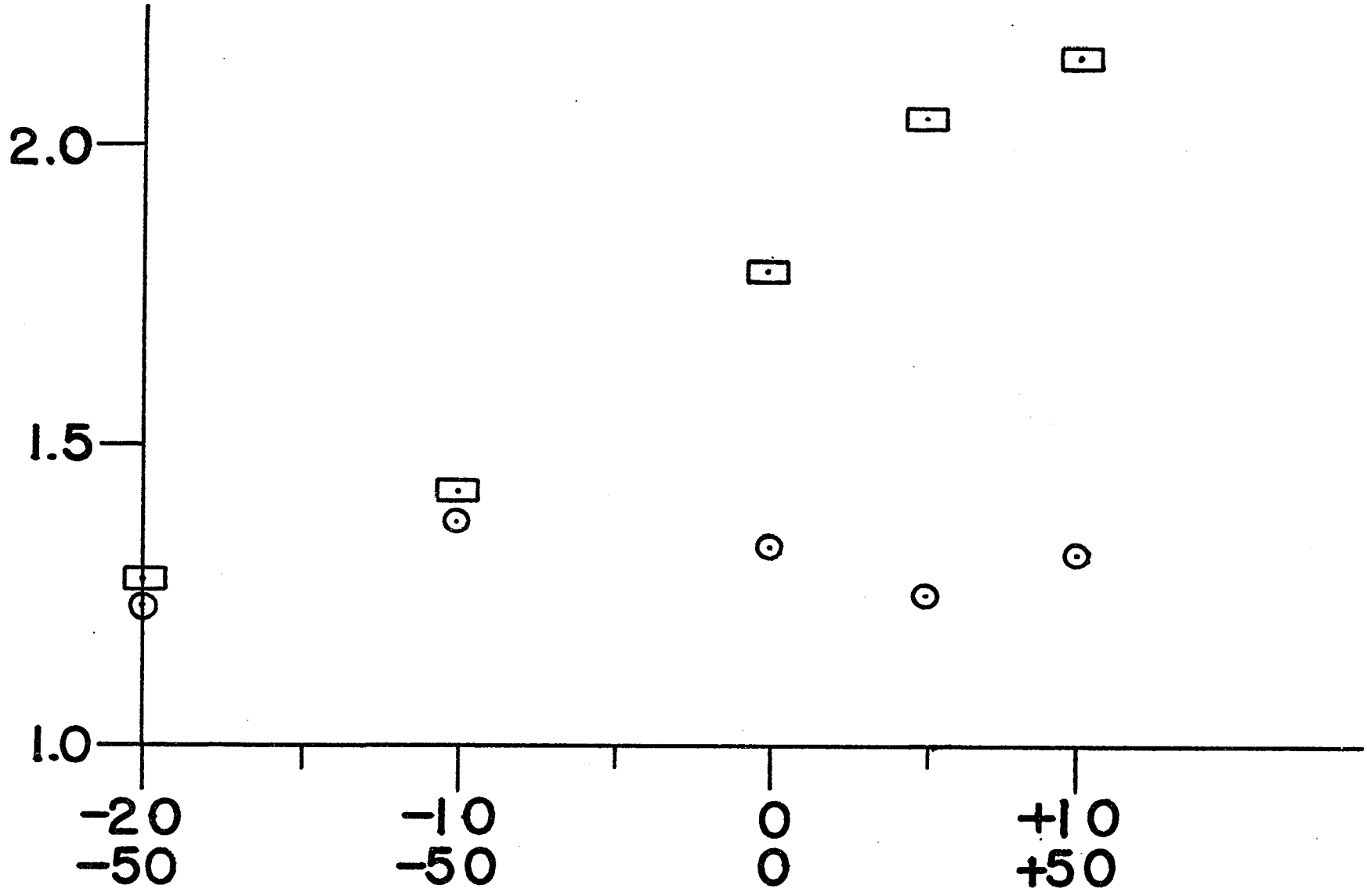

Reproduced with permission of the copyright owner. Further reproduction prohibited without permission.

Figure 11

Photoelectron Spectrum of the HBr in the Energy Range Corresponding to Ionization into $HBr^+ \ ^2\Sigma^+$ Vibronic States.

Reproduced with permission of the copyright owner. Further reproduction prohibited without permission.

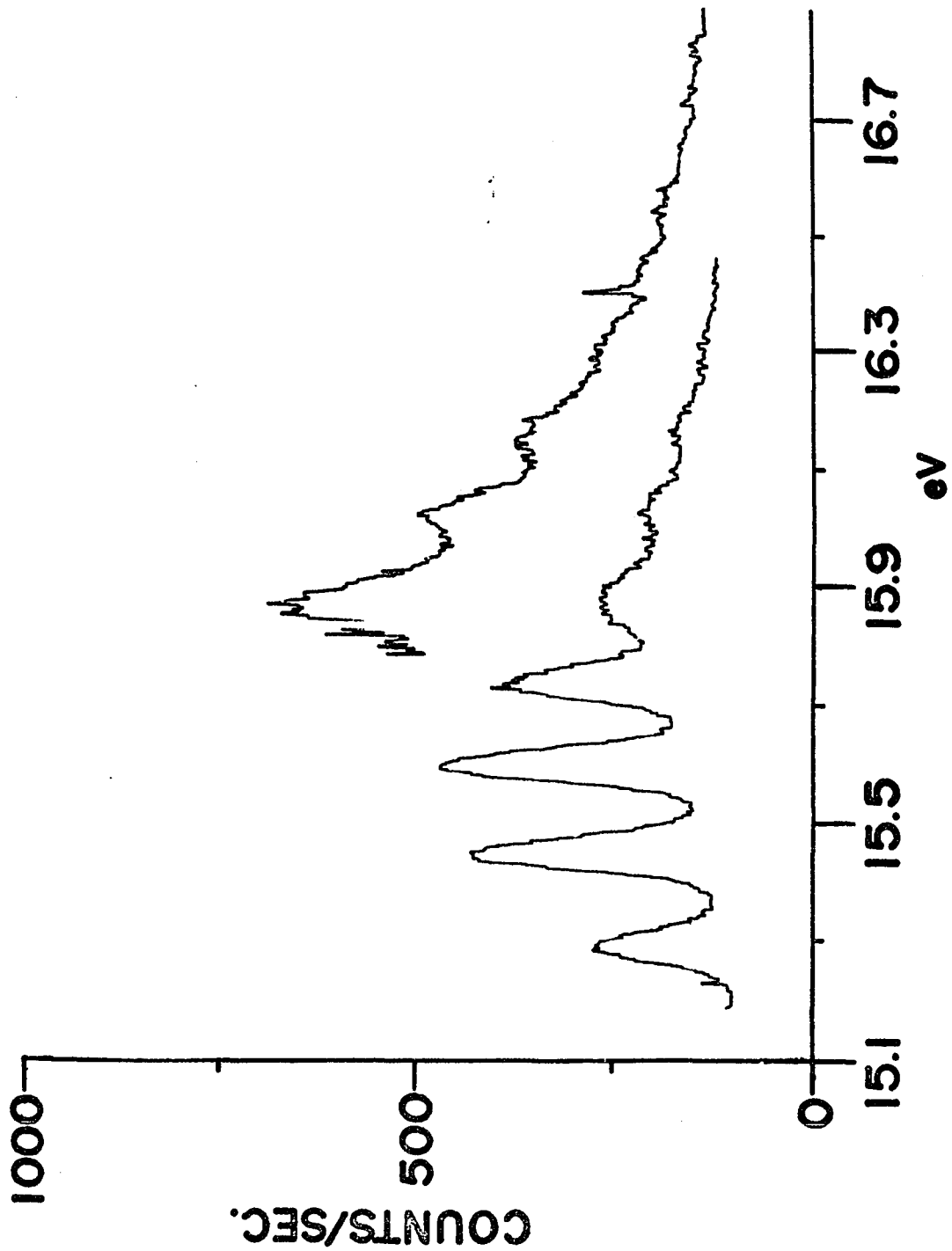

Reproduced with permission of the copyright owner. Further reproduction prohibited without permission.

Figure 12

Birge-Sponer Plot Derived from the Photoelectron Spectrum in Fig. 11.

Reproduced with permission of the copyright owner. Further reproduction prohibited without permission.

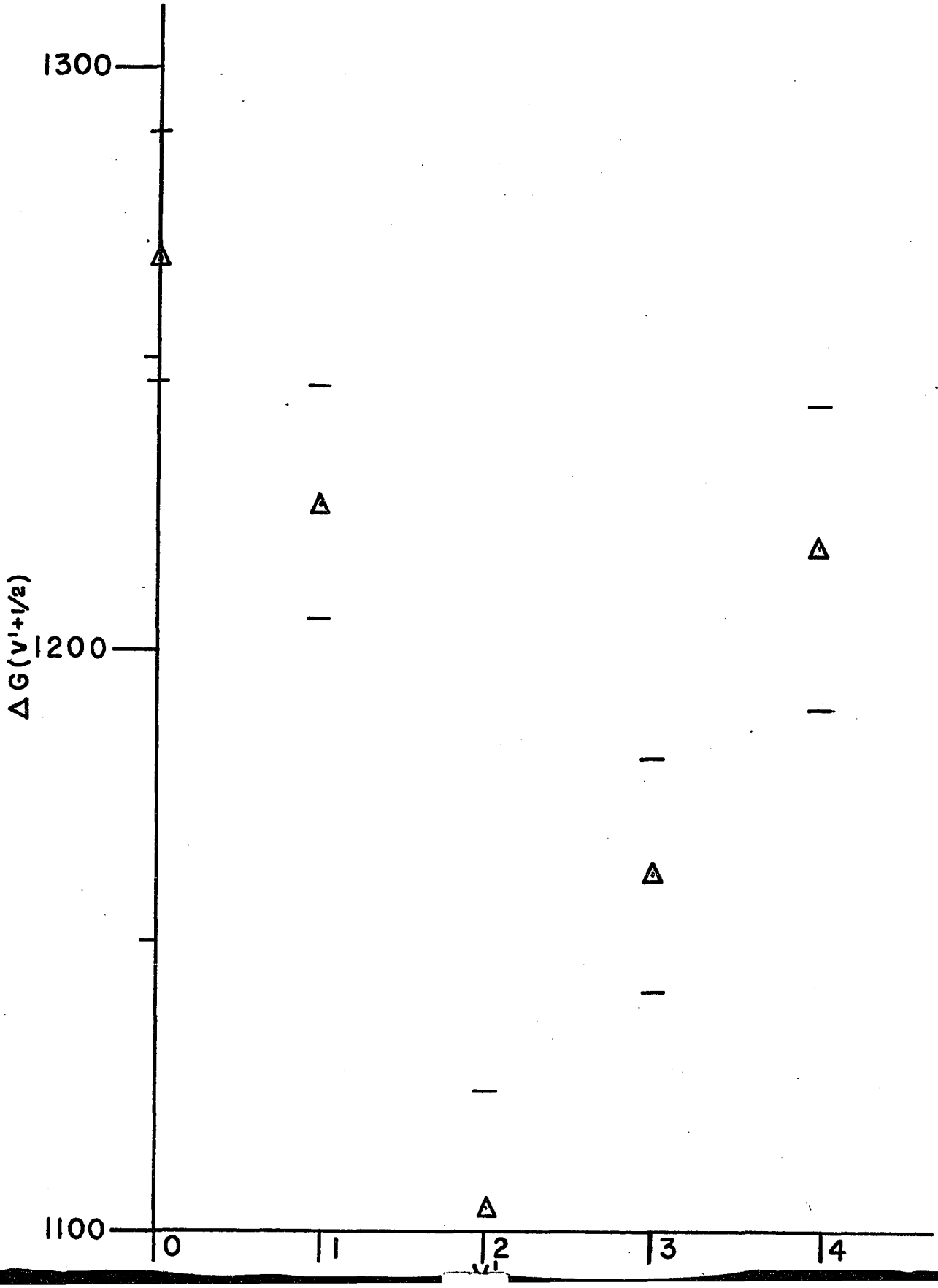

Reproduced with permission of the copyright owner. Further reproduction prohibited without permission.

Figure 13

Relative Positions of $\tilde{A}\ ^2\Sigma^+$ and

$X\ ^2\Pi$ Potential Energy Curves.

Reproduced with permission of the copyright owner. Further reproduction prohibited without permission.

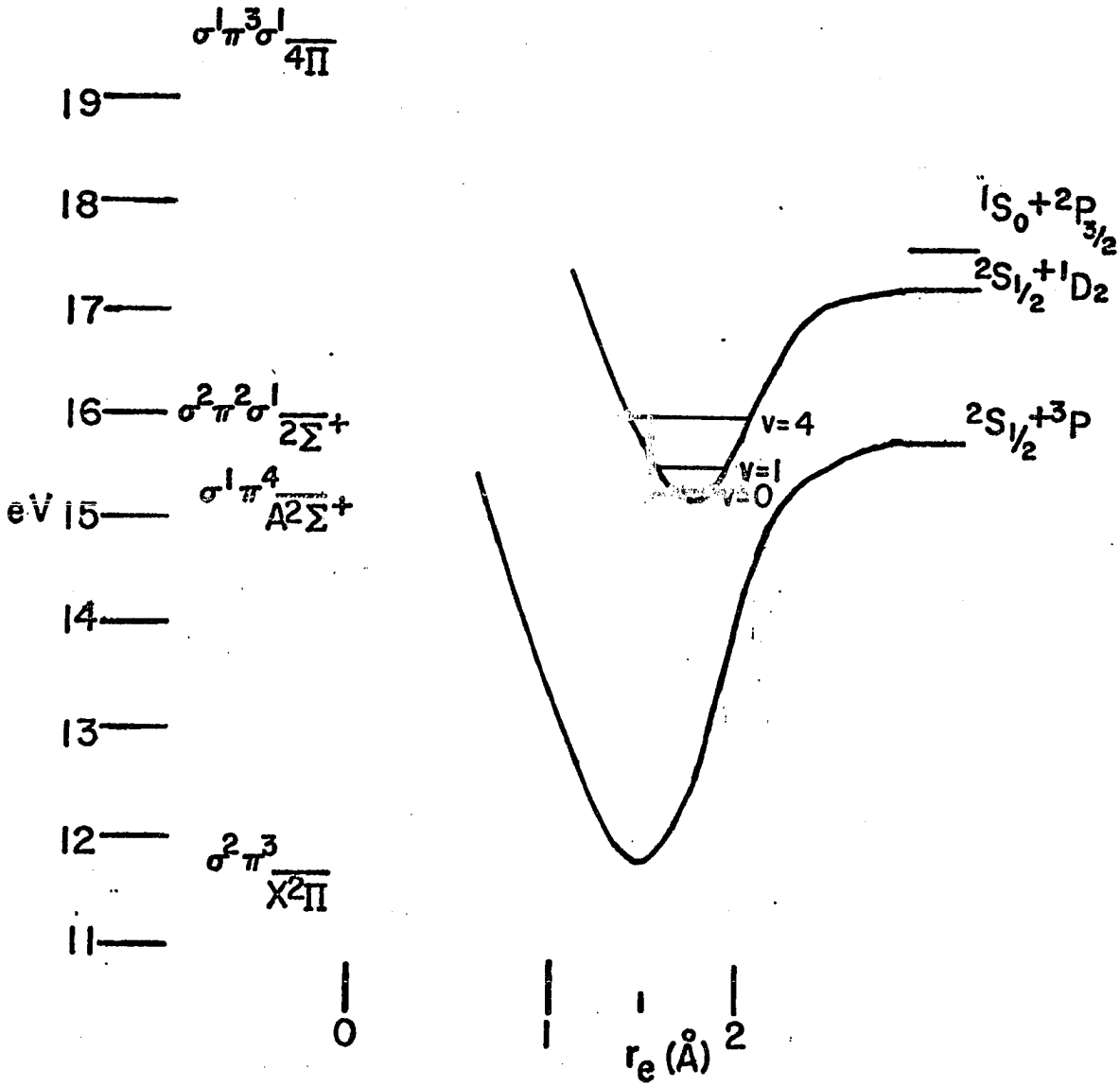

Reproduced with permission of the copyright owner. Further reproduction prohibited without permission.

Figure 14

Diagram Showing all Possible Curve Crossings in HBr^+ Without Consideration to Interaction Between States.

Reproduced with permission of the copyright owner. Further reproduction prohibited without permission.

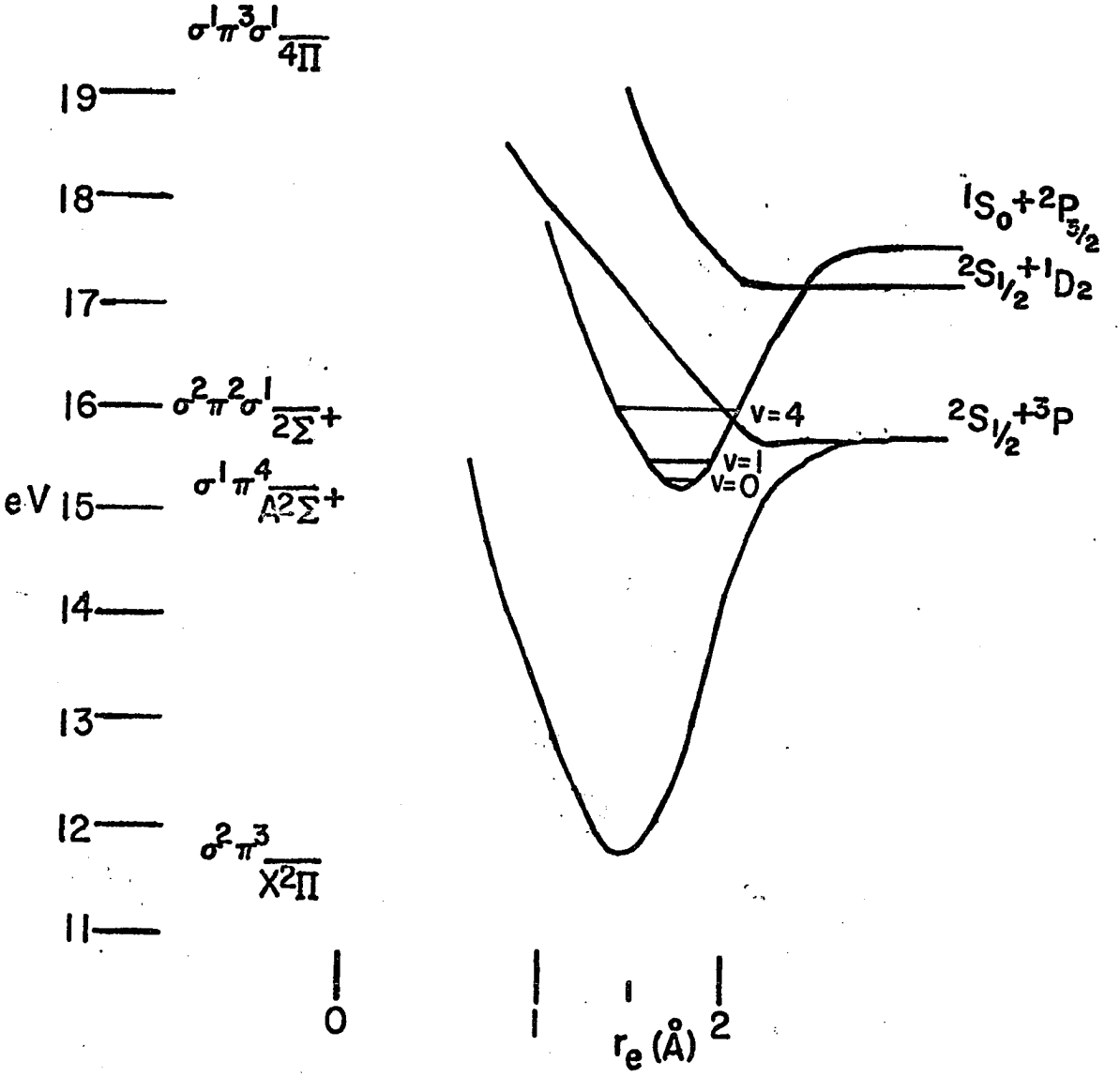

Reproduced with permission of the copyright owner. Further reproduction prohibited without permission.

Figure 15

Diagram Showing Resultant Potential Energy Curves When Interactions Between States are Considered.

Reproduced with permission of the copyright owner. Further reproduction prohibited without permission.

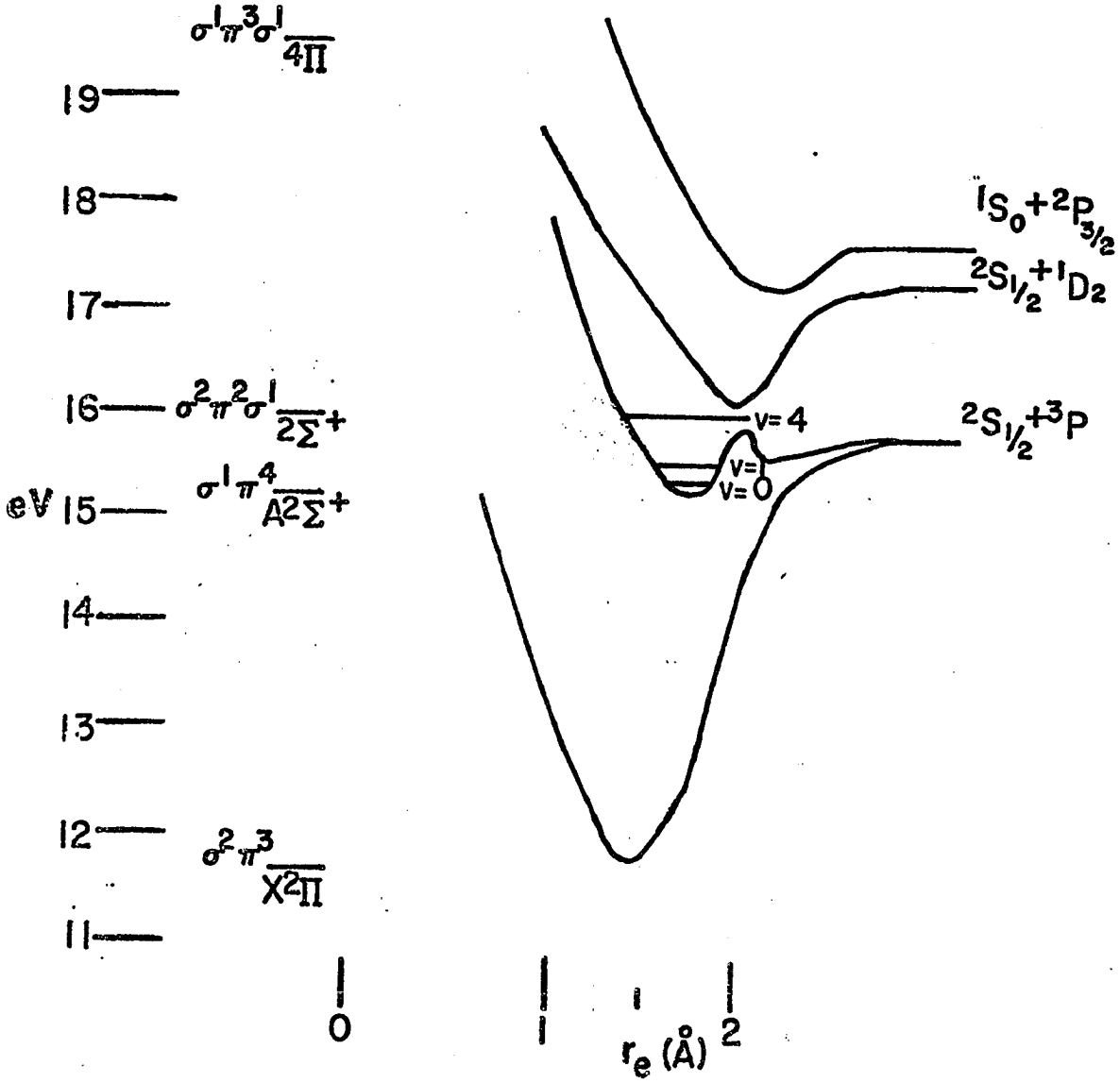

Reproduced with permission of the copyright owner. Further reproduction prohibited without permission.

CS_2^+ AND N_2O^+

Previous Work

Qualitative theoretical predictions of the electronic structure of molecules began not long after the advent of the quantum mechanics. However, since the early 1930's there have been three important papers which discuss the electronic structure of triatomic molecules: Mulliken's LCAO-MO description of CO_2,[1] Walsh's paper on the geometries of AB_2 molecules,[2] and Peyerimhoff and Buenker's paper on the geometry and spectra of nitrous oxide.[3] Each of the preceding three theoretical studies have predicted the orbital bonding characteristics of triatomics in general or have done calculations on a specific triatomic and then extended the findings to all triatomics.

Since N_2O^+ and CS_2^+ both have 15 valence electrons, the electron configurations of the ground state are $KKK(3\sigma_g)^2\ (2\sigma_u)^2\ (4\sigma_g)^2\ (3\sigma_u)^2\ (1\Pi_u)^4\ (1\Pi_g)^3$ in CS_2^+ and $KKK(4\sigma)^2\ (5\sigma)^2(6\sigma)^2\ (1\Pi)^4\ (7\sigma)^2\ (2\Pi)^3$ in N_2O^+, (the configurations and symmetries of excited states appear in Table 6). Our fluorescent spectroscopic studies of N_2O^+ and CS_2^+ have been concerned with the first three electronic states . The bonding characteristics of the $3\sigma_u$ (7σ), $1\Pi_u$ (1Π), $1\Pi_g$ (2Π) orbitals

Reproduced with permission of the copyright owner. Further reproduction prohibited without permission.

seem to be most germain to this discussion. Fig. 16 contains descriptions of these orbitals advanced by the aforementioned authors. In addition, orbital correlation diagrams [2,3] between the bent and linear geometries of triatomics appear in Fig. 17. (A further analysis of the bonding character of these orbitals will appear in the discussion section).

The emission spectra of both N_2O^+ and CS_2^+ have been analyzed by Calloman.[4,5] Photographic detection was used for both molecules to obtain accurate rotational and vibrational constants, (see Table 7). However, because photographic means were employed, accurate intensity measurements could not be made. Partial photoionization cross-sections for both N_2O^+ and CS_2^+ have been measured,[6] but ion-ion F.C.F.'s are available for only N_2O^+.

Tanaka[8] has observed a number of Rydberg series converging to I.P.'s in both N_2O^+ and CS_2^+; these I.P.'s for N_2O and CS_2 are thus known to .001ev,(see Table 8). Dibeler's[9,10] photoionization mass-spectrometry experiments determined appearance potentials for N^+, N_2^+ and for S^+ and CS^+.

Reproduced with permission of the copyright owner. Further reproduction prohibited without permission.

EXPERIMENTAL RESULTS

Observed Transitions

Spectra of N_2O^+ and CS_2^+ taken on our fluorescent emission apparatus are presented in Figs. 18-21. The N_2O^+ spectrum in the region 3000-4000Å shows five broad peaks. These peaks were assigned to vibronic components of the $\tilde{A}\ ^2\Sigma^+ \rightarrow \tilde{X}\ ^2\Pi_i$ transitions by comparison with Calloman's results. The CS_2 spectrum similarly exhibits five peaks, but they are in the 2000-3000Å range. Two of these peaks correspond to the 000-000 vibronic transition of the $B\ ^2\Sigma^+ \rightarrow\ ^2\Pi_{g3/2,1/2}$ transition of CS_2^+. This assignment was also made by comparison to Calloman's work.

The other three peaks in the CS_2 spectrum do not correspond to any transition observed by Calloman, nor can they be assigned by comparison with transition energies predicted from photoelectron data. A quick look at Fig.3A in the experimental section proves that these peaks are not scattered light. These remaining peaks must therefore be due to emission from fragments of the parent ion or the neutral. S_2 does not emit in the 2500Å range, but the transition $A\ ^1\Pi \rightarrow X^1\Sigma^+$ in CS does correspond closely to the three unassigned peaks.[11] The CS bands which probably contribute to the peaks at 2698, 2587, and 2531Å are indicated on the figure.

Reproduced with permission of the copyright owner. Further reproduction prohibited without permission.

Two peaks which are not attributable to scattered light, or fragment emission appear in the energy range predicted by photoelectron spectroscopy for the $A\ ^2\Pi_u \rightarrow X\ ^2\Pi_g$ transition in CS_2^+, (see Fig. 19). Thus they are probably due to CS_2^+ emission. However, it is impossible to make any vibronic assignments based on just two peaks, especially when the splitting between the $^2\Pi_{u1/2}$ and $^2\Pi_{u3/2}$ states has only been determined from the convergence limits of Rydberg series.[11a] Photographic emission spectra of CS_2^+ in this spectral region have been recently obtained by S. Leach and his collaboratos[12] who are carrying out a vibrational analysis with the aid of transition energies predicted from the photoelectron spectrum of CS_2^+. Similarly the spectrum of N_2O^+ in the 2000-3000Å region exhibits two broad maxima in the energy range expected for the $B\ ^2\Pi \rightarrow X\ ^2\Pi$ transition in N_2O^+. This is just a very tentative assignment and higher resolution work must be done to state anything definite.

Intensity Measurements

Dayton, Dalby and Bennett[13] have observed N_2O^+ emission using an electron impact source. They monitored the $\tilde{A} - \tilde{X}$ fluorescence emission both photographically with high dispersion and photoelectrically at low dispersion. The low dispersion spectrum is almost

Reproduced with permission of the copyright owner. Further reproduction prohibited without permission.

identical to the spectrum taken in this thesis. This suggests that neutral-ion population rates for the $\tilde{A}$ state of N_2O^+ are about the same for electron impact and photon excitation. The high dispersion spectrum of Dayton et. al. indicates that there are other unresolved bands underlying the N_2O^+ vibronic transitions observed in this thesis. Creutzberg and Calloman[14] have recently taken high resolution spectra of N_2O^+ which prove that the three N_2O^+ peaks we detected at 3390, 3488, and 3542Å are composites of two or more vibronic bands. Photodensitometer studies,[14] although accurate to only ± 30% imply that various transitions, (e.g. $^2\Sigma^+_{(010)} \rightarrow {}^2\Pi_{3/2(010)}$ and $^2\Sigma^+_{(100)} \rightarrow {}^2\Pi_{3/2(100)}$), contribute approximately 20% of the intensity of the peak at 3542Å, and that the peaks at 3390Å and 3488Å have significant contributions from the transitions indicated in Fig. 20.

Relative intensities for the (000-n00) progression are given in Table 9, (note the intensity for the 000-000 band is only approximate in view of Creutzberg's results). Our low resolution prohibits even an approximate estimate of the relative intenisties for the (000-n00) progression. Haugh and Bayes have given relative intensities for the (000-n00) progression but their value of 1.66 for $I^{em}_{(100-100)}/I^{em}_{(100-000)}$ disagrees radically with Creutzberg's[14] estimate of 0.25. Thus

Reproduced with permission of the copyright owner. Further reproduction prohibited without permission.

Haugh and Bayes probably also did not have enough resolution to accurately determine relative intensities.

DISCUSSION

Fragmentation Processes

Since accurate relative intensities for the (100-n00) progression, and thus a value of $K_n^{(100)}/K_r^{(000)}$ cannot be estimated with our present resolution, additional information about fragmentation processes occurring in N_2O^+ is unobtainable from the present data. The appearance of fluorescence from CS in the CS_2^+ spectra indicates that some dissociation to produce electronically excited CS must be occurring from the manifold of electronic states of CS_2 or CS_2^+ at energies less than 21.2ev. There are four possible processes which can produce CS from CS_2 with a helium resonance lamp as a source: (1) dissociative ionization, i.e. $CS_2 + h\nu \rightarrow [CS_2^{+*}] \rightarrow CS\ (\tilde{A}\ ^1\Pi) + S^+ + e^-$; (2) photodissociation, i.e. $CS_2 + h\nu \rightarrow CS\ (\tilde{A}\ ^1\Pi)$ + S(neutral) + kinetic energy caused by excitation into a dissociation continuum of a CS_2 Rydberg state; (3) Impurities present in the source produce radiation in the 8-12ev region which causes photodissociation, i.e. excitation into the dissociation continuum of a CS_2^* (non-Rydberg) or CS_2 (Rydberg state); (4) CS_2 diffused into the helium

Reproduced with permission of the copyright owner. Further reproduction prohibited without permission.

light source thus producing CS($\tilde{A}$ - $\tilde{X}$) radiation in the scattered light spectrum.

To help understand the energetics involved in the dissociation of CS_2^+ or CS_2, Fig. 22 was made using thermochemical and photoelectron data. The least energetic pair of symmetry-allowed and spin-allowed dissociation products which contains CS($^1\Pi$) occurs at 21.06ev. (A spin forbidden dissociation pair including CS($^1\Pi$) occurs at 19.16ev). Since Turner[16] has stated that peaks originally observed at 19.3ev and 21.0ev in the CS_2 photoelectron spectrum were spurious, it is doubtful that process (1) is occurring.

Cook and Ogawa[15] have done photoionization and fluorescence yield experiments on CS_2 using excitation energies between 1000Å and 600Å. They attributed the onset of fluorescence at 976.5Å to the $\tilde{A}\ ^2\Pi_u \rightarrow \tilde{X}\ ^2\Pi_g$ transition, (which our observations confirm), but could not identify CS emission because they did not disperse the fluorescence. However, a short extrapolation of Cook and Ogawa's photoionization yield curves for CS_2 indicates only 80-90% photoionization efficiency at 584Å. Therefore sufficient excitation to a continuum of a Rydberg state, (i.e. process(2)), to account for the large CS intensity is possible.

The visible scattered light spectrum of the helium resonance source exhibits only a few weak lines with

Reproduced with permission of the copyright owner. Further reproduction prohibited without permission.

intensities $\leq$ 10 photons/sec. Thus it is possible but unlikely that V.U.V. radiation from impurities in the photoionizing source is adequate to produce observed CS intensities of 250 photons/sec. The occurrence of process (4) can be proven by inserting the retractable mirror in the optical path of the excitation source and taking a spectrum. If a large increase in CS emission is not observed, process (4) can be eliminated. (This experiment has not been performed yet).

A fluorescent photoionization experiment of the type performed by Judge et. al. on CO_2 could definitely determine what type of dissociation process is occurring. The source excitation energy could be varied until fluorescence due to CS ($A^1\Pi - X^1\Sigma_g$) is observed. If no CS ($A^1\Pi - X^1\Sigma_g$) vibronic transitions are observed, process (3) or process (4) must be responsible for our observation of CS emission. If CS fluorescence is seen, the lowest excitation energy which produces this fluorescence will (one would hope) correspond to a Rydberg state of CS_2 or a vibronic state of CS_2^+. Thus either process (1) or process (2) can be eliminated.

Electron Structure and Bonding Characteristics

As can be seen from Fig. 16, Mulliken[1] has interpreted the $3\sigma_u(7\sigma)$, $1\Pi_u(1\Pi)$, $1\Pi_g(2\Pi)$ orbitals as weakly antibonding, strongly bonding, and non-bonding

Reproduced with permission of the copyright owner. Further reproduction prohibited without permission.

respectively. Peyerimhoff[3] and Walsh[2] have predicted these orbitals to be weakly bonding, strongly bonding, and non-bonding. The ordering of orbitals in N_2O^+ and CS_2^+ has been determined by information from ionic emission spectroscopy and photoelectron spectroscopy. Calloman has observed the (000-000) band in N_2O^+ and CS_2^+[4,5] at 3.492ev and 4.398ev respectively. The rotational analysis of these bands discloses the electronic transition in N_2O^+ to be $^2\Sigma^+ \rightarrow {}^2\Pi_{3/2}$ and $^2\Sigma_u^+ \rightarrow {}^2\Pi_{g3/2}$ in CS_2^+. Turner's[6] photoelectron spectra show a 3.486ev separation between the first and second I.P.'s in N_2O^+ and a 4.410ev separation between the first and third I.P. of CS_2^+. Therefore it is apparent that the orbital energy ordering is:

$$N_2O^+ \rightarrow KKK\ 4\sigma\ 5\sigma\ 6\sigma\ 1\Pi\ 7\sigma\ 2\Pi$$
$$CS_2^+ \rightarrow KKK\ 3\sigma_g\ 2\sigma_u\ 4\sigma_g\ 3\sigma_u\ 1\Pi_u\ 1\Pi_g$$

For N_2O^+, the difference in equilibrium normal coordinate lengths between the configurations

$$KKK\ (4\sigma)^2\ (5\sigma)^2\ (6\sigma)^2(1\Pi)^4\ (7\sigma)^2\ (2\Pi)^3 \text{ and}$$
$$KKK\ (4\sigma)^2\ (5\sigma)^2\ (6\sigma)^2(1\Pi)^4\ (7\sigma)^1\ (2\Pi)^4$$

should depend on the relative bonding characteristics of the 2Π and 7σ orbitals. The more bonding in nature

Reproduced with permission of the copyright owner. Further reproduction prohibited without permission.

an orbital, the more its occupation shortens the bond lengths. Qualitative considerations of F.C.F.'s can determine whether the equilibrium normal coordinates of the initial and final electron states are equal, (i.e. the closer the (000-000) F.C.F. is to unity, the closer the correspondence between r_e' and r_e''). If rotational analysis of transitions is available a quantitative measure of r_e's is possible. Thus from consideration of F.C.F.'s and rotational spectra (if available), relative equilibrium normal coordinates for different electron states can be deduced, and therefore the relative bonding characteristics of orbitals can be obtained. In linear molecules the frequency of the symmetric vibration is also a good measure of bonding nature; the higher the frequency of the vibration in a particular electronic state, the more bonding the configuration corresponding to this state.

Using neutral-ion F.C.F.'s and symmetric stretch frequencies Turner[16] deduced that the 1Π ($1\Pi_u$), 7σ ($3\sigma_u$), and 2Π ($1\Pi_g$) orbitals are strongly bonding, slightly bonding or non-bonding, and non-bonding respectively. The F.C.F.'s in Table 9 for the $A\ ^2\Sigma^+ \rightarrow X\ ^2\Pi$ transition in N_2O^+ and the observation of only $B\ ^2\Sigma^+_{u(000)} \rightarrow X\ ^2\Pi_{g(000)}$ emission in CS_2^+ indicate that r_e' and r_e'' are equal for the CS_2^+ $\tilde{B}$-$\tilde{X}$ transition

Reproduced with permission of the copyright owner. Further reproduction prohibited without permission.

but are not the same for the N_2O^+ $\tilde{A}$-$\tilde{X}$ transition. Assuming, as Turner believes that the 2Π ($1\Pi_g$) orbital is non-bonding, ion-ion F.C.F.'s indicate that the N_2O^+ 7σ orbital is slightly bonding and the CS_2^+ $3\sigma_u$ orbital is non-bonding. The ν_1 values of 1140 and 1350cm.$^{-1}$ given by Turner[16] for the symmetric modes of the N_2O^+ X $^2\Pi$ and A $^2\Sigma^+$ states respectively, reinforces the argument for the slightly bonding nature of the 7σ state. It also appears to me that there is appreciable charge density in the N-N and N-O bonds indicated in Peyerimhoff's orbital contour, (see Fig. 16). I feel that Peyerimhoff's results suggest a slightly bonding nature for the 7σ orbital, not the non-bonding characteristic that Turner infers. In addition, Calloman's[17] normal coordinate analysis on N_2O^+ gives the r_e's in Table 10. These r_e's reinforce the argument that the 7σ orbital is slightly bonding.

Turner[16] has noted that the X $^2\Pi_g$ and C $^2\Sigma_g^+$ states of CS_2^+ have a much lower bending frequency than the ground state of the neutral. However, in the X $^2\Pi$ and C $^2\Sigma^+$ states of N_2O^+ the bending frequency is almost the same as in the neutral ground state. Although Turner's assignment of bending frequencies for N_2O^+ and CS_2^+ are not conclusive, it is interesting to speculate on Turner's observation. Correlation diagrams such as those in Fig. 17 can be used to explain the preceding

Reproduced with permission of the copyright owner. Further reproduction prohibited without permission.

observation. It is reasonable to assume that the more stable the linear geometry of a molecule whose equilibrium configuration is linear, the higher the frequency of the bending mode. The diagram in Fig. 17 for AB_2 type molecules shows that removing an electron from the $^2\Pi_g$ or $3\sigma_u$ orbital decreases the stability of the linear geometry compared to the ground state. However, the diagram for N_2O indicates that removing an electron from the 2Π or 7σ orbital has little effect on the stability of the linear geometry. Thus Turner's observations about the bending frequencies in N_2O^+ and CS_2^+ can be explained with correlation diagrams. Since a LCAO-MO calculation has not been done on CS_2, this argument is not entirely conclusive, but it does seem to be the most probable considering existing information.

Conclusion

The importance of this chapter lies in the suggestion of significant future experiments rather than the presentation of results per se. High resolution spectra should be taken of CS_2^+ and N_2O^+. In CS_2^+ the goal would be to better define the emission in the 4500Å area. In N_2O^+ the purpose would be to obtain better F.C.F.'s in the 3000-4000Å range so $K_n^{(100)}/K_r^{(000)}$ can be obtained and to elucidate the continuum observed

Reproduced with permission of the copyright owner. Further reproduction prohibited without permission.

in the 2000-3000Å region. (A V.U.V. monochromator might be best for use in the region below 3000Å). Finally, a fluorescent photoionization experiment with a variable V.U.V. excitation source should be used to determine the details of the fragmentation occurring in CS_2.

Reproduced with permission of the copyright owner. Further reproduction prohibited without permission.

Reproduced with permission of the copyright owner. Further reproduction prohibited without permission.

TABLE 6

Ground and First Two Excited Configurations for N_2O^+ and CS_2^+

N_2O^+

Configuration	State
KKK $(4\sigma)^2$ $(5\sigma)^2$ $(6\sigma)^2$ $(1\Pi)^4$ $(7\sigma)^2$ $(2\Pi)^3$	$\tilde{X}\ ^2\Pi_{3/2,1/2}$
KKK $(4\sigma)^2$ $(5\sigma)^2$ $(6\sigma)^2$ $(1\Pi)^4$ $(7\sigma)^1$ $(2\Pi)^4$	$\tilde{A}\ ^2\Sigma^+$
KKK $(4\sigma)^2$ $(5\sigma)^2$ $(6\sigma)^2$ $(1\Pi)^3$ $(7\sigma)^2$ $(2\Pi)^4$	$\tilde{B}\ ^2\Pi_{3/2,1/2}$

CS_2^+

KKK $(3\sigma_g)^2$ $(2\sigma_u)^2$ $(4\sigma_g)^2$ $(3\sigma_u)^2$ $(1\Pi_u)^4$ $(1\Pi_g)^3$	$\tilde{X}\ ^2\Pi_{g1/2,3/2}$
KKK $(3\sigma_g)^2$ $(2\sigma_u)^2$ $(4\sigma_g)^2$ $(3\sigma_u)^2$ $(1\Pi_u)^3$ $(1\Pi_g)^4$	$\tilde{A}\ ^2\Pi_{u1/2,3/2}$
KKK $(3\sigma_g)^2$ $(2\sigma_u)^2$ $(4\sigma_g)^2$ $(3\sigma_u)^1$ $(1\Pi_u)^4$ $(1\Pi_g)^4$	$\tilde{B}\ ^2\Sigma_u^+$

TABLE 7

Spectroscopic Constants for N_2O^+ and CS_2^+

N_2O^+	B_0	D_0	$^2\Sigma^+ - ^2\Pi_{1/2}$ ν_0	$^2\Sigma^+ - ^2\Pi_{3/2}$ ν_0	ν_1
$A^2\Sigma^+$	0.43287	1.42×10^{-7}	28,229.82	28,096.73	1345
$\tilde{X}^2\Pi$	0.41146	1.77×10^{-7}			1119
CS_2^+					
$\tilde{B}\ ^2\Sigma_u^+$	0.10776	1.4×10^{-8}			$\approx 610\pm100$ cm.$^{-1}$
$\tilde{X}\ ^2\Pi_g$	0.10914	———	35,017.87	35,458.48	———

Reproduced with permission of the copyright owner. Further reproduction prohibited without permission.

TABLE 8

Appearance Potentials for N_2O^+ and CS_2^+ Parent Ions

	A.P. NO^+	A.P. N_2^+	A.P. CS^+	A.P. S^+
N_2O^+	17.3ev	15.65ev	—	—
CS_2^+	—	—	16.16ev	14.81ev

****

TABLE 9

Relative Intensities and F.C.F.'s for

$N_2O^+ \ ^2\Sigma^+_{(000)} \rightarrow \ ^2\Sigma^+_{(n00)}$ Transitions

	Relative Intensity		F.C.F.'s	
	Schneider -Smith	Haugh -Bayes	Schneider -Smith	Haugh -Bayes
000-000	.61	.61	.57	.57
000-100	.30	.30	.32	.32
000-200	.09	.090	.11	.11

****

TABLE 10

Equilibrium Internuclear Separations for N_2O^+

	$r_0(NN)^*$	$r_0(NO)^*$
A $^2\Sigma^+$	1.140	1.141
X $^2\Pi_i$	1.155	1.185

*all measurements in Å

Reproduced with permission of the copyright owner. Further reproduction prohibited without permission.

Figure 16

Charge Density Diagrams for the

$7\sigma(3\sigma_u)$, $1\Pi(1\Pi_u)$, and

$2\Pi(1\Pi_g)$ Orbitals of NNO (NON).

Reproduced with permission of the copyright owner. Further reproduction prohibited without permission.

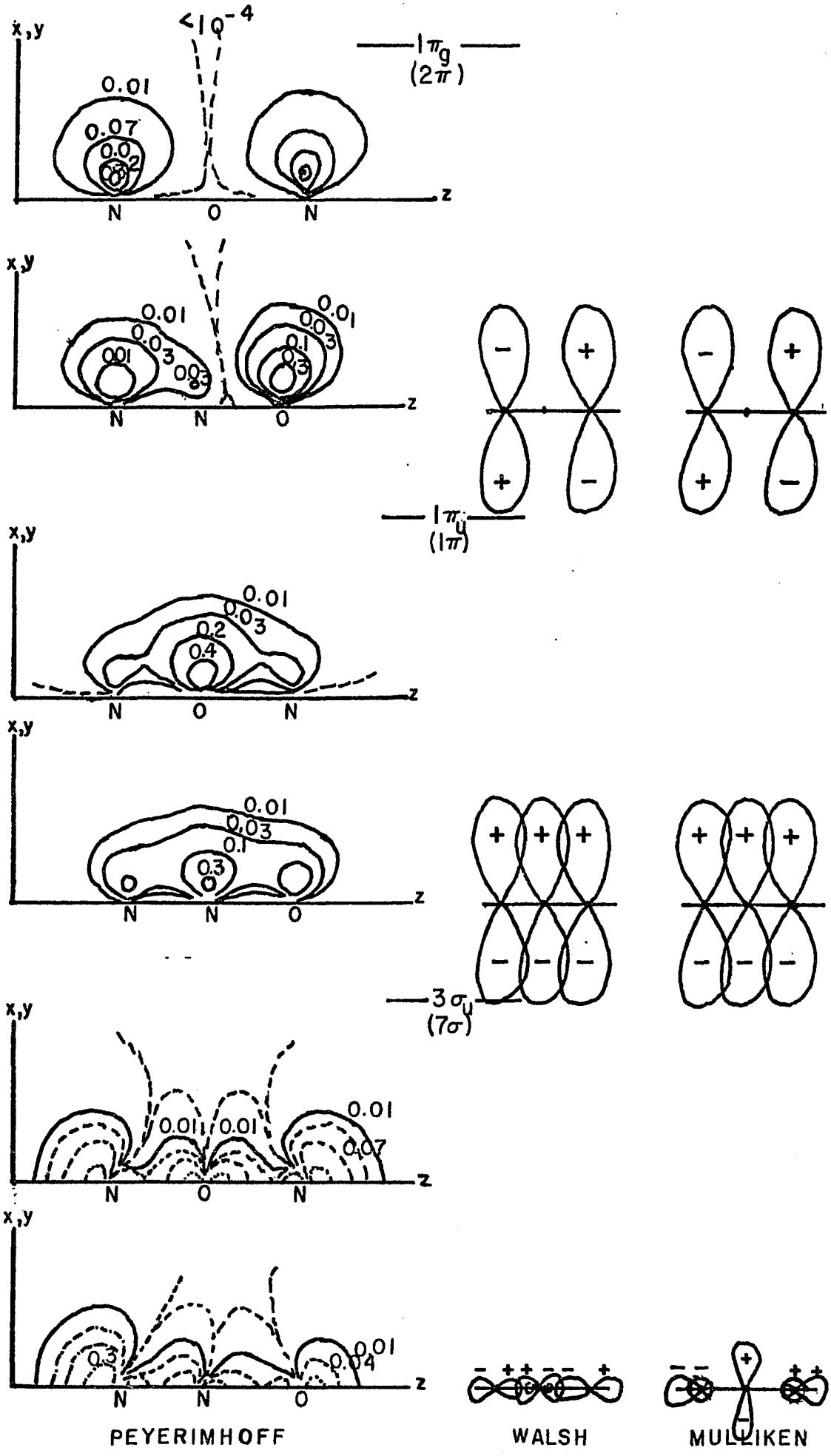

Reproduced with permission of the copyright owner. Further reproduction prohibited without permission.

Figure 17

Correlation Diagrams Between Bent and Linear Geometries for N_2O and ABA Type Molecules.

Reproduced with permission of the copyright owner. Further reproduction prohibited without permission.

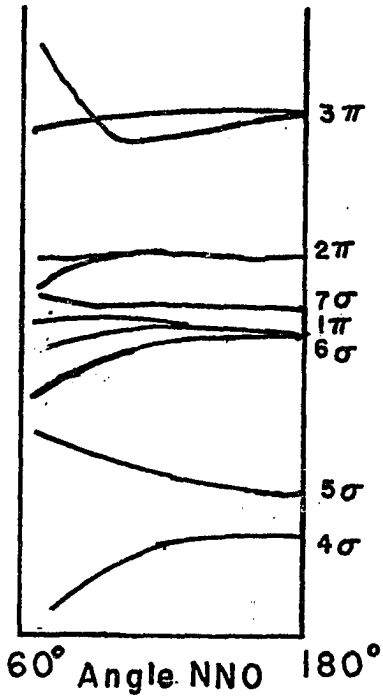

PEYERIMHOFF's

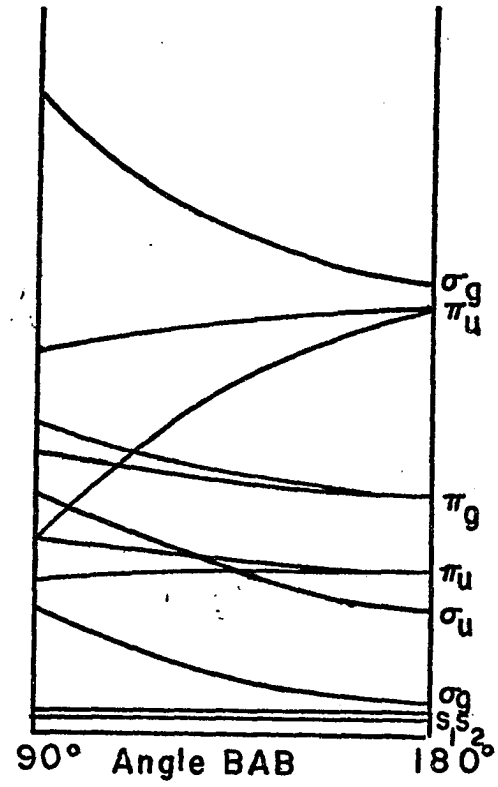

WALSH's

Reproduced with permission of the copyright owner. Further reproduction prohibited without permission.

Figure 18

Fluorescent Photoionization Spectrum of CS_2^+ in the 2000Å - 2800Å Range. Experimental Conditions: 500μ Slits, 18Å FWHM, 2 Runs, 100μ Pressure of CS_2. Peaks Marked (a) and (b) are the

$$^2\Sigma^+_{u\,(000)} \rightarrow {}^2\Pi_{g1/2\,(000)} \text{ and}$$

$$^2\Sigma^+_{u(000)} \rightarrow {}^2\Pi_{g3/2(000)}$$

Transitions Respectively.

Reproduced with permission of the copyright owner. Further reproduction prohibited without permission.

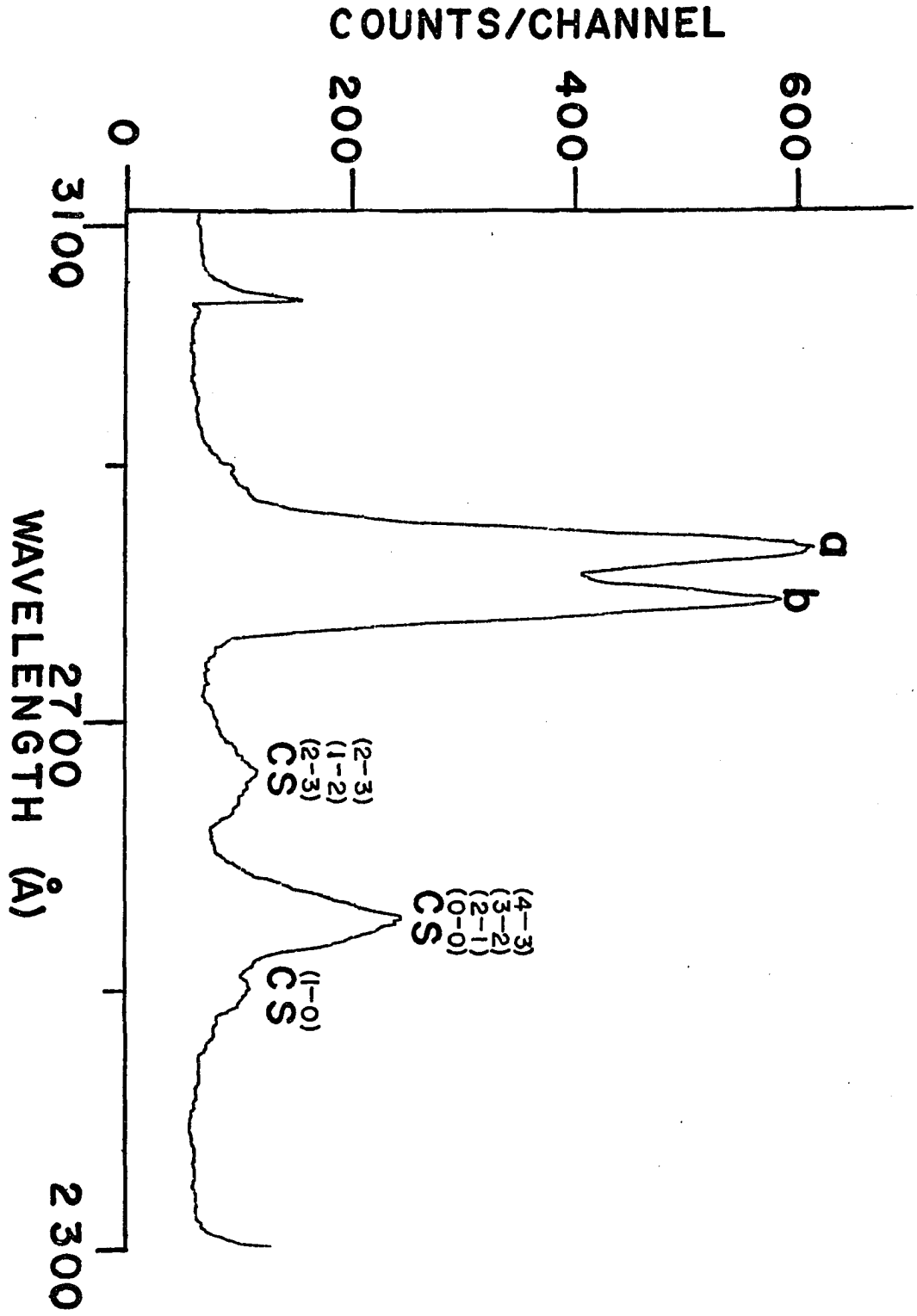

Reproduced with permission of the copyright owner. Further reproduction prohibited without permission.

Figure 19

Fluorescent Photoionization Spectrum of CS_2^+ in the 4000Å - 5000Å region. Experimental Conditions: 500μ Slits, 18Å FWHM, 4 Runs, 100μ Pressure of CS_2. Peaks Marked by (a) are Scattered Light.

Reproduced with permission of the copyright owner. Further reproduction prohibited without permission.

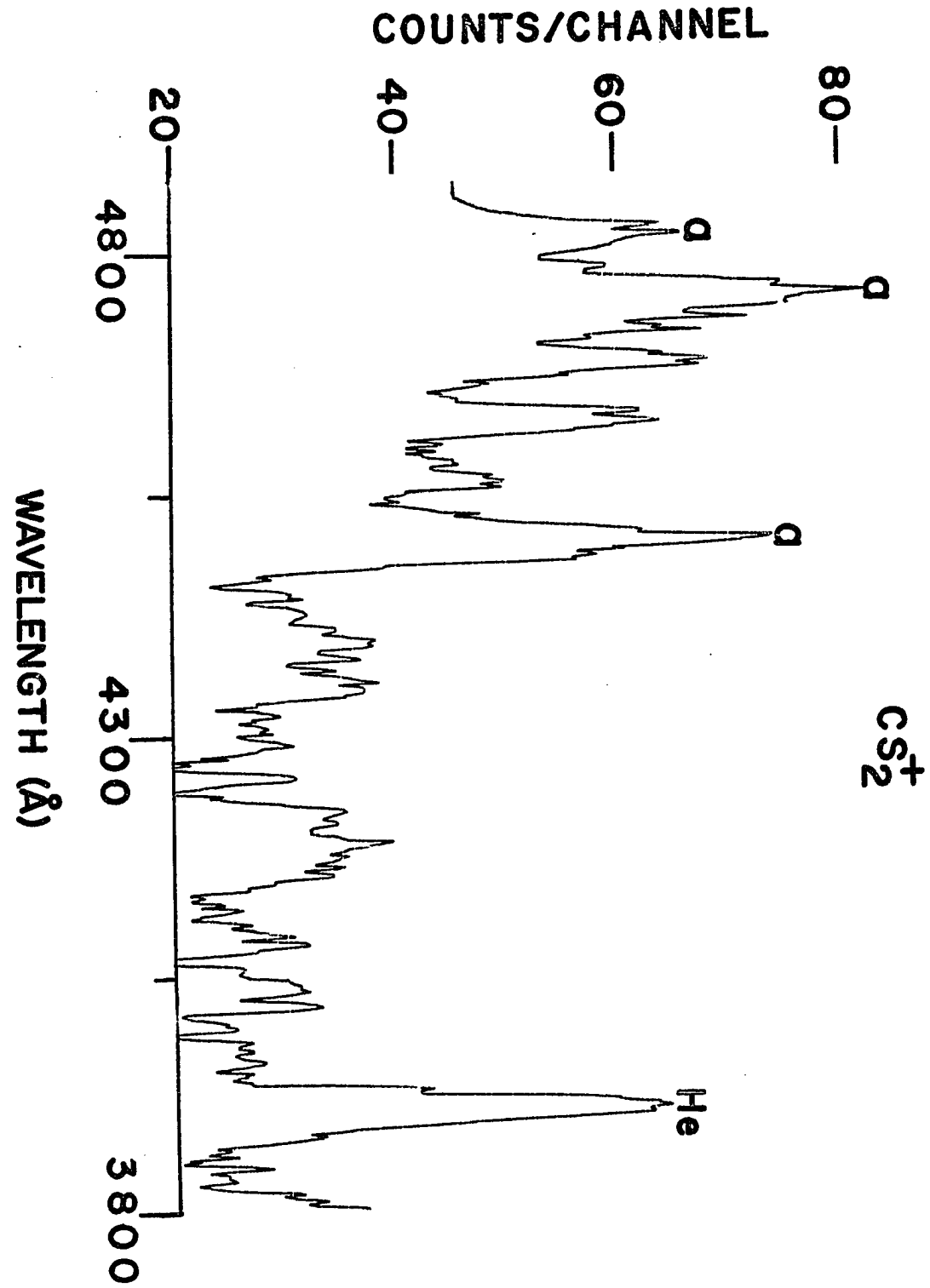

Reproduced with permission of the copyright owner. Further reproduction prohibited without permission.

Figure 20

Fluorescent Photoionization Spectrum of N_2O^+ in the 3000Å - 4000Å Region. Experimental Conditions: 500μ Slits, 18Å FWHM, 2 Runs, 100μ N_2O Pressure.

Reproduced with permission of the copyright owner. Further reproduction prohibited without permission.

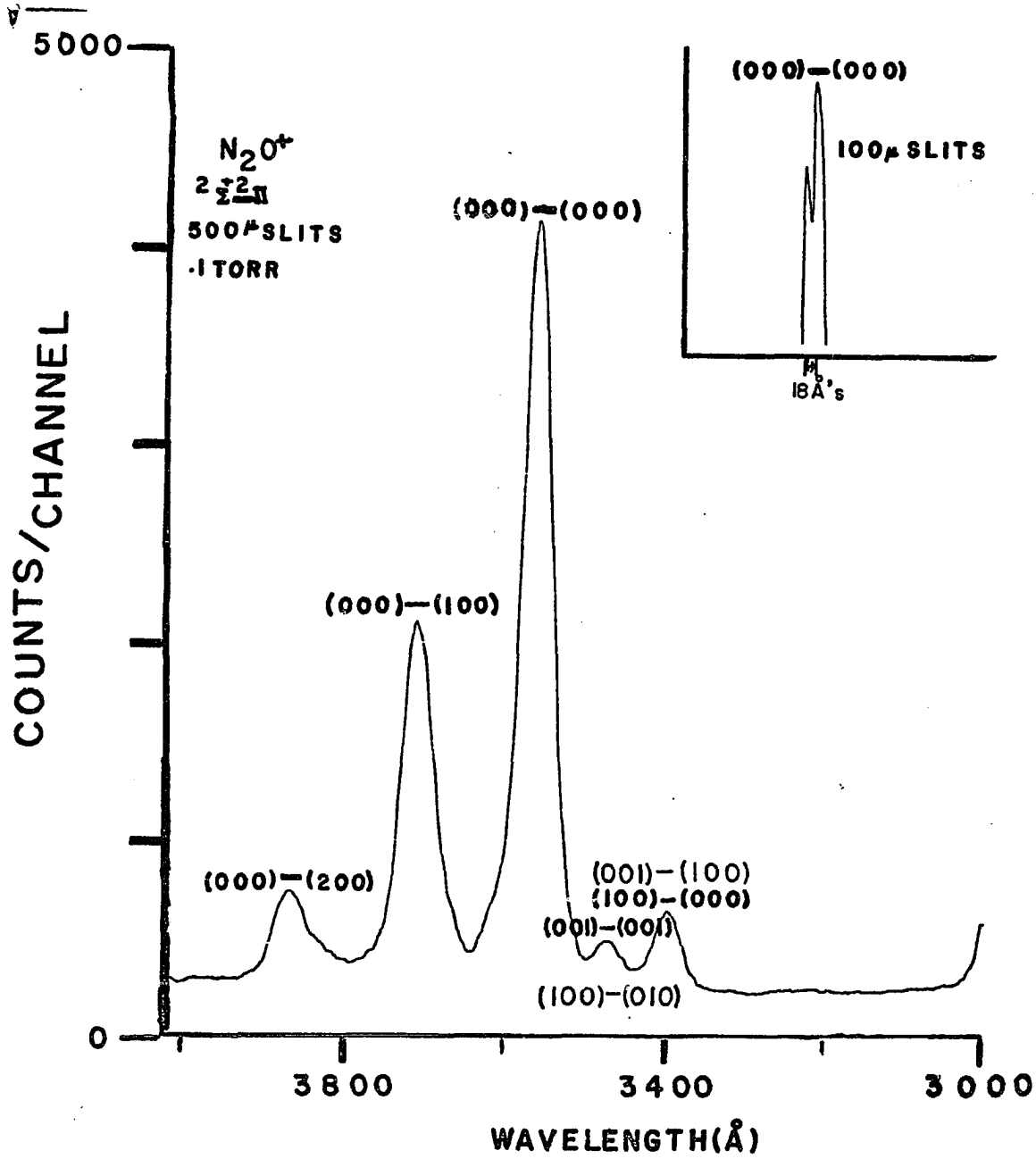

Reproduced with permission of the copyright owner. Further reproduction prohibited without permission.

Figure 21

Fluorescent Photoionization Spectrum of N_2O^+ in the 2000Å - 3000Å region. Experimental Conditions: 500μ Slits, 18Å FWHM, 5 Runs, 100μ N_2O Pressure.

Reproduced with permission of the copyright owner. Further reproduction prohibited without permission.

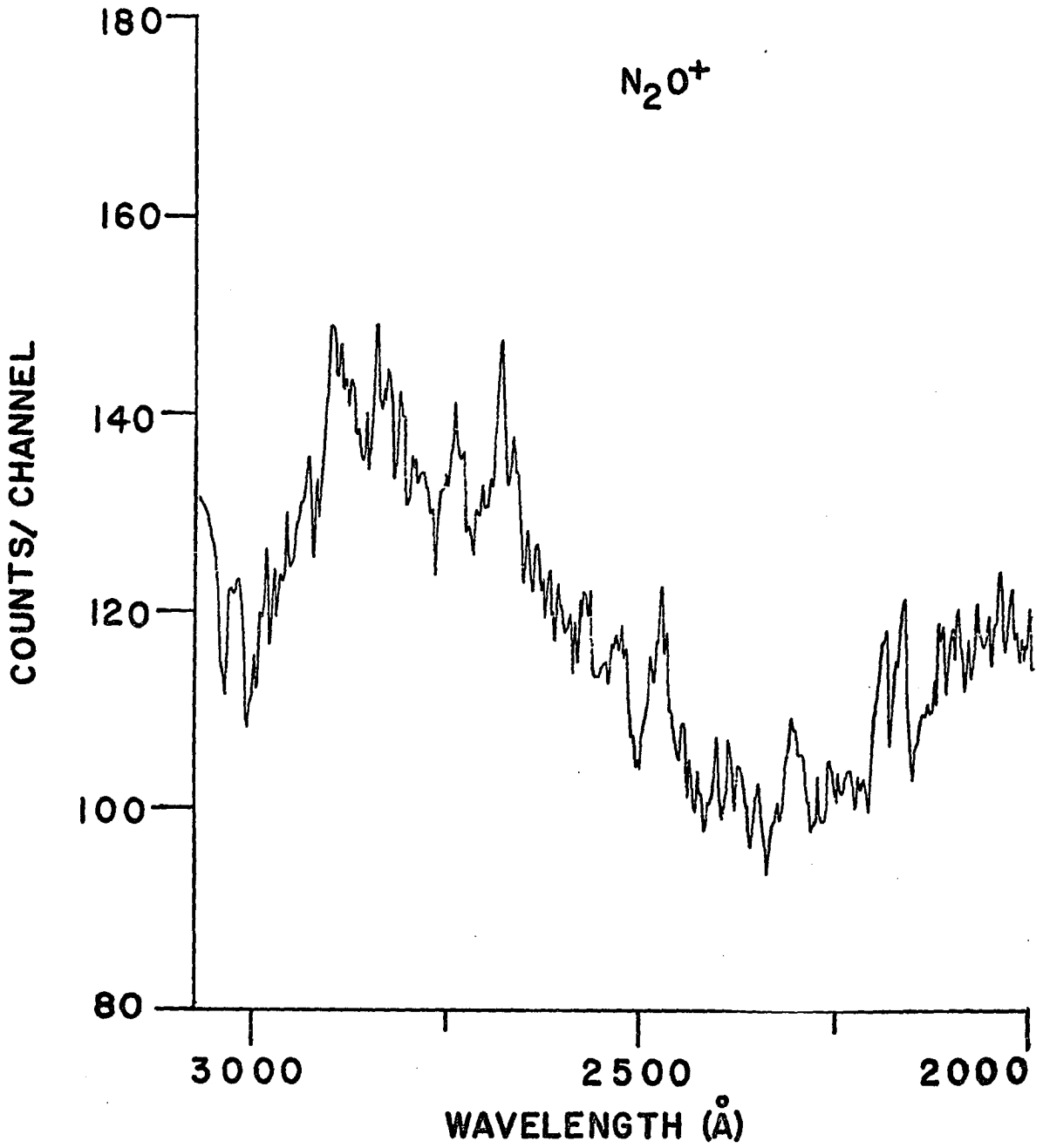

Reproduced with permission of the copyright owner. Further reproduction prohibited without permission.

Figure 22

Energy Diagram of the CS_2 - CS_2^+ Manifold

of States and Their Possible Dissociation Products.

I.P. of S was obtained from
I.P.'s, A.P.'s and Heats of Formation of Gaseous Positive Ions, N.S.R.D.S. -NBS -26 (1969)

Electronic energy level separations in CS were obtained from Ref. 11, N_2O^+ and CS_2^+ section

Energy levels of S and S^+ were obtained from
Atomic Energy Levels N.B.S. Circular 467

Dissociation energy for the ground state of CS_2 was obtained from
J.A.N.A.F. "Thermochemical Tables," Dow Chemical Co., Midland, Mich., Aug. 1965

Note if Dibeler's value for D(S-CS) from Ref. 9 of the N_2O^+ and CS_2^+ section is used, all dissociation limits in this fig. would be raised 0.4ev.

Reproduced with permission of the copyright owner. Further reproduction prohibited without permission.

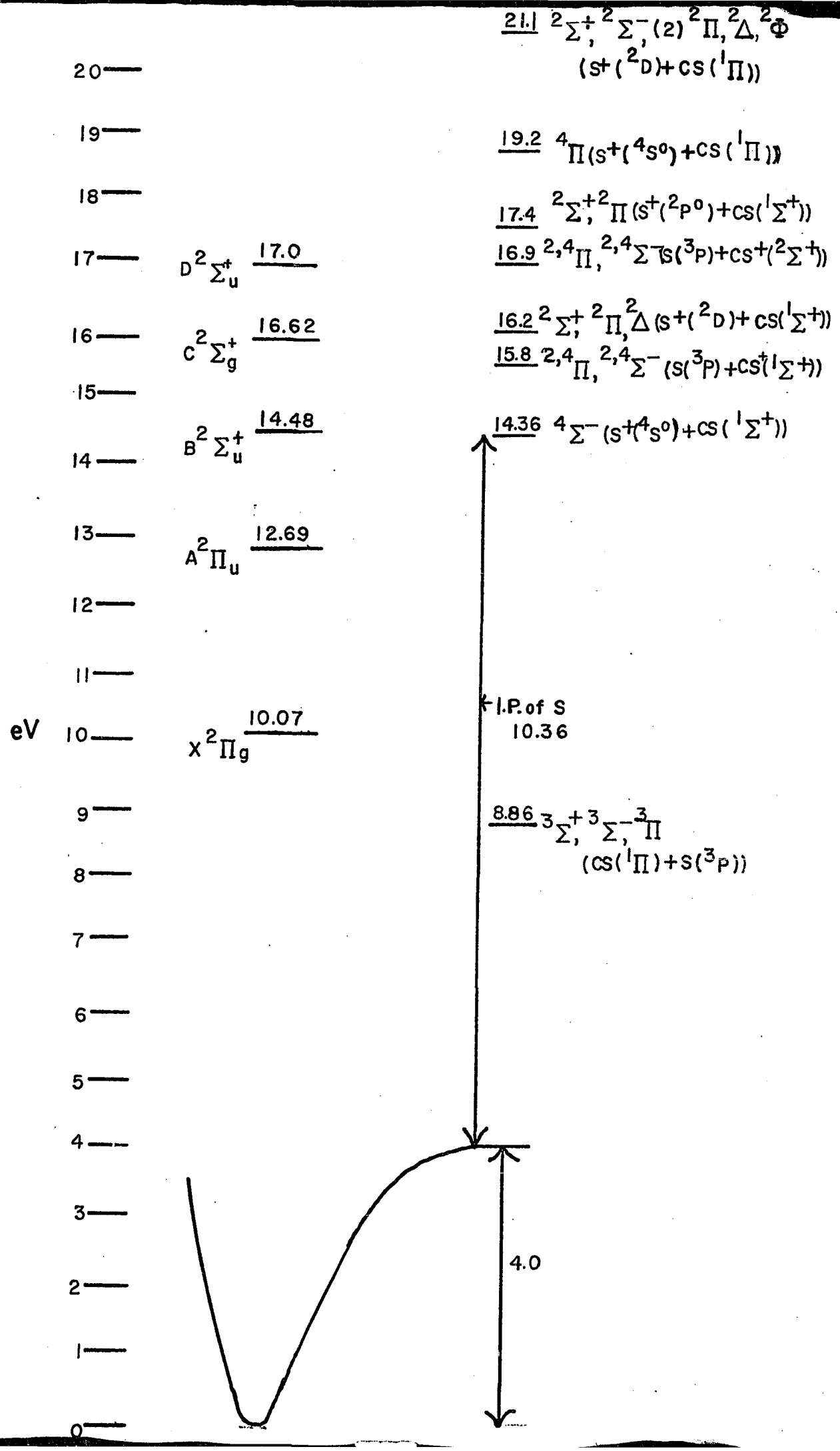

Reproduced with permission of the copyright owner. Further reproduction prohibited without permission.

Appendix I

Program for Computing Rotational Spectrum of $^2\Sigma \rightarrow {}^2\Pi$ Transitions

Reproduced with permission of the copyright owner. Further reproduction prohibited without permission.

This program computes transition energies for $^2\Sigma \rightarrow {}^2\Pi$ emission. Intensities of rotational lines are also computed and used in combination with the transition energies to plot a spectrum on the C.R.T. The rotational lines are convoluted with a triangle to introduce the appropriate resolution.

Outputs include: (1) energies ordered by rotational branch; (2) energies ordered by wavelength; (3) arrays used to plot on the C.R.T.; (4) upper and lower state rotational energies.

The following are appropriate units for input

BVPP = The upper state rotational constant in $cm.^{-1}$
DVPP = The upper state rotational constant in $cm.^{-1}$
ZLAMO = The upper state γ_0 in $cm.^{-1}$
BV = The lower state rotational constant in $cm.^{-1}$
DV = The lower state rotational constant in $cm.^{-1}$
VOO = The band origin for no splitting in $cm.^{-1}$
A = The lower state coupling constant in $cm.^{-1}$
F = The lower state q_0 in $cm.^{-1}$
P = The lower state p_0 in $cm.^{-1}$
XLAST = The longest wavelength desired on the C.R.T. plot in Å
XFIRS = The shortest wavelength desired on the C.R.T. plot in Å
LINE = The number of lines in each rotational branch calculated
SLIT = The slit width of the Jarrel-Ash 1/4 meter in mm.
QUANT = The Ω quantum number of the lower state
BE = The equilibrium rotational number for the lower state in $cm.^{-1}$
DE = The equilibrium rotational constant for the lower state in $cm.^{-1}$
NOPUNCH = Cue to computer whether or not to punch energy transitions and differentials with respect to BV out

Reproduced with permission of the copyright owner. Further reproduction prohibited without permission.

Reproduced with permission of the copyright owner. Further reproduction prohibited without permission.


```
      DIMENSION ANGST(2000),STREN(2000),SF2(30),PF1U(30),PF1L(30),
     1BOLT1(30),FP(6,30),STP(6,30),SF1(30),Q(6,30),AP(6,30),
     2AAP(6,30),RFR(5),BOLT2(30)
      DIMENSION BRANCH(12),XFREQ(300),FREQ(300),ISUM(300)
      DIMENSION DPF1U(30),DPF1L(30)
      DIMENSION ZLAM1(30),DSF1(30),DDSF(6,30)
      DIMENSION DSF2(30)
      DIMENSION FMT15(11),FMT05(11)
      DATA BRANCH/3HF11,3HQ11,3HR11,3HP21,3HQ21,3HR21,3HP22,3HQ22,3HR22,
     13HP12,3HQ12,3HR12/
      DATA FMT15/6H(2X,'K,6H',4X,',6HP11',7,6HX,'Q11,6H',7X,',6HR11',7,6
     1HX,'P21,6H',7X,',6HQ21',7,6HX,'R21,6H')     /
      DATA FMT05/6H(2X,'K,6H',4X,',6HP22',7,6HX,'Q22,6H',7X,',6HR22',7,6
     1HX,'P12,6H',7X,',6HQ12',7,6HX,'R12,6H')     /
      READ(5,99)DVPP,DVPP                                              1
   99 FORMAT(F10.4,F10.4)
      READ(5,69)BV,ZLAMO,A,E,PO,V00,DV                                 2
   69 FORMAT(5F10.4,F10.2,F10.7)
      READ(5,70)E,DE                                                   3
   70 FORMAT(2F7.4)
      READ(5,193)TEMP,XFIRS,XLAST                                      4
  193 FORMAT(3F10.4)
      READ(5,826)LINES,SLIT                                            5
  826 FORMAT(I2,F8.4)
      READ(5,830)QUANT                                                 7
  830 FORMAT(F3.1)
      READ(5,1001)NOPNCH                                               8
 1001 FORMAT(I2)
      NLAST=IFIX((XLAST-XFIRS)/SLIT)
      DO 43 IINT=1,NLAST
      IINT=IINT-1
      ANGST(IINT)=XLAST-SLIT*FLOAT(IINT)
      STREN(IINT)=0.0
   43 CONTINUE
      SLIT1=16.0*SLIT*0.25
      LINE2=LINES+2
      DO 20 L=1,LINE2
      K=L-1
      IF(QUANT.EQ.0.5)AJ=FLOAT(K)-0.5
      IF(QUANT.EQ.1.5)AJ=FLOAT(K)+0.5
      Y=A/BV
      IF(AJ.LT.0.0) GO TO 31
      W=32.0*(AJ**2+AJ)
      U=(Y**2-4.0*Y+(2.0*AJ+1.0)**2)**.5                               32
      Z=1.0/U
      T=2.0*AJ+1.0
      TT=4.0*(AJ**2)+4.0*AJ
   31 C=DVPP*FLOAT(K)*(FLOAT(K)+1.0)-DVPP*(FLOAT(K))**2*(FLOAT(K)+1.)**2
      ZLAM=ZLAMO/(1.0+(DE*FLOAT(K)*(FLOAT(K)+1.0))/BE)
      ZLAM1(L)=ZLAM/ZLAMO
      IF(K.EQ.0)GO TO 30
      SF2(L)=C-ZLAM*(FLOAT(K)+1.)**.5
      DSF2(L)=(SF2(L)-C)/ZLAMO
      WRITE(6,111)K,SF2(L)                                             41
      X=(Y*(Y-4.0)+(AJ+.5)**2)**.5                                     43
```

```
      DX=(4.0*Y/BV-2.0*Y/BV)*.5/X
      P=1.0/(1.0+DV*AJ*(AJ+1.0)/BV)
      DP=P0*DV*AJ*(AJ+1.0)/(BV**2*(1.0+DV*AJ*(AJ+1.0)/BV)**2)
      IF(QUANT.EQ.1.5)GO TO 29
      D=BV*((AJ+.5)**2-1.0+.5*(4.0*(AJ+.5)**2+Y*(Y-4.))**.5)-DV*((AJ+1.)
     1**4)                                                              47
      DD=((AJ+.5)**2-1.+.5*(4.*(AJ+.5)**2+Y*(Y-4.))**.5)+((4.*Y-2.*Y*
     1*2)*.25*(1.0/(4.0*(AJ+.5)**2+Y*(Y-4.0))**.5))                     48    49
      DDU=((.5*P+F)*(2.0/X-Y/X+1.0)+2.0*F*(AJ-.5)*(AJ+1.5)/X)*(AJ+.5)*0.
     15
      DDDU=((.5*DP+F)*(2.0/X+1.0-Y/X)+(.5*P+F)*(Y/(BV*X)+Y*D
     1X/X**2)-2.0*F*DX*(AJ-.5)*(AJ+1.5)/X**2)*(AJ+.5)*.5
      GO TO 133
   29 D=BV*((AJ+.5)**2-1.0-.5*(4.0*(AJ+.5)**2+Y*(Y-4.))**.5)-DV*AJ**4   52
      DD=((AJ+.5)**2-1.-.5*(4.*(AJ+.5)**2+Y*(Y-4.))**.5)-((4.*Y-2.*Y*
     1*2)*.25*(1.0/(4.0*(AJ+.5)**2+Y*(Y-4.0))**.5))                     53    54
      DDU=((.5*P+F)*(2.0/X-Y/X-1.0)+2.0*F*(AJ-.5)*(AJ+1.5)/X)*(AJ+.5)*0.
     15
      DDDU=((.5*DP+F)*(2.0/X-1.0-Y/X)+(.5*P+F)*(Y/(BV*X)+Y*D
     1X/X**2)-2.0*F*DX*(AJ-.5)*(AJ+1.5)/X**2)*(AJ+.5)*.5
  133 PF1U(L)=D+DDU
      DPF1U(L)=DD+DDDU
      WRITE(6,299)L,PF1U(L)                                             58
      PF1L(L)=D-DDU
      DPF1L(L)=DD-DDDU
   30 SF1(L)=C+ZLAM*FLOAT(K)*.5
      DSF1(L)=(SF1(L)-C)/ZLAM
      IF(AJ.LE.0.0)GO TO 20
      BOLT1(L)=1.0/(EXP(1.4384*SF1(L)/TEMP))                            70
      BOLT2(L)=1.0/(EXP(1.4384*SF2(L)/TEMP))                            73
      IF(QUANT.EQ.0.5)GO TO 123
      FP(1,L)=(T**2+T*Z*(TT+1.0-2.0*Y))/(32.0*AJ)
      STP(1,L)=FP(1,L)*BOLT1(L-1)
      FP(2,L)=(T*(TT-1.0+Z*(8.0*AJ**3+12.0*AJ**2-2.0*AJ-7.0+2.0*Y)))/W
      STP(2,L)=FP(2,L)*BOLT1(L)
      FP(3,L)=(T**2+T*Z*(TT-7.0+2.0*Y))/(32.0*(AJ+1.0))
      FP(4,L)=(T**2-T*Z*(TT-7.0+2.0*Y))/(32.0*AJ)
      STP(4,L)=FP(4,L)*BOLT2(L)
      FP(5,L)=(T*(TT-1.0-Z*(8.0*AJ**3+12.0*AJ**2-2.0*AJ+1.0-2.0*Y)))/W
      FP(6,L)=(T**2-T*Z*(TT+1.0-2.0*Y))/(32.0*(AJ+1.0))
      GO TO 124
  123 FP(1,L)=(T**2+T*Z*(TT-7.0+2.0*Y))/(32.0*AJ)
       STP(1,L)=FP(1,L)*BOLT2(L-1)
      FP(2,L)=(T*(TT-1.0+Z*(8.0*AJ**3+12.0*AJ**2-2.0*AJ+1.0-2.0*Y)))/W
      STP(2,L)=FP(2,L)*BOLT2(L)
      FP(3,L)=(T**2+T*Z*(TT+1.0-2.0*Y))/(32.0*(AJ+1.0))
      FP(4,L)=(T**2-T*Z*(TT+1.0-2.0*Y))/(32.0*AJ)
      STP(4,L)=FP(4,L)*BOLT1(L-2)
      FP(5,L)=(T*(TT-1.0-Z*(8.0*AJ**3+12.0*AJ**2-2.0*AJ-7.0+2.0*Y)))/W
      STP(5,L)=FP(5,L)*BOLT1(L-1)
      FP(6,L)=(T**2-T*Z*(TT-7.0+2.0*Y))/(32.0*(AJ+1.0))
      STP(6,L)=FP(6,L)*BOLT1(L)
  124 WRITE(6,299)K,SF1(L)                                              116
   20 CONTINUE
      IF(QUANT.EQ.0.5)GO TO 443
      DO 34) L=2,LINES
```

Reproduced with permission of the copyright owner. Further reproduction prohibited without permission.

```
      STP(3,L)=FP(3,L)*BOLT1(L+1)
      STP(5,L)=FP(5,L)*BOLT2(L+1)
      STP(6,L)=FP(6,L)*BOLT2(L+2)
  389 CONTINUE
      GO TO 433
  443 DO 405 L=2,LINES
      STP(3,L)=FP(3,L)*BOLT2(L+1)
  405 CONTINUE
  433 IF(QUANT.EQ.0.5)GO TO 88
      DO 45 I=2,LINES
      Q(1,I)=SF1(I-1)-PF1L(I)+VDD
      Q(2,I)=SF1(I)-PF1U(I)+VDD
      Q(3,I)=SF1(I+1)-PF1L(I)+VDD
      Q(4,I)=SF2(I)-PF1U(I)+VDD
      Q(5,I)=SF2(I+1)-PF1L(I)+VDD
      Q(6,I)=SF2(I+2)-PF1U(I)+VDD
      DDSF(1,I)=-DPF1L(I)
      DDSF(2,I)=-DPF1U(I)
      DDSF(3,I)=-DPF1L(I)
      DDSF(4,I)=-DPF1U(I)
      DDSF(5,I)=-DPF1L(I)
      DDSF(6,I)=-DPF1U(I)
   45 CONTINUE
      GO TO 531
   88 DO 397 I=3,LINES
      Q(1,I)=SF2(I-1)-PF1U(I)+VDD
      Q(2,I)=SF2(I)-PF1L(I)+VDD
      Q(3,I)=SF2(I+1)-PF1U(I)+VDD
      Q(4,I)=SF1(I-2)-PF1L(I)+VDD
      Q(5,I)=SF1(I-1)-PF1U(I)+VDD
      Q(6,I)=SF1(I)-PF1L(I)+VDD
      DDSF(1,I)=-DPF1U(I)
      DDSF(2,I)=-DPF1L(I)
      DDSF(3,I)=-DPF1U(I)
      DDSF(4,I)=-DPF1L(I)
      DDSF(5,I)=-DPF1U(I)
      DDSF(6,I)=-DPF1L(I)
  399 CONTINUE
  531 NUMB=IFIX(3.5-QUANT)
      NUMBE=IFIX(15.5-QUANT)
      IF(ACRNCT.EQ.0)GO TO 3461
      WRITE(7,3462)((Q(N,M),M=NUMB,NUMBE),N=1,6)                    232
      WRITE(7,3462)((DDSF(N,M),M=NUMB,NUMBE),N=1,6)                 242
 3462 FORMAT(F10.3)
 3461 DO 336 N=1,6
      DO 337 M=NUMB,LINES
      AWAVE=(10.0**8)/Q(N,M)                                        258
      IF(AWAVE.LT.XFIRS.OR.AWAVE.GT.XLAST)GO TO 337
      AP(N,M)=((XLAST-AWAVE)/SLIT)
      AAP(N,M)=AP(N,M)-AINT(AP(N,M))
      IF(AAP(N,M).LE.0.5)GO TO 203
      RR=AINT(AP(N,M))+2.0
      IF(RR.EQ.0.0)RR=1.0
      GO TO 209
  203 RR=AINT(AP(N,M))+1.0
  209 DO 556 M=1,4
```

Reproduced with permission of the copyright owner. Further reproduction prohibited without permission.

```
SCHNEIDER ALSES          CHM455-3788                          DATE 06/23/71     TIME  23 29'34''  737  PAGE  4
      LARRY      -  EFN   SOURCE STATEMENT  -  IFN(S)  -

      NN=MN-1
      RRR(MN)=(STR(N,M)*(SLIT1-FLOAT(NN)*SLIT1*.25))/SLIT1
      KATM=IFIX(RR)-NN
      KAT=IFIX(RR)+NN
      STREN(KAT)=STREN(KAT)+RRR(MN)
      IF(NN.EQ.0)GO TO 556
      STREN(KATM)=STREN(KATM)+RRR(MN)
  556 CONTINUE
  337 CONTINUE
  336 CONTINUE
      WRITE(6,52)                                                          300
   52 FORMAT(1H1,'TRANSITIONS')
      IF(QUANT.EQ..5)GO TO 3000
      IF(QUANT.EQ.1.5)GO TO 4000
 3000 WRITE(6,FMT05)                                                       307
      GO TO 5000
 4000 WRITE(6,FMT15)                                                       309
 5000 DO 202 M=NUMB,LINES
      L=M-1
      WRITE(6,201)L,Q(1,M),Q(2,M),Q(3,M),Q(4,M),Q(5,M),Q(6,M)              314
  201 FORMAT(1X,I2,6F10.2)
  202 CONTINUE
  999 FORMAT(1X,I6,F10.3)
      WRITE(6,55)                                                          323
   55 FORMAT(1H1,'ORDERED TRANSITIONS')
      WRITE(6,942)                                                         324
  942 FORMAT(1X,'BRANCH',5X,'    K   ',7X,'FREQUENCY',4X,'INTENSITY',2X,
     1'LINE STRENGTH',1X,'BOLTZ FACTOR')
      JJJ=0
      DO 91 M=1,6
      DO 82 N=NUMB,LINES
      JJJ=JJJ+1
      XFREQ(JJJ)=Q(M,N)
      ISUM(JJJ)=100*M+N
   82 CONTINUE
   91 CONTINUE
      LINE3=6*(LINES-IFIX(2.5-QUANT))
      CALL SORTAL(-1)                                                      341
      CALL SORT(XFREQ(1),XFREQ(2),LINE3,ISUM(1))                           343
      DO 25 I=1,LINE3
      IY=ISUM(I)/100
      IZ=ISUM(I)-IY*100
      FREQ(I)=10.0**8/XFREQ(I)                                             352
      ABR=STP(IY,IZ)/FP(IY,IZ)
      IX=IFIX(2.5-QUANT)*IY
      IW=IZ-1
      WRITE(6,444)BRANCH(IX),IW,FREQ(I),STP(IY,IZ),FP(IY,IZ),ABR           358
  444 FORMAT(1X,A6,5X,I6,5X,4F13.4)
   25 CONTINUE
      WRITE(6,1022)(STREN(I),ANGST(I),I=1,NLAST)                           365
 1022 FORMAT(1X,2F12.4)
 1322 FORMAT(F12.3)
      LABC=3000-NLAST
      CALL ISPLOT(NLAST,LABC,XFIRS,XLAST,ANGST,STREN,III)                  374
      STOP
      END
```

Reproduced with permission of the copyright owner. Further reproduction prohibited without permission.

```
      SUBROUTINE BSPLOT(NLAST,LABC,XFIRS,XLAST,X,Y,III)
      DIMENSION Y(NLAST),X(NLAST)
      DIMENSION NLX(12),NLY(12),NUX(12),NAME(12),NRY(12)
      READ(5,846)(NLX(I),NLY(I),NAMC(I),NUX(I),NRY(I),I=1,12)                    1
  846 FORMAT(5A6)
      CALL PENBGN(LX,LY)                                                         12
  836 CALL SCLPLT(2,3,3,3,2,2,),2,1,2,XLAST,0.0,XFIRS,1.0,0.0,0.0,25.0,
     125.0,-12.5,-12.5,1.0,NLX,NLY,NUX,NRY,NAME,LX,LY)                          14
      CALL GENPLT(1,1,2,X,Y,1,NLAST,XLAST,0.0,XFIRS,2.3,FIRSTX,FIRSTY,
     1FINALX,FINALY,25.0,25.0,-12.5,-12.5,1.0,DUMM,LX,LY)                       16
      CALL PENRLF(LX,LY)                                                         18
      CALL PENEND(LX,LY)                                                         20
  835 RETURN
      END
```


Reproduced with permission of the copyright owner. Further reproduction prohibited without permission.

[illegible]	[illegible]
1	9.536
2	-1309.990
1	12.743
2	31.907
3	-1270.352
2	37.167
3	65.889
4	-1214.842
3	73.250
4	111.501
5	-1143.603
4	120.960
5	168.704
6	-1055.550
5	130.257
6	237.446
7	-953.766
6	251.087
7	317.566
8	-835.299
7	333.390
8	409.292
9	-701.209
8	427.092
9	512.241
10	-551.562
9	532.110
10	626.423
11	-386.434
10	643.352
11	751.734
12	-205.909
11	775.713
12	883.060
13	-10.077
12	914.081
13	1035.280
14	200.959
13	1063.330
14	1193.260
15	427.093
14	1223.327
15	1361.454
16	664.207
15	1393.928
16	1540.911
17	924.175
16	1574.976
17	1730.264
18	1194.864
17	1766.307
18	1929.739
19	1480.132
18	1967.746
19	2139.152
20	1779.829
19	2179.106
20	2358.306
21	2093.796
20	2400.191
21	2586.996
22	2421.166
21	2630.766

Reproduced with permission of the copyright owner. Further reproduction prohibited without permission.

TRANSITIONS

K	P11	Q11	R11	P21	Q21	R21
1	29214.59	29227.33	29251.76	29224.18	29246.50	29260.48
2	29187.63	29212.12	29248.20	29206.86	29240.84	29266.45
3	29156.64	29192.73	29240.44	29185.37	29230.98	29268.19
4	29121.45	29169.16	29228.45	29159.70	29216.90	29265.65
5	29082.10	29141.41	29212.72	29129.85	29198.58	29278.82
6	29036.60	29109.45	29191.73	29095.81	29176.91	29267.66
7	28990.95	29073.29	29166.96	29057.56	29149.16	29252.14
8	28939.15	29032.90	29137.87	29015.10	29118.00	29232.23
9	28883.19	28988.27	29104.45	28968.40	29082.52	29207.90
10	28823.05	28938.39	29066.76	28917.46	29042.68	29179.09
11	28758.75	28886.22	29024.48	28862.24	28998.46	29145.79
12	28690.25	28828.76	28977.87	28802.74	28941.82	29107.94
13	28617.55	28766.77	28926.79	28738.92	28896.73	29065.50
14	28540.52	28700.33	28871.22	28670.77	28839.15	29018.42
15	28459.46	28630.32	28811.11	28596.25	28777.04	28966.66
16	28374.04	28555.40	28746.42	28521.34	28710.38	28910.16
17	28284.34	28476.04	28677.11	28440.00	28639.10	28848.89
18	28190.34	28392.21	28604.14	28354.21	28563.18	28782.77
19	28092.01	28303.48	28524.45	28263.92	28482.57	28711.77

Reproduced with permission of the copyright owner. Further reproduction prohibited without permission.

ORDERED TRANSITIONS

BRANCH	K	FREQUENCY	INTENSITY	LINE STRENGTH	BOLTZ FACTOR
P21	3	3414.3460	0.1991	0.3234	0.6155
P21	2	3414.5479	0.1518	0.2092	0.7256
P21	4	3414.6417	0.2214	0.4383	0.5051
R21	1	3415.2447	0.0813	0.0982	0.8273
R21	5	3415.4386	0.2217	0.5529	0.4010
P21	6	3416.7408	0.2054	0.6667	0.3081
R21	7	3418.5533	0.1786	0.7795	0.2291
R11	1	3418.6581	0.0915	0.1018	0.8986
R11	2	3419.0137	0.1777	0.2194	0.8100
Q21	1	3419.2129	0.3606	0.3152	0.9123
Q21	2	3419.8744	0.5572	0.6735	0.8273
R11	3	3419.9214	0.2424	0.3433	0.7061
R21	8	3420.8815	0.1470	0.8911	0.1650
Q21	3	3421.0261	0.6746	0.9297	0.7256
P11	4	3421.3255	0.2803	0.4709	0.5954
Q11	1	3421.4547	0.3902	0.4048	0.9640
P21	1	3421.8243	0.4835	0.4970	0.9728
Q21	4	3422.6766	0.7238	1.1760	0.6155
P11	1	3422.9472	0.5030	0.5030	1.0000
R11	5	3423.2244	0.2919	0.6011	0.4856
Q11	2	3423.2367	0.6272	0.6930	0.8986
R21	9	3423.7317	0.1152	1.0015	0.1150
P21	2	3423.8532	0.5408	0.5928	0.9123
Q21	5	3424.8237	0.7152	1.4160	0.5051
Q11	3	3425.5102	0.7898	0.9751	0.8100
R11	6	3425.6272	0.2811	0.7335	0.3832
P11	2	3426.1014	0.5853	0.6071	0.9640
P21	3	3426.3742	0.5804	0.7015	0.8273
R21	10	3427.1111	0.0863	1.1105	0.0777
Q21	6	3427.4734	0.6621	1.6512	0.4010
Q11	4	3428.2790	0.8814	1.2493	0.7061
R11	7	3428.5371	0.2540	0.9678	0.2927
P21	4	3429.3900	0.5902	0.8134	0.7256
P11	3	3429.7499	0.6533	0.7270	0.8986
Q21	7	3430.6308	0.5799	1.8823	0.3081
R21	11	3431.0274	0.0620	1.2182	0.0509
Q11	5	3431.5493	0.9056	1.5211	0.5954
R11	8	3431.9595	0.2172	1.0040	0.2164
P21	5	3432.9042	0.5700	0.9260	0.6155
P11	4	3433.8955	0.6910	0.8531	0.8100
Q21	8	3434.3013	0.4633	2.1097	0.2291
Q11	6	3435.3102	0.3717	1.7950	0.4856
R21	12	3435.4391	0.0428	1.3246	0.0323
R11	9	3435.9006	0.1768	1.1418	0.1549
P21	6	3436.9208	0.5244	1.0383	0.5051
Q21	9	3438.4914	0.3849	2.3335	0.1650
P11	5	3438.5416	0.6940	0.9329	0.7061
Q11	7	3439.5833	0.7936	2.0707	0.3832
R11	10	3440.3674	0.1376	1.2813	0.1074
R21	13	3440.5056	0.0284	1.4295	0.0199
P21	7	3441.4446	0.4610	1.1498	0.4010
Q21	10	3443.2080	0.2938	2.5541	0.1150
P11	6	3443.6921	0.6640	1.1153	0.5954
Q11	8	3444.3682	0.6674	2.3466	0.2927
R11	11	3445.3676	0.1026	1.4224	0.0721
R21	14	3446.0872	0.0182	1.5331	0.0119
P21	8	3446.4813	0.3852	1.2603	0.3081
Q21	11	3448.4591	0.2154	2.7714	0.0777

Reproduced with permission of the copyright owner. Further reproduction prohibited without permission.

P11	7	3449.3518	0.6070	1.2499	0.4856	
Q11	9	3449.6709	0.5688	2.6239	0.2164	
P11	12	3450.9095	0.0735	1.5650	0.0469	
P21	9	3452.0370	0.3138	1.3696	0.2291	
R21	15	3452.2450	0.0113	1.6352	0.0069	
Q21	12	3454.2531	0.1519	2.0955	0.0509	
Q11	10	3455.4483	0.4510	2.7118	0.1549	
P11	8	3455.5262	0.5313	1.3864	0.3832	
P11	13	3457.0026	0.0506	1.7092	0.0296	
P21	10	3458.1187	0.2437	1.4776	0.1650	
R21	16	3458.4410	0.0067	1.7760	0.0039	
Q21	13	3460.5497	0.1032	3.1365	0.0323	
Q11	11	3461.8581	0.3433	3.1074	0.1074	
P11	9	3462.2214	0.4403	1.5247	0.2227	
R11	14	3463.6569	0.0436	1.8850	0.0181	
P21	11	3466.7163	0.1622	1.5844	0.1150	
P21	12	3468.2361	0.0039	1.3353	0.0021	
Q21	14	3467.5090	0.0677	2.4065	0.0189	
Q11	12	3466.7565	0.2513	3.4157	0.0721	
P11	11	3469.4443	0.3402	1.6647	0.2164	
R11	15	3470.4335	0.0216	2.0022	0.0108	
P21	13	3471.8922	0.1213	1.6498	0.0777	
R21	17	3474.3003	0.0022	1.9333	0.0011	
Q21	15	3474.9322	0.0423	3.0035	0.0119	
Q11	13	3476.2059	0.1773	3.7767	0.0469	
P11	11	3477.2025	0.2797	1.9063	0.1549	
R11	16	3479.6942	0.0134	2.1510	0.0062	
P21	14	3479.6017	0.0913	1.7938	0.0509	
R21	18	3480.4026	0.0012	2.0258	0.0006	
Q21	16	3483.0813	0.0263	3.8414	0.0069	
Q11	14	3484.2193	0.1206	4.0705	0.0296	
P11	12	3485.5646	0.2093	1.9499	0.1074	
R11	17	3487.1017	0.0040	2.3012	0.0035	
P21	15	3487.8732	0.0612	1.8964	0.0423	
Q21	17	3491.7284	0.0156	4.0104	0.0039	
Q11	15	3492.8005	0.0702	4.3671	0.0181	
P11	13	3494.3596	0.1510	2.0942	0.0721	
R11	18	3496.1201	0.0046	2.4529	0.0019	
P21	15	3496.7177	0.0397	1.9976	0.0109	
Q21	18	3501.0105	0.0089	4.2065	0.0021	
Q11	16	3501.9944	0.0503	4.6665	0.0108	
P11	14	3503.7779	0.1052	2.2495	0.0469	
R11	19	3505.7641	0.0026	2.4051	0.0010	
P21	16	3506.1471	0.0249	2.0575	0.0119	
Q21	19	3510.4196	0.0050	4.3996	0.0011	
Q11	17	3511.7238	0.0309	4.8684	0.0062	
P11	15	3513.7701	0.0707	2.3083	0.0296	
P21	17	3516.1743	0.0151	2.1959	0.0069	
Q11	18	3522.0924	0.0184	5.2738	0.0035	
P11	16	3524.3484	0.0470	2.5376	0.0181	
P21	18	3526.8134	0.0089	2.2929	0.0039	
Q11	19	3532.0149	0.0106	5.5917	0.0019	
P11	17	3535.6253	0.0340	2.6684	0.0104	
P21	19	3538.0793	0.0051	2.3925	0.0021	
P11	18	3547.3148	0.0176	2.1406	0.0062	
P11	19	3559.7315	0.0104	2.9943	0.0035	
		0.0000	3445.0000			
		0.0000	3444.9100			
		0.0000	3444.8200			
		0.0000	3444.7300			

Reproduced with permission of the copyright owner. Further reproduction prohibited without permission.

0.1713	3444.6400
0.3437	3444.5500
0.5155	3444.4600
0.6874	3444.3700
0.5155	3444.2800
0.3437	3444.1900
0.1713	3444.1000
0.0000	3444.0100
0.1440	3443.9200
0.3320	3443.8300
0.4540	3443.7400
0.6640	3443.6500
0.4590	3443.5600
0.4055	3443.4700
0.3129	3443.3800
0.2293	3443.2900
0.2013	3443.2000
0.2203	3443.1100
0.1469	3443.0200
0.0734	3442.9300
0.0000	3442.8400
0.0000	3442.7500
0.0000	3442.6600
0.0000	3442.5700
0.0000	3442.4800
0.0000	3442.3900
0.0000	3442.3000
0.0000	3442.2100
0.0000	3442.1200
0.0000	3442.0300
0.0000	3441.9400
0.0000	3441.8500
0.0000	3441.7600
0.1153	3441.6700
0.2305	3441.5800
0.3453	3441.4900
0.4610	3441.4000
0.3459	3441.3100
0.2305	3441.2200
0.1153	3441.1300
0.0000	3441.0400
0.0000	3440.9500
0.0000	3440.8600
0.0071	3440.7700
0.0446	3440.6800
0.0901	3440.5900
0.1316	3440.5000
0.1583	3440.4100
0.1174	3440.3200
0.0759	3440.2300
0.0344	3440.1400
0.0000	3440.0500
0.0000	3439.9600
0.1384	3439.8700
0.3668	3439.7800
0.5992	3439.6900
0.7916	3439.6000
0.5992	3439.5100
0.3668	3439.4200
0.1384	3439.3300

Reproduced with permission of the copyright owner. Further reproduction prohibited without permission.

0.0000	3439.2400
0.0000	3439.1500
0.0000	3439.0600
0.0000	3438.9700
0.0000	3438.8800
0.2637	3438.7900
0.5355	3438.7000
0.4062	3438.6100
1.0793	3438.5200
0.8092	3438.4300
0.5395	3438.3400
0.2697	3438.2500
0.0000	3438.1600
0.0000	3438.0700
0.0000	3437.9800
0.0000	3437.8900
0.0000	3437.8000
0.0000	3437.7100
0.3077	3437.6200
0.0000	3437.5300
0.0000	3437.4400
0.0000	3437.3500
0.0000	3437.2600
0.1311	3437.1700
0.3622	3437.0800
0.3933	3436.9900
0.5244	3436.9000
0.3933	3436.8100
0.2622	3436.7200
0.1311	3436.6300
0.0000	3436.5400
0.0000	3436.4500
0.0000	3436.3600
0.0000	3436.2700
0.0642	3436.1800
0.0784	3436.0900
0.1426	3436.0000
0.1763	3435.9100
0.1325	3435.8200
0.0991	3435.7300
0.0656	3435.6400
0.2500	3435.5500
0.4746	3435.4600
0.6953	3435.3700
0.6631	3435.2800
0.6844	3435.1900
0.4354	3435.1000
0.2179	3435.0100
0.0000	3434.9200
0.0000	3434.8300
0.0000	3434.7400
0.0000	3434.6500
0.1209	3434.5600
0.2417	3434.4700
0.3625	3434.3800
0.4833	3434.2900
0.6042	3434.2000
0.6772	3434.1100
0.6491	3434.0200
0.6211	3433.9300

Reproduced with permission of the copyright owner. Further reproduction prohibited without permission.

0.5183	3433.8400
0.3455	3433.7500
0.1728	3433.6600
0.0000	3433.5700
0.0000	3433.4800
0.0000	3433.3900
0.0000	3433.3000
0.1425	3433.2100
0.2850	3433.1200
0.4275	3433.0300
0.5700	3432.9400
0.4275	3432.8500
0.2850	3432.7600
0.1425	3432.6700
0.0000	3432.5800
0.0000	3432.4900
0.0000	3432.4000
0.0000	3432.3100
0.0543	3432.2200
0.1086	3432.1300
0.1629	3432.0400
0.2172	3431.9500
0.1629	3431.8600
0.3350	3431.7700
0.5071	3431.6800
0.6792	3431.5900
0.5056	3431.5000
0.6792	3431.4100
0.4683	3431.3200
0.2574	3431.2300
0.0465	3431.1400
0.0620	3431.0500
0.0465	3430.9600
0.1760	3430.8700
0.3054	3430.7800
0.4349	3430.6900
0.5799	3430.6000
0.4349	3430.5100
0.2899	3430.4200
0.1450	3430.3300
0.0000	3430.2400
0.0000	3430.1500
0.1633	3430.0600
0.3266	3429.9700
0.4900	3429.8800
0.6533	3429.7900
0.6375	3429.7000
0.6217	3429.6100
0.6060	3429.5200
0.5902	3429.4300
0.4427	3429.3400
0.2951	3429.2500
0.1475	3429.1600
0.0000	3429.0700
0.0000	3428.9800
0.0000	3428.8900
0.0635	3428.8000
0.1270	3428.7100
0.1905	3428.6200
0.4743	3428.5300

Reproduced with permission of the copyright owner. Further reproduction prohibited without permission.

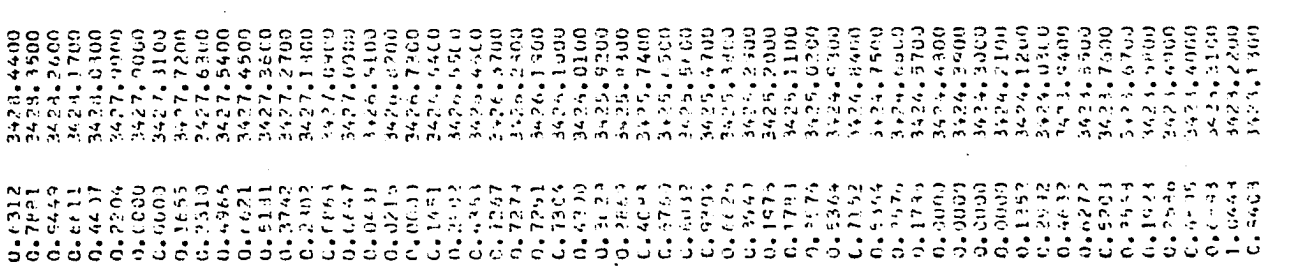

Reproduced with permission of the copyright owner. Further reproduction prohibited without permission.

0.4364	3424.0400
0.9137	3422.9500
0.7331	3422.8600
0.7444	3422.7700
0.8475	3422.6800
0.5423	3422.5900
0.3013	3422.5000
0.1913	3422.4100
0.1000	3422.3200
0.0000	3422.2300
0.0000	3422.1400
0.1200	3422.0500
0.2417	3421.9600
0.3625	3421.8700
0.4835	3421.7800
0.4032	3421.6900
0.5239	3421.6000
0.6537	3421.5100
0.7605	3421.4200
0.7415	3421.3300
0.7425	3421.2400
0.7804	3421.1500
0.8181	3421.0600
0.8162	3420.9700
0.8443	3420.8800
0.8789	3420.7900
0.8735	3420.7000
0.8367	3420.6100
0.8000	3420.5200
0.8000	3420.4300
0.8000	3420.3400
0.8000	3420.2500
0.8000	3420.1600
0.8000	3420.0700
0.8000	3419.9800
0.7695	3419.8900
0.8557	3419.8000
0.8953	3419.7100
0.9000	3419.6200
0.9000	3419.5300
0.9000	3419.4400
0.9000	3419.3500
0.9249	3419.2600
0.8494	3419.1700
0.4037	3419.0800
0.3530	3418.9900
0.2463	3418.9000
0.1792	3418.8100
0.2023	3418.7200
0.2754	3418.6300
0.2472	3418.5400
0.1707	3418.4500
0.1122	3418.3600
0.0446	3418.2700
0.0000	3418.1800
0.0000	3418.0900
0.0000	3418.0000
0.0000	3417.9100
0.0000	3417.8200
0.0000	3417.7300

Reproduced with permission of the copyright owner. Further reproduction prohibited without permission.

0.0000	3417.6400
0.0033	3417.5500
0.0000	3417.4400
0.0000	3417.3700
0.0000	3417.2300
0.0000	3417.1300
0.0000	3417.1000
0.0013	3417.0100
0.1127	3416.9200
0.1140	3416.8300
0.2054	3416.7400
0.1440	3416.6500
0.1027	3416.5600
0.0513	3416.4700
0.0000	3416.3800
0.0000	3416.2900
0.0000	3416.2000
0.0000	3416.1100
0.0000	3416.0200
0.0000	3415.9300
0.0000	3415.8400
0.0054	3415.7500
0.1080	3415.6600
0.1663	3415.5700
0.2429	3415.4800
0.2069	3415.3700
0.1718	3415.3000
0.1367	3415.2100
0.0960	3415.1200

Reproduced with permission of the copyright owner. Further reproduction prohibited without permission.

REFERENCES FOR INTRODUCTION, EXPERIMENTAL AND THEORY SECTIONS

1. C.F. Meyer, Phys. Rev. 10 91 (1917).
2. W. Wein, Ann. Physik 69, 331 (1923).
3. W.A. Chupka, J. Chem. Phys. 30, 191 (1959).
4. V.H. Dibeler and R.M. Reese, J. Res. N.B.S. 68A, No 4, 409 (1964).
5. V.H. Dibeler and J.A. Walker, Adv. in Mass Spect. 4, 767 (1967).
6. W.A. Chupka, J. Chem. Phys. 54, 1936 (1971).
7. W.C. Price and D.W. Simpson, Proc. Roy. Soc. A165, 272 (1938).
8. Y. Tanaka, A.S. Jursa, and F.J. LeBlanc, J. Chem. Phys. 32 1199 (1960).
9. For a complete review of the theory of Rydberg series, see R.S. Mulliken, J. Amer. Chem. Soc. 86, 3183 (1964).
10. C.R. Brundle et. al., Chem Phys. Lett. 3, 292 (1969).
11. E. Linholm, Arkiv Für Fysik 40, 97 (1967).
12. V.M. Ellsworth and J.J. Hopfield, Phys. Rev. 29, 79 (1927).
13. G. Herzberg, Ann. Physic 86, 189 (1928).
14. M. Haugh and K. Bayes, Phys. Rev. A2, 1778 (1970).
15. M. Bayes, to be published.
16. M.I. Al-Jouboury and D.W. Turner, J. Chem. Soc. 5141 (1963).
17. D.W. Turner, Phys. Meth. in Adv. Inorg. Chem. 74 (1958).
18. D.W. Turner, Molecular Photoelectron Spectroscopy (Wiley, 1970).

Reproduced with permission of the copyright owner. Further reproduction prohibited without permission.

19. E. Lindholm, Chem. Phys. Lett. 1, 543 (1967).

20. D.L. Judge, A.L. Morse, and G.L. Weissler, Proc. VIth Int. Conf. on Ion Phenomena in Gases 373 (1963).

21. D.L. Judge and G.L. Weissler, J. Chem. Phys. 48, 4590 (1968).

22. B.S. Schneider and A.L. Smith, to be published.

23. D.W. Turner and D.P. May, J. Chem. Phys. 46, 1156 (1967).

24. D.L. Judge, G.S. Bloom, and A.L. Morse, Can. J. Phys. 47, 489 (1969).

25. F. Maak and C.M. Sellars, J. Sci. Inst. 42, 900 (1965).

26. The catalyst can be purchased from BSAF, P.O. Box 389, Paramus, New Jersey, under the name Catalyst R 3-11.

27. F.C. Fehsenfeld, K.M. Evenson, and H.P. Broida, Rev. Sci. Instr. 36, 294 (1965).

28. J.R. Samson, Techniques of Vacuum Ultraviolet Spectroscopy (Wiley, 1967).

29. D.L. Akins, S.E. Schwartz, and C.B. Moore, Rev. Scien. Inst. 39, 715 (1968).

30. G.A. Morton, Applied Optics 7, 1 (1968).

31. A good qualitative description can be found in Herzberg, Molecular Spectra and Molecular Structure (Van Nostrand, 1966). For a good mathematical treatment refer to R. Nicholls and A.L. Stewart in Bates, Atomic and Molecular Processes (Chapter 2).

32. G. Herzberg, ref. 31.

33. M. Vestal, A. Wahrhaftig, and W. Johnston, J. Chem. Phys. 37, 1276 (1962).

34. H.M. Rosenstock et. al., Proc. Nat. Acad. Sci. U.S. 38, 667 (1952).

35. G.F. Marr, Photoionization Processes in Gases (Academic Press, 1967).

Reproduced with permission of the copyright owner. Further reproduction prohibited without permission.

REFERENCES FOR HBr^+ SECTION

1. F. Norling, Z. Phys. 95, 179 (1935).

2. R.F. Barrow and A.D. Caunt, Proc. Phys. Soc. 66, 41 (1953).

3. L. Marsigny et. al., C.R. Acad. Sci. Paris 266, 176 (1968).

4. G. Pennetier et. al., J. Chimie Phys. 61, 1162 (1964).

5. L. Marsigny et. al., C.R. Acad. Sci. Paris 266, 1731 (1968).

6. D. Turner, Molecular Photoelectron Spectroscopy (Wiley, 1970).

7. J.M. Lemka, T.R. Passmore and W.C. Price, Proc. Roy. Soc. (London) 304A, 53 (1968).

8. M.T. Haugh and K. Bayes, to be published in J. Chem. Phys.

9. R.W. Nicholls, J. Quant. Spect. Rad. Trans. 2, 433 (1962).

10. D.L. Judge and G.L. Weissler, J. Chem. Phys. 48, 4590 (1968).

11. R.N. Zare and J.K. Cashion, U.C.R.L. - 10881 (June 1963).

12. Herzberg ref. 31, Introduction.

13. D.A. Ramsay, J. Chem. Phys. 20, 1920 (1952).

14. E.L. Hill and J.H. Van Vleck, Phys. Rev. 32 250 (1923).

15. L.T. Earls, Phys. Rev. 48, 423 (1935).

15A. F.W. Birss et. al., Can. J. Phys. 48, 1230 (1970).

16. R.G. Turner and R.W. Nicholls, Can. J. Phys. 32, 468 (1954).

17. R.N. Zare, E.O. Larsson, and R.A. Berg, J. Mol. Spect. 15, 117 (1965).

Reproduced with permission of the copyright owner. Further reproduction prohibited without permission.

18. T.C.James, J. Mol. Spect. 20, 77 (1966).

19. A.L. Smith, J. Mol. Spect. 28, 269 (1968).

20. Private Communication.

21. M.J. Haugh, Ph. D. Dissertation (U.C.L.A., 1970).

Reproduced with permission of the copyright owner. Further reproduction prohibited without permission.

REFERENCES FOR N_2O^+ AND CS_2^+ SECTION

1. R.S. Mulliken, Can. J. Phys. 36, 10 (1958).

2. A.D. Walsh, J. Chem. Soc. 2266 (1953).

3. S.D. Peyerimhoff and R.J. Buenker, J. Chem. Phys. 49, 2473 (1968).

4. J.H. Calloman, Proc. Chem. Soc. 313 (1959).

5. J.H. Calloman, Proc. Roy. Soc. (London) 244A, 220 (1968).

6. C.R. Brundle and D.W. Turner, Int. J. Mass. Spect. and Ion Phys. 2, 195 (1969).

7. M.J. Haugh and K.O. Bayes, Phys. Rev. A 2, 1778 (1970).

8. Y. Tanaka, A.S. Jursa, and F.J. LeBlanc, J. Chem. Phys. 32 1199, 1205 (1960).

9. V.H. Dibeler and J.A. Walker, Adv. in Mass Spect. 4, 767 (1967).

10. V.H. Dibeler, J.A. Walker, and S.K. Liston, J. of Res. N.B.S. 71A, 371 (1967).

11. R.F. Barrow et. al., Arkiv Fysik 18, 543 (1960).

11A. M. Ogawa and H.C. Chang, Can. J. Phys. 48, 2455 (1970).

12. S. Leach, Private Communication.

13. I.E. Dayton, F.W. Dalby, and R.G. Bennett, J. Chem. Phys. 33, 179 (1960).

14. F.C. Creutzberg, Ph. D. Dissertation (University College, London, 1965).

15. G.R. Cook and M. Ogawa, J. Chem. Phys. 51, 2419 (1969).

16. D.W. Turner, Molecular Photoelectron Spectroscopy (Wiley, 1970).

17. J.H. Calloman and F.C. Creutzberg, Proc. Int. Conf. Spectrosc. 1st Bombay, 1, 171 (1954).

Reproduced with permission of the copyright owner. Further reproduction prohibited without permission.